Synthesis and characterization of undoped and Ag doped TiO_2, ZnO and ZnS nanoparticles for the photocatalytic degradation of 2-chlorophenol under UV irradiation

by

Shirley Priscilla ONKANI (Student number: **211036250)**

Supervisors

Prof. FanyanaM. Mtunzi

Dr. Paul N. Diagboya

Dr. Michael Klink

Synthesis and characterization of undoped and Ag doped TiO_2, ZnO and ZnS nanoparticles for the photocatalytic degradation of 2-chlorophenol under UV irradiation

Subject code: 615001

08/07/2019

Submitted by: **Shirley Priscilla ONKANI** Student number: **211036250**

To the Department of Chemistry for the degree of Masters in Chemistry

Under the supervision of

Prof. Fanyana M. Mtunzi

Co-supervisions

Dr. P.N. Diagboya

Dr. Michael Klink

Faculty of Applied and Computer Sciences, Department of Chemistry

Vaal University of Technology,

Andries Potgieter Boulevard,

P.O. Box 1900,

Vanderbijlpark, South Africa

Dedicated

To My Family

Certification

This is to certify that the dissertation entitled “Synthesis and characterization of undoped and Ag doped TiO_2, ZnO and ZnS nanoparticles used as photocatalyst for degradation of 2–chlorophenol under UV irradiation” submitted by Shirley Priscilla Onkani is in fulfillment of the requirements for the degree of Master in Chemistry at Vaal University of Technology. The work is an authentic work carried out by me under the supervisions of Prof FM Mtunzi, Dr PN Diagboya and Dr MKlink.

To the best of my knowledge, the work done in this dissertation has not been submitted to any other University/Institute for the award of any degree or diploma.

Date: 08/07/2019

Miss SP Onkani,
Department of Chemistry
Vaal University of Technology,
Vanderbijlpark,
1900, South Africa.

Acknowledgement

I would like to thank my family members: my mother, my father, my two younger brothers, grand-mothers, uncles and aunts for their mental support, encouragements and good wishes. I especially thank my father, who has been immensely helpful to me for my University studies and my living during all these years.

Sincere gratitude goes to my supervisors for their continuous encouragement and invaluable responsibilities throughout my research work.

I gratefully acknowledged the NCAP group member from chemistry department Prof M.J Moloto, Dr Elvera Viljoen, Prof Vusumi Pakade and Dr Thokozani Xaba for their many useful comments and discussions.

I solemnly thank Dr. E.O. Oseghea, Dr C.Y. Abasi, Mr Emmanuel Ba'aku AttahDaniel, Miss D.S More, Mr.Patric Ngoyi and Dr Kate Kotlhao for their assistance during the course of my work.

I also thank Vaal University of Technology for the opportunity to be a master student and use the laboratory facilities.

Once again I will like to thank the Research Directorate Office for their financial support especially via VUT award scholarship which was been a huge help.

I also acknowledged the Departments of Metallurgy and Biotechnology at Vaal University of Technology for giving me the opportunities to analyze my samples using the XRD and FTIR equipment. I would like to acknowledge the support of my laboratory colleagues (past and present) for their help, encouragement and for the friendly atmosphere in the laboratory. Lastly I would like to thank the almighty God my help and strength.

Abstract

Phenol, 2-chlorophenol (2-CP) is used in the manufacture of several chemical compounds including other chlorophenols, dyes, dentifrice and pesticides. The usage of these chemicals results in the discharge of 2-CP that is harmful to most biota in the environment. Therefore there is need to remove or degrade 2-CP from the environment, especially in water. This research focused on the synthesis, characterization and application of Ag doped semiconductor (TiO_2, ZnO, and ZnS) nanoparticles for the removal of 2-CP from water. Sol-gel and co-precipitation methods were used to synthesize the nanoparticles with different Ag contents (1%, 3% and 5%). Silver metal was used as a doping agent due to its antibacterial activity and ability to improve the photocatalytic activity of the semiconductors for 2-CPdegradation under UV irradiation. Characterization techniques such as *X*-ray diffraction (XRD), Fourier transform infrared (FTIR), Ultra-violet visible spectroscopy (*UV*-Vis) and photoluminescence spectra (PL) were used to characterize the structural, optical and physical properties of the nanoparticles, while Transmission electron microscopy (TEM) was used to characterize the surface of the nanoparticles. The XRD results confirmed the formation of anatase, wurtzite and blend phases of TiO_2, ZnO and ZnS nanoparticles, respectively. The band gaps of the synthesized nanoparticles were 3.42 eV, 3.23 eV and 3.12 eV for TiO_2, ZnO and ZnS nanoparticles respectively. The TEM images showed that all synthesized nanoparticles were uniform in shape. Photocatalytic degradation of 2-CP under UV irradiation confirmed that the semiconductor's photocatalytic activities improved with the addition of Ag ions. The best removal percentage was obtained at doped Ag percentages of 5, 1 and 5 % using TiO_2, ZnO and ZnS, respectively. In addition, the effects of various parameters affecting the photocatalytic degradation such as pH, initial concentrations of 2-CP and amount of catalyst (Ag doped TiO_2, ZnO and ZnS, respectively) loading were examined and optimized. At the different initial concentrations of 2-CP, namely, 8, 20 and 50 ppm, the highest degradation efficiency was obtained at pH of 10.5 and 5 mg of catalyst dosage. However a decrease in initial concentration of 2-CP showed an increase in the photocatalytic efficiency. The degradation percentage of 2-CP obtained with Ag doped TiO_2; ZnO and ZnS nanoparticles were 74.74, 57.8 and 45.49 %, respectively. Doping of these materials with Ag enhanced their photocatalytic activity; thus, they have the potential of degrading phenolic compounds, especially 2-chlorophenol, in water.

Table of Contents

List of figures

List of tables

List of symbols and abbreviations

Greek symbol	
Ă:	Armstrong
β:	Beta
Cos:	Co sinus
θ:	Theta
μm:	Pico meter
λ:	Wavelength
English symbol	
K:	Adsorption coefficient of the reactant
A_0:	Adsorption in initial time
A_t:	Adsorption of reactant time (t)
K_{app}:	apparent first order constant
cm^{-1}:	per centimetre
C:	Concentration
C_0:	Concentration reaction at initial time (t_0)
C_t:	Concentration of reactant time (t)
C:	Concentration
D :	Diameter
^oC:	Degree Celsius
eV:	Electron Volt (J)
L/mg:	Litre per milligrams
Ln:	Natural Logarithm
m:	Meter
mg/L:	Milligram per litre
mg/L min:	Milligram per litre per min
mL:	Milliter
min:	Minute
ppm:	Parts per million
nm:	Nanometer
D%:	Percentage Degradation
k:	The reaction rate constant
rpm:	Revolutions per min
m^2/g:	Square meter per gram
Ksp:	Solubility product
%:	Percentage
pzc :	Point of Zero charge :
PKa:	negative base-10 logarithm of the acid dissociation constant of a solution pKa= -log 10 Ka
PCP:	Pentachlorophenol

TIPO:	Tetra isopropyl oxide
AOP:	Advance Oxidative Process
E_g:	Band gap
BiOCl:	Bismuth oxychloride
CdS:	Cadmium sulphide
CL:	Cathodoluminescence
CO_2:	Carbon dioxide
2-CP:	2-chlorophenol
Cr-ZnS:	Chronium-Zinc sulfide
Co(II):	Cobalt (II) ion
Co-La-TiO_2:	Cobalt-Lanthanum doped titanium dioxide
Co-ZnO:	Cobalt zinc oxide
Co-doped TiO_2:	Cobalt doped titanium dioxide
CD:	Conduction band
2,4-DCP:	2,4-dichlorophenol
2,4-D:	Dichloroprop
2,4-DP:	Dichloroprop-p
e^- / h^+:	Electron-hole pairs
EL:	Electroluminescence
EU:	European union
FTIR:	Fourier Transform Infrared Spectroscopy
GC-MS:	Gas chromatography-mass spectrometry
Au:	Gold
HLPW:	High level panel on water
HPLC:	High performance liquid chromatography
HCl:	Hydrochloric acid
H_2O_2:	Hydrogen peroxide
H_2:	Hydronium
H^+:	Hydronium ion
OH^-:	Hydroxyl radical
IARC:	International Association for Research on Cancer
Fe_2O_3:	Iron (III) oxide or ferric oxide
JCPDS:	Joint Committee on Powder Diffraction Standards
La doped TiO_2:	Lanthanum doped Titanium dioxide
LSPR:	Localized Surface Plasmon Resonance
MEF:	Metal Fluorescence
Ni^{2+}:	Nickel(ii) ion
Ni-ZnO:	Nickel Zinc oxide
Pd:	Palladium
Pt:	Platinium
PL:	Photolominescence
SCE:	Saturated Calomnel Electrode
SERS :	Scattering

Ag:	Silver
Ag^{2+}:	Silver (ii) ion
Ag^{3+}:	Silver (iii) ion
Ag doped BiOCl:	Silver doped bismuth oxychloride
AgO:	Silver Oxide
Ag_2S:	Silver sulfide
NaOH:	Sodium hydroxide
SPR:	Surface Plasmonic Resonance
H_2O_2:	Superhydroxyl peroxide
O^-_2:	Superoxide
O^{2-}:	Superoxide ion
SO^-_4:	Sulphate radical
TTIP:	Tetraisopropoxide
Th-ZnO:	Thorium zinc oxide
SnO_2:	Tin dioxide (stannic oxide)
TiO_2:	Titanium dioxide
TiOH:	Titanium hydroxide
$TiOH_2^+$:	Titanium hydroxide
Ti^{4+}:	Titanium (iv) ion or titanic ion
TiO^-:	Titanium (II) oxide
TEM:	Transmission electron microscope
W:	Tungsten
2,4,6-TCP:	2,4,6 Trichlorophenol
UVC:	Ultraviolet light
UV:	Ultra-violet
US EPA:	US Environment Protection Agency
WO_3:	Tungsten (VI) oxide
VB:	Valence band
V dopedTiO_2:	Vanadium doped Titanium dioxide
H_2O:	Water
WHO:	World Health Organisation
XRD:	*X*-ray diffraction
Zn $(CH_3COO)_2 2H_2O$:	Zinc acetate dehydrate
$Zn(OH)_2$:	Zinc hydroxide
Zn $(NO_3)_2.6H_2O$:	Zinc nitrate hexahydrate
ZnO:	Zinc Oxide
ZnS:	Zinc Sulfide

Chapter 1: Introduction

1.1 Introduction

It has been reported that the world may face a 40% water shortage by 2030 and this will affect at least 1.80 billion people (HPLW, 2017). For instance, water demand in South Africa will increase by 1% each year from 15-billion cubic meters a year in 2016 to 18 billion cubic meters in 2030. “This is equal to 17% supply deficit (HPLW, 2017). Water quality is a crucial resource for human life and the entire earth’s ecology. One of the greatest challenges with water is pollution (Water, 2017). Water pollution is any undesirable change in water purity and quality caused by the introduction of harmful substances. For the World Health Organization (WHO) (1997), the term ‘water pollution’ is defined as any change in the physical, chemical and biological properties of water that has a harmful effect on living things (Helmer et al., 1997).

Developed countries such as China, Australia, Italy, United States of America, India, Japan, Germany, Indonesia, and Brazil are listed amongst the highest water polluted countries in the world because of urbanization and the use of several chemical products (All-About-Water-Filters, 2019). South Africa, a semi-arid country, with a low chance of rainfall each year is faced by growing water pollution as in the rest of Africa. In South Africa, pollution leads to high priority problems because of the relative scarcity of water. Urbanization contributes to the deterioration of water quality in water sources (lakes, rivers and streams) in urban centres (Moyo and Phiri, 2002).

Pollution has several sources such as growth of the population, deforestation, damming of rivers, destruction of wetlands, industry, mining, agriculture and energy use. In the past, water pollution was linked to the energy industry. It has been stated that around 450 tons of organic waste is produced annually in South Africa (Heath et al., 2009). Recently, population growth and the industrial development have been identified as the major contributory factors to South Africa’s water pollution (Musingafi, 2014). Waste water is discharged by industries and domestic activities into rivers, lakes and ending up in oceans contain chemicals such as dyes, pesticides and herbicides, as well as biological pollutants (bacteria and viruses).Conventional treatment methods such as flocculation, activated carbon adsorption and filtration have been applied to clean polluted water.

However, these methods are expensive and not very efficient (Mohamed, 2011; Oturan and Aaron, 2014; Krishnan et al., 2017).Advanced oxidative process (AOP) is a new efficient technique for non-biodegradable pollutants compared to biological process (Gnanaprakasam et al., 2015). The AOP uses stronger oxidants than molecular oxygen such as ozone and especially $OH^{\cdot}$ radicals, generated either by UV light, ultrasound and/or catalyst in the degradation of organic pollutants (Vora et al., 2009). The use of a semiconductor in the AOP process is based on the generation of electron–hole pair by photo-activation of the semiconductor's material. In the presence of a catalyst, low energy ultraviolet rays may be utilized for degradation of recalcitrant wastewater pollutants by using photo-generated positives holes and electrons as powerful oxidants and good reductant, respectively (Bamuza-Pemu, 2014).

Amongst the different semiconductors TiO_2 (3.2eV), ZnO (3.3eV) and ZnS (3.66eV) nanoparticles attracted attention due to their different potential applications in different areas, such as catalysis, biomedical, sensors, electrical, and electronics (Ibhadon and Fitzpatrick, 2013). Heterogeneous semiconductors have attracted much attention recently because of their low toxicity, low cost, optical, chemical, electrical properties, and environmentally friendly characteristics which make them suitable photocatalysts in the photocatalytic process. Their rapid rate recombination photogenerated electron-hole pair is one of the disadvantages (Ibhadon and Fitzpatrick, 2013).

Doping is the introduction of an impurity into the lattice of a pure material. During the past decade the introduction of impurities into semiconductor materials has been studied by researchers for the purpose of regulating their properties. Multiple elements from the periodic table have been used as dopant ions into the range of semiconductor nanoparticles and the results showed an improvement of their properties compared to the pure semiconductors nanoparticles (Hosseini et al., 2015; Munir et al., 2019). However, the incorporation of Ag can bring new properties to the semiconductor and improve their photocatalytic activity by reducing the rapid recombination of electron-hole (e^-/h^+) pair which will make the nano-semiconductor suitable for the degradation of persistent organic pollutants (Boxi and Paria, 2014).

This study will focus on the use of a semiconductor photocatalyst doped with silver for the elimination of a phenolic derivative compound.

1.2. Problem Statement

Phenolic compounds and its derivatives are ubiquitous contaminants in the environment. Their discharge to the environment causes serious problems such as odour, change of taste, and water turbidity. Among them, chlorinated phenols known as chlorophenols are an important class of aromatic pollutants in industrial wastewater. They enter the environment via industrial activities such as chemical and pharmaceutical waste deposits. For instance, 2-chlorophenol, one of chlorinated compounds released to the environment is an intermediate product in the production of phenoxy herbicides (or phenoxies) and it is employed by municipalities for water disinfection. The ingestion of drinking water and fish contaminated with 2-chlorophenol threatens human health. 2-cholrophenol is a significant pollutant threat in the environment due to its toxicity, carcinogenicity, poor biodegradability, even at low concentrations. Its removal from water has become a big challenge to researchers (Ku et al., 2010; Taleb, 2014; Rashid et al., 2015a).

In the removal of 2-chlorophenol from water, photocatalytic processes assisted by semiconductor nano-photocatalysts (TiO_2, ZnO, and ZnS) has gained significant attention over conventional techniques. The TiO_2, ZnO, and ZnS semiconductor nanoparticles are mainly used due to their light induced free radical catalytic degradation of 2-chlorophenol. The photocatalytic applications of semiconductor nano-photocatalysts under UV irradiation light rely on their band gap, crystallinity, surface area and electrons-holes recombination. The development of less expensive and efficient photocatalysts for the complete or partial mineralization of recalcitrant organic pollutants by turning them to CO_2 and H_2O is still a problem for the industries (Babu and Khadar, 2011; Boxi and Paria, 2014; Bechambi et al., 2015).

1.3. Aim

The aim of this research is to determine the photocatalytic activity of undoped and silver doped TiO_2, ZnO and ZnS nanoparticles for the degradation of 2-chlorophenol under UV irradiation.

1.4. Objectives

The objectives of this research are:

1. To synthesize TiO_2, ZnO and ZnS nanoparticles

2. To synthesize doped TiO_2, ZnO and ZnS with different percentages (1, 3 and 5 %) of Ag nanoparticles.

3. To characterize the nanoparticles using, Ultra-violet visible spectroscopy (*UV*-Vis), Photoluminescence spectra (PL), *X*-ray diffraction (XRD), Fourier transform infrared (FTIR) and Transmission electron microscopy (TEM).

4. To assess the synthesized nanoparticles for the photocatalytic degradation of 2-chlorophenol under UV irradiation.

5. To investigate various operating variables such as effect of pH, catalyst concentration and pollutant concentration on the catalyst photo activity efficiency.

Chapter 2: Literature Review

2.1. Background

Pollution of drinking water sources by chemical substances is a major challenge due to the diverse sources of pollutants; industrial and municipal wastewater as well as agricultural sources. Pollution has an adverse effect on humans, the ecosystem and may lead to production of toxins, bad taste and odour in water (Bamuza-Pemu, 2014). Some of these compounds are endocrine disrupting compounds (Bisphenol A, 2-chlorophenol, 2,4-dichlorophenol, 2,3,4,6-tetrachloropheno etc) and pose potential threat on human and animal health (Choquette-Labbé et al., 2014).The increasing levels of organic pollutants originating from autogenic sources such as pesticides, aromatic compounds from industrial effluent, or pharmaceuticals have been detected in water sources. There is a need to enhance the drinking water treatment technologies to meet safety requirements and to mitigate the presence of unwanted pollutants. A new technology called advanced oxidation process has been judged to be the best method for the removal of these resistant and recalcitrant pollutants (Gupta et al., 2012).

2.2. Chlorophenols

Chlorophenols (CP_s) are poorly biodegradable with a half-life that can exceed 10 years in organic sediments. Over 166 chlorinated phenol compounds are on the list of 14667 national priority pollutant and 6 of them (2-CP, 4-CP, 2,4-DCP, 2,4,6- TCP and PCP) have been named by the US Environmental Protection Agency (US EPA) as priority pollutants in water pollution (Callahan et al., 1979; Zhu and Shan, 2009; Zhu et al., 2011). Other groups of chlorinated phenolic compound such as 2,4,5-Trichlorophenol, 2,3,4,6-Tetrachlorophenol (TTC) have been classified as 2B group environmental carcinogens by the International Association for Research on Cancer (Czaplicka, 2004).

2.2.1. 2-Chlorophenol

The compound 2-chlorophenol is also known as ortho-chlorophenol or 2-choro-1-hydroxybenzene. The molecular formula is C_6H_4ClOH and the structure shown in Figure 2.1. 2-chlorophenol is formed by a reaction between chlorine molecule and phenol in a presence of an acidic catalyst. It is a colorless to yellow-brown liquid, toxic with an unpleasant, repulsive odour, and has a pKa = 8.5 at 25℃ (Zorba, 2015).

The C-Cl bond in the 2-chlorophenol compound is highly stable and it is responsible for its toxicity and persistence in biological environments (Rao et al., 2003b). It is introduced into the aquatic environment by the effluents discharged of several industries such as pharmaceutical, dyestuff, textiles, plastics, petroleum as well as from effluents when it is used as an intermediate product for the production of large synthetic molecules (Zorba, 2015). In addition, it also enters water during the purification process via the use of chlorine (Rao et al., 2003b). Kool et al. (1982) and Lucas and Kopfler (1984) qualitatively identified the presence of 2-chlorophenol in drinking water in United States. In Australia, 2-chlorophenol was found in ground water samples collected near a chemical manufacturing plant (Stepan et al., 1981). People consuming 2-chlorophenol contaminated water above its standard exposure limit (0.2 – 0.5 µg/L) may develop defects such as lung, liver, and kidney damage, and in some cases death (Zorba, 2015).

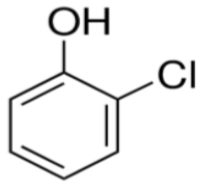

Figure 2. 1: 2-chlorophenol structure (Zorba, 2015)

It has been observed that water containing more 200 mg/L of 2-CP cannot be treated by biological methods (Rao et al., 2003a). However, the advanced oxidation process has been promoted or judged as an appropriate technique for a complete oxidation of resistant and toxic organic compounds to harmless products such as CO_2 and H_2O (Ba-Abbad et al., 2017).

2.3. Advanced Oxidation Method

In the 1980s, an advanced oxidative process (AOPs) was proposed for potable water treatment. Since then, AOPs have been proposed for the treatment of various wastewaters due to their ability to degrade recalcitrant organic and inorganic pollutants in wastewater (Deng and Zhao, 2015). The advanced oxidation process involves the generation of hydroxyl radicals ($OH^{\bullet}$) in sufficient quantity for water purification. Some recently advanced oxidative processes have used sulphate radicals ($SO_4^{\bullet-}$).

Contrary to the functioning of common oxidants such as chlorine and ozone that play double role of decontamination and disinfection, AOPs are applied for the destruction of organic pollutants in wastewater for the complete oxidation and mineralization to CO_2 and H_2O (Zhou and Smith, 2002; Augugliaro et al., 2006; Deng and Zhao, 2015). Advanced oxidation processes may be used in combination with chemical and/or physical agents; for example, combination of oxidizing agents with UV, catalyst or ultrasound and a catalyst plus ultraviolet (Choquette-Labbé et al., 2014).

These advanced oxidation processes can be grouped into different classes such as (i) the photolytic system (use only UV irradiation), (ii) the photochemical system (combination of UV and chemical oxidation), and (iii) physical system (photocatalysis and cavitation).

Advance oxidative processes use reactive oxygen species as the principal oxidizing agent. The use of external sources such as ultraviolet radiation (UV) or solar light makes AOPs (Ibhadon and Fitzpatrick, 2013) more expensive than biological wastewater treatment. The AOPs have certain advantages and disadvantages as described below.

Advantages

i. Destroys toxic organic compounds without transferring them into another phase
ii. Works for air and water disinfection
iii. Adaptable in small scales

Disadvantages

i. Relatively high operation cost due to chemical or energy input
ii. Formation of oxidation intermediates potentially more toxic

Several methods are classifieds under the broad definition on AOPs and these may be grouped into non-photochemical and photochemical driven methods (Table 1).

Table 1: List of some AOPs

Process occur in Darkness	Light driven AOPs
Ozone (O_3)	**Photolysis (UV + H_2O_2)**
Fenton (Fe^{2+} + H_2O_2)	**Photocatalysis (light + catalyst)**
Electrolysis (electrodes + current)	**Photo- Fenton (Solar lights + Fenton)**
Sonolysis (ultrasounds)	**Hydrogen peroxide and ozone ($UV/O_3/H_2O_2$)**

2.3.1. Advanced Oxidation Process Mechanism

Advanced oxidation process involves several steps.

i. Formation of strong oxidants (e.g. $OH^{\bullet}$)
ii. Reaction of oxidant with organic compounds in water producing biodegradable intermediates
iii. Reaction of biodegradable intermediates with oxidants referred to as mineralization (i.e. production of water (H_2O) + carbon dioxide (CO_2) and inorganic salts.

2.3.2. $OH^{\cdot}$ radicals – based advanced oxidative process

The hydroxyl radicals ($OH^{\bullet}$) are reactive and strong oxidizing agents in water treatment with a potential oxidation of between 2.8 V and 1.95 V for pH = 0 and at pH = 14 vs SCE (saturated calomel electrode used commonly as a reference electrode) (Metcalf et al., 2003; Deng and Zhao, 2015).

They are non-selective and react rapidly with organic pollutant species with a constant rate between 10^8-$10^9 ms^{-1}$. The hydroxyl radical attacks organic pollutants using one of four ways: hydrogen abstraction, radical addition, electron transfer and radical recombination. Any of these results in carbon-center radicals with the organic pollutants and the carbon-centre reacts with O_2 to produce reactive species such as H_2O_2 (hydrogen peroxide) and O^{-}_2 (superoxide) which is known as the more reactive species compared to $OH^{\cdot}$ for chemical degradation and mineralization of organic pollutants (Deng and Zhao, 2015).

A summary of $OH^{\cdot}$ generation mechanisms of major AOPs for wastewater treatment are depicted below:

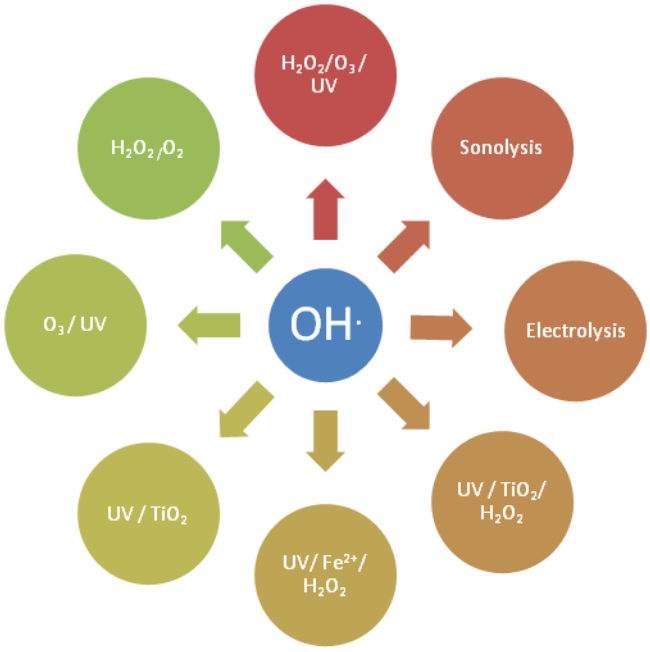

Figure 2.2: Main advanced oxidation processes (AOPs)

Photochemical oxidation processes based on UV can be classified in two groups: homogeneous photooxidation and heterogeneous photocatalysis which rely on different mechanisms of $OH^{\cdot}$ generation (Gupta et al., 2012).

2.3.3. Homogeneous Photo Oxidation

Homogeneous photodegradation applications in the treatment of contaminated water use an oxidant to generate radicals that attack the organic pollutants to initiate oxidation. Several photochemical methods (Figure 2.2) may be used in a homogeneous solution such as: (i) Hydrogen peroxide (UV/H_2O_2), (ii) Ozone (UV/O_3), (iii) Photo- Fenton system (Fe^{3+}/H_2O_2) and (iv) Hydrogen peroxide and ozone ($UV/O_3/H_2O_2$); This combination increases the rate of oxidative degradation (Sunder and Hempel, 1997; Safarzadeh-Amiri, 2001).

The majority of AOPs listed in Figure 2.2involves the use of hydrogen peroxide as oxidizing agents. The oxidizing strength of H_2O_2 alone has been observed to be weak in the absence of UV light. The light improves the rate and the strength of oxidation for the production of enough $OH^{\cdot}$. The H_2O_2 can also be used to improve other AOPs if it is added at low concentrations, as the molecule splits in two hydroxyl radicals (Deng and Zhao, 2015).

Table 2: List of homogeneous photo-oxidation (Mohamed, 2011)

Methods	Reaction	Disadvantages
UV /O_3	$O_3 + H_2O + hv \longrightarrow O_3 + H_2O_2$ $O_3 + H_2O_2 \longrightarrow OH^{\cdot} + 2HO_2^{\cdot} + O_2$	pH dependence Absorb λ ‹ 300 nm, a lesser component in solar radiation. Continuous supplies of feed chemicals are required
UV/H_2O_2	$H_2O_2 + hv \longrightarrow 2HO^{\cdot}$	Absorb λ ‹ 300 nm, a lesser component in solar radiation. pH dependence Continuous supply of feed chemicals is required
UV/H_2O_2/O_3	$O_3 + H_2O \longrightarrow OH^{\cdot} + 2HO_2^{\cdot} + O_2$	Absorb λ ‹ 300 nm, a lesser component in solar radiation. Applicable over a wider pH range.
Fe^{3+}/H_2O_2	$H_2O_2 + Fe^{2+} \longrightarrow Fe^{3+} + {\cdot}OH + OH^-$ $Fe^{3+} + H_2O + hv \longrightarrow Fe^{2+} + {\cdot}OH + H^+$	Sludge disposal problem during the process Process is expensive

2.3.4. Heterogeneous Photocatalysis

Heterogeneous photocatalysis with the use of UV or visible light illumination on the surface of a semiconductor has been applied mainly and recognized to be efficient for water and air purification (Pera-Titus et al., 2004; Mahmoodi et al., 2006; Fujishima et al., 2007; Wang et al., 2009). Heterogeneous photocatalyst implies the presence of reactants and photocatalyst in two or more phases. The principle of the photocatalysis is a photoexcitation of a semiconductor solid which results in the absorption of radiation but not in the near ultraviolet spectrum (Mohammadi et al., 2011).

It has many advantages compared to other processes such as (i) complete mineralization, (ii) no waste disposal problem, (iii) low cost, and (iv) uses mild temperature and pressure conditions (Fujishima et al., 2007).

A good semiconductor material near UV irradiation may be excited by high energy photons equal to its band gap to produce electrons in the conduction band and in the valence band holes. These charge carriers are able to produce reduction or oxidation that can react with water and organic pollutants (Mohamed, 2011). The positive holes left in the valence band are oxidative and can react with hydroxyl ions to form hydroxyl radicals (Mills and McFarlane, 2007; Gaya and Abdullah, 2008).

2.3.4.1. Semiconductors Photocatalysis

Recently, the use of semiconductors in the photocatalysis process has attracted much attention in the resolution of environmental problems. Semiconductor photocatalysts are substances which accelerates a chemical reaction by absorption of light which can be solar light, UV light, visible light etc (Kaur, 2010; Gupta et al., 2012; Ibhadon and Fitzpatrick, 2013).

A semiconductor is a solid material which has electrical conductivity between that of a conductor and insulator. An example is shown in Figure 2.3. In a semiconductor electronic structure characterized by a filled valence band and empty conduction band, the energy difference between the valence and conduction band is called the band gap energy (E_g) (Linsebigler et al., 1995). When the surface of the semiconductor is irradiated with a photon which has an energy equal or greater to its band gap, electrons seated at the valence band are excited and move to the conduction band by leaving the holes in the valence band (Fox and Dulay, 1993; Linsebigler et al., 1995; Hoffmann et al., 1995; Bahnemann, 2004; Mohamed, 2011).

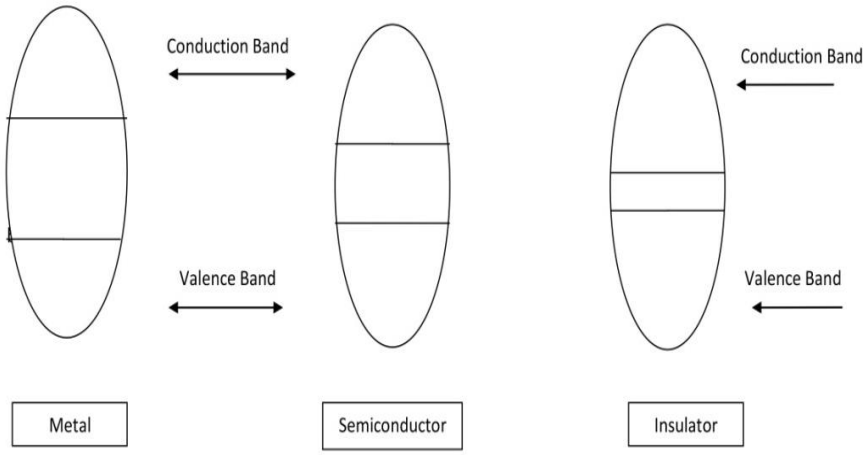

Figure 2.3: Band gap comparison (Mohamed, 2011)

Semiconductor photocatalysts over other chemical oxidation methods are more effective due to some advantages such as being inexpensive and can mineralize different organic compounds. Based on the literature, semiconductors such as TiO_2, WO_3, Fe_2O_3, ZnO, and metal chalcogenides CdS and ZnS which have photocatalytic properties (Salem et al., 2003; Rodríguez and Fernández-García, 2007) have been used as photocatalysts. Table 3 shows some common semiconductors employed as photocatalysts, their band gap energies and absorption wavelength.

Table 3: Band gap energy and absorption wavelength of commonly used semiconductors (Stumm, 1992)

Semiconductor	**Eb_g (eV)**	**λ (nm)**
Fe_2O_3	2.3	539
TiO_2 (rutile)	3.0	413
TiO_2 (anatase)	3.2	388
WO_3	2.8	443
ZnO	3.2	388
CdS	2.42	512
ZnS	3.6	344

Recently, research in photocatalysis has focused on better understanding of the oxidative degradation principles of organic pollutants in the aqueous phase. The use of semiconductor photocatalysts for pollutant reduction in water and air has been attractive owing to their unique advantage over conventional treatment methods as it presents a "green treatment" approach with a complete mineralization of organic pollutants into CO_2 and H_2O using photonic energy (Rao et al., 2003a; Zhao and Yang, 2003; Herrmann et al., 2007)

Researchers struggled to find an appropriate semiconductor photocatalyst in the field of photocatalysis due to specifc requirements. A good photocatalyst must have an energy band gap higher or equal to 2.4 eV, be photostable, chemically and biologically inert, easy to be formed and highly photoactive.

However, amongst the semiconductors used, TiO_2has been proven to be the most suitable and efficient for the removal of organic pollutants in water (Fernández et al., 2004; Sim et al., 2005). Mills et al. (1993), Gogate and Pandit (2004), Malato et al. (2007) used titanium dioxide because of its chemical, biological inertness and stability with respect to photocorrosion, non-carcinogenicity, non-toxicity, low cost and its anatase phase has the best catalytic performance and degradation efficiency.

2.3.4.2. Photocatalysis

Photocatalysis results in the modification of the rate of a photoreaction by using a light source. It is a chemical reaction which involves firstly a catalysed photolysis where the light is absorbed by the substrate and secondly a photogenerated catalysis where the photocatalytic activity depends on the ability of the catalyst to create electron-hole pairs, which generate reactive radicals (mainly hydroxyl radicals ($OH^{\bullet}$)) (Kaur, 2010).

2.3.4.2.1. Principle and Mechanisms of Photocatalysis

The photocatalysis principle is simple and may follow two simultaneous reactions: oxidation from the photogeneration hole and reduction from the photogenerated electron (Saravanan et al., 2017). The full explanation of photocatalytic degradation of organic pollutant by a semiconductor photocatalyst has been reviewed by several authors (Kaur, 2010; Zorba, 2015;Gnanaprakasam et al., 2015; Saravanan et al., 2017). Figure 2.4 shows the schematic representation of the semiconductor photocatalytic mechanism.

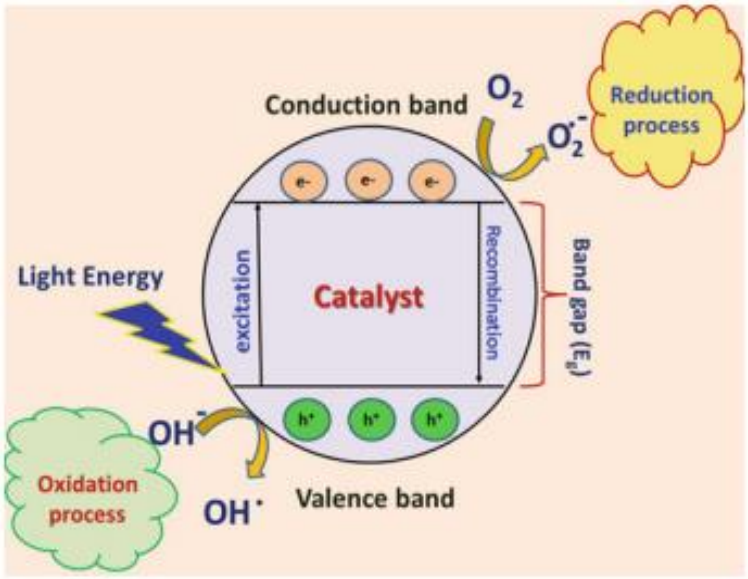

Figure 2.4: Schematic representation of semiconductor photocatalytic mechanism (Saravanan et al., 2017)

The surface of the photocatalyst is illuminated by a photon which has energy equal to or higher than the band gap energy (E_{bg}) of the catalyst. When the photon is absorbed it creates a charge separation due to promotion of electrons from the valence band of the semiconductor catalyst to the conduction band by leaving holes in the valence band. However, this hole in the valence band can react with a molecule of water to produce hydroxyl radicals which can degrade the organic pollutant.

On the other hand, electrons seated in the conduction band can also react with different species present in the solution such as oxygen absorbed on the photocatalyst surface or/with the dissolve O_2 to give superoxides radicals ($O_2^{\bullet-}$); then the superoxide radicals can react with molecules of water (H_2O) to produce hydroperoxy radicals ($HO_2^{\bullet}$) and hydroxyl radicals ($OH^{\bullet}$) known as the strong oxidizing agents for the decomposition of organic pollutants. Finally, hydroxyl radicals ($OH^{\bullet}$) will oxidize the organic molecule to carbon dioxide and water. In the meantime, the electron-hole pair recombination can take place and this reduces the photocatalytic activity of the photocatalyst (Saravanan et al., 2017).

There are several organic pollutants treated by photocatalysis degradation using different semiconductor photocatalysis. Ku et al. (1996) investigated the decomposition of 2-chloropbenol in aqueous solution by UV/TiO_2 oxidation process under various solution pH values, light intensities and types of TiO_2. The removal of 2-chlorophenol was highly dependent on solution pH. The highest percentage degradation was obtained at an adequate catalyst dosage. Priya and Madras (2006) investigated the photocatalytic degradation of nitrobenzene with synthesized nano-TiO_2 and P 25 under UV irradiation. The photocatalytic degradation followed the pseudo-first-order kinetics and the highest degradation was obtained with nano-TiO_2 compared to P 25. Chiou et al. (2008a) studied the degradation of phenol under UV irradiation TiO_2.They observed that the degradation of phenol increased with UV/TiO_2 compared to the commercial TiO_2. An addition of H_2O_2 improves the degradation efficiency of phenol. On the other hand the degradation of 2,4- dichlorophenol under UV irradiation was investigated by Gaya et al. (2010) using ZnO nanoparticles. Parameters such as pollutant concentration, pH, and catalyst dosage were investigated. A higher degradation was obtained with a catalyst dosage of 1.5 g l^{-1} with 50 ppm of 2, 4- dichlorophenol. Benhebal et al. (2013) investigated the photocatalytic degradation of phenol and benzoic acid under UV irradiation. Key parameters such as pH, catalyst dosage, and pollutant concentration were investigated. A maximum degradation of 69.75% for phenol and 67.98% for benzoic acid was obtained after 120 min.

2.4. Doping

Doping is the combination of pure nanoparticles with a dopant to obtain the doped nanomaterial. Dopant materials can improve the efficiency of the photocatalyst in multiple ways by: bringing a change on the band gap of the semiconductor (Sathishkumar et al., 2013), forming a level of impurity (Cao et al., 2013), creating oxygen vacancies (Wu et al., 2010), giving unique surface area for the adsorption of organic molecules and acting as an electron trapper (Barakat et al., 2014). There are two ways of doping, interstitial and substitutional. In the interstitial way, the radius of the doped ion is smaller than the radius of the lattice ions or lattice space which allows the crystal cell of the metal oxide surface to be pierced by the doped ion. On the other hand, substitutional doping occurs when the dopant replaces the lattice ion or lattice oxide (Cao et al., 2013).

Moreover it has been noticed that a doped ion incorporated into the catalyst crystal lattice can modify the electronic property of the synthesized nanocatalyst and enhance its adsorption in the visible region (Tian et al., 2008; Pouretedal et al., 2009a;Tian et al., 2009; Cao et al., 2013).

Semiconductor materials such as nanoscale metal oxides and chalcogenides have been investigated due to their various shapes (spherical, cubic, hexagonal, triangle, square etc.), properties and applications (photocatalysis, photoluminescence, sensors, antimicrobial and more). Researchers sought to improve the semiconductor materials via incorporation of dopant materials. Doping may be carried out using one or more dopant ions (co-dopant) (Boxi and Paria, 2014).

The effect of doping on a photocatalyst activity is determined by a number of factors: initial concentration of pollutants, physico-chemicals properties of the catalyst, type and concentration of the dopant. If the dopant concentration is higher than the optimum concentration of doping value, the photocatalytic activity decreases. This results in the decrease of surface area of the catalyst and narrows the space charge region and the penetration of radiation light on the photocatalyst surface which may be more than the space layer. Thus, the recombination of electron hole pairs will happen easily (Xu et al., 2002; Gnanaprakasam et al., 2015).

Doped materials can behave as an electron-hole pair recombinator when the distance between the trap sites is reduced with the increase of doping particle concentration and leads to decrease in the photocatalytic activity of a nanocatalyst (Chen et al., 2008). A semiconductor can be doped with a transition, non-metal, metal, alkaline earth metal or a noble metal. The use of noble metals such as Ag, Pt and Au as doping agents has attracted attention due to their capacity to scavenge photogenerated electrons and to promote electron hole pair separation in the photocatalysis process, thereby enhancing the photocatalytic activity of the semiconductor (Awazu et al., 2008; Yu et al., 2010) and finally by improving the adsorption of organic pollutants on the phototocatalyst surface (Kumar et al., 2010). The choice of silver nanoparticles as a dopant has become attractive amongst the other noble metals due to its catalytic activity, size, shape-dependent optical properties, as well as its promising use in chemical and biological sensing in surface enhanced Raman scattering (SERS) and metal fluorescence (MEF), localized surface Plasmon resonance (LSPR) and its antibacterial activity (Bechambi et al., 2015). In addition, silver is one of the cheapest noble metals.

2.4.1. Metal Oxide Semiconductors

Metal oxides such as TiO_2, PbO, ZnO, CdO, Fe_2O_2 and CeO_2have been studied in several photocatalysis applications. However, amongst the metal oxide semiconductors applied in photocatalysis, TiO_2 and ZnO have proven to be the most suitable for environmental purposes such as water treatment (Gnanaprakasam et al., 2015). Thus, these two shall be discussed below.

2.4.1.1. Titanium Dioxide

Titanium dioxide (TiO_2) exists in three different polymorphs in nature, namely, anatase phase (tetragonal), rutile phase (tetragonal) and brookite phase (orthorhombic) (Bakardjieva et al., 2006). Amongst these phases, anatase and rutile phases are widely used in photocatalysis as compared to brookite which is not photoactive. Both phases have the same crystal structure but differ in their distortion of each octahedron and by assembly patterns of their octahedral chains. In addition, the difference in the lattice structure is based on their density (Ullattil and Periyat, 2017). The structure of TiO_2 in the three phases are shown in Figure 2.5.

The anatase conduction band is 0.2 eV higher than that of rutile (Kawahara et al., 2002). Their photocatalytic efficiency is brought about by their band gap differences (3.2-3.3 eV for anatase and 3.0 - 3.1 eV for rutile).

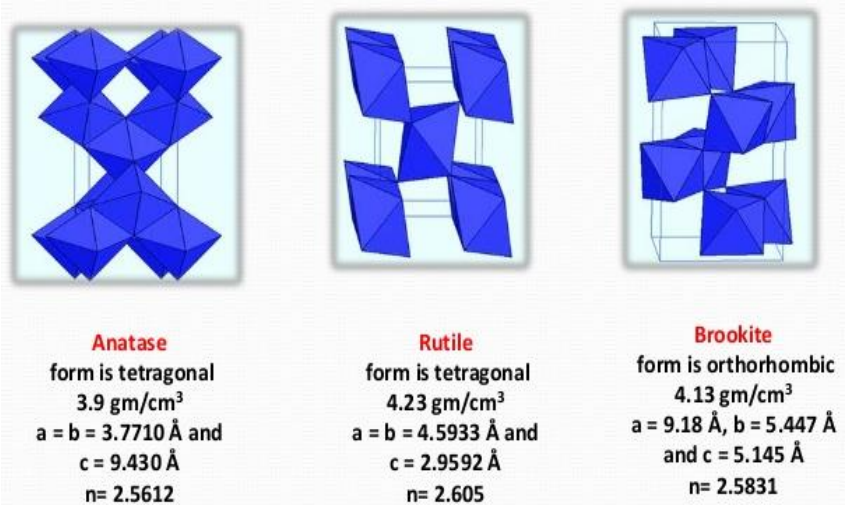

Figure 2.5 : Crystal structures of TiO_2 (Sankar and Gopchandran, 2009)

TiO_2 has been judged as an excellent semiconductor photocatalyst due to its low cost, non-toxicity, chemical stability and ability to possess high photocatalytic activity (Elsalamony and Mahmoud, 2017). Its wide band gap (3.2 eV for anatase and 3.06 eV for rutile) makes it to use just 5% of the solar spectrum. Moreover, the pure TiO_2 has a high rate of recombination of electrons-holes. It has been reported that the photocatalytic efficiency of TiO_2can affect its morphological and structural characteristics (Linsebigler et al., 1995). However, to overcome these limitations, researchers came up with a novel approach by doping semiconductors with metals or metal oxides. This approach has double effects:

i. To reduce the catalyst band gap, increasing the wavelength range of the semiconductor and thus shifting it into the visible region.
ii. To delay the rapid electron-hole pairs recombination by increasing the charge trapping.

Doping TiO_2 with a noble-metal such as Ag improves its photocatalytic activity by reducing the rapid recombination rate of photogenerated electron-hole pairsand in some cases, increases the adsorption surface area. In some studies, Ag doped TiO_2 has been found to enhance its antibacterial activity (Boxi and Paria, 2014).

Ilyas et al. (2011) reported on the photocatalytic degradation of nitro-and chloro-phenols using doped and undoped titanium dioxide nanoparticles. The study showed that higher percentage degradation was obtained for both groups of pollutants in the range of 83 and 96 - 99%, respectively by doping Ag with TiO_2. Cao et al. (2008) studied the preparation of Ag doped TiO_2 nanoparticles for photocatalytic degradation of acetamiprid in water; according to the results Ag added to TiO_2 nanoparticles improved its photocatalytic activity and the photocatalytic degradation of acetamiprid.

Several methods have been reported for the synthesis of Ag-TiO_2 nanoparticles. These include Liquid Impregnation (LI) (Ilyas et al., 2011), photodeposition (Parastar et al., 2013, Kumar et al., 2015), solvothermal method (Wu et al., 2012) and sol-gel (Saravanan et al., 2018, Nainani et al., 2012, Cao et al., 2008).

2.4.1.2. Zinc Oxide

Zinc Oxide (ZnO) is a versatile semiconductor of II-VI group with a wide band gap of 3.37 eV, and large excitonic binding energy of 60 meV at room temperature (Shah et al., 2014). ZnO exists in nature in two forms, wurtzite and blende (Figure 2.6). ZnO nanocrystalline material has attracted a great interest for its unique optical, chemical and electronic properties and potential applications in several fields including: light emitting diodes, solar cells, transparent electronics, chemical sensor and spintronics (Nomura et al., 2003; Pearton et al., 2004). All of these make it an ideal nanocrystalline material in the field of nanotechnology (Chauhan et al., 2010).

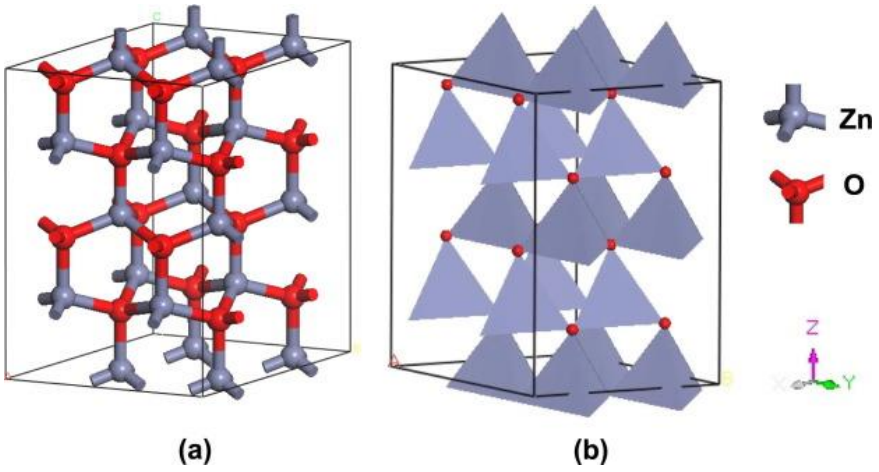

Figure 2.6: ZnO crystal structures: a) blende, b) wurtzite (Mohamad et al., 2017)

The semiconductor ZnO has widely attracted researchers due to its low cost, high chemical stability, and mass production. In addition, ZnO has won much attention in the photocatalytic degradation process and mineralization of pollutants in the environments. It absorbs more light quanta, generates high oxidizing power holes, highly efficient photocatalysis in acid and basic medium and attracts an extensive variety of solar powered light range compared to other oxide semiconductors (Jang et al., 2010; Wu et al., 2010). However, due to its high surface activity, crystalline nature, morphological features, and texture, ZnO nanoparticles are considered as the most favorable catalyst for the degradation of organic pollutants. The high recombination rate electron-hole pair is one of the problems of ZnO because it reduces the degradation efficiency of organic pollutants (Yıldırım et al., 2013).

In order to solve these limitations, the combination of a transition metal doping or a deposition of noble metal such as Ag to the semiconductor catalyst was found to improve the photocatalytic activity efficiency of synthesized nanoparticles, surface defects and the optical properties of ZnO (Bechambi et al., 2015).

Further, doping ZnO with Ag can also delay or avoid the fast recombination of e^-/h^+ pairs produce during light illumination. This allows the hole to migrate along the catalyst surface for oxidizing the absorbed organic molecules (Chen et al., 2004). Recent investigations have been done for photocatalytic application using ZnO modified with metal ion such as palladium, gold, Cu and Ag (Singh et al., 2017).

2.4.2. Chalcogenides Semiconductors

Compounds consisting of at least one chalcogen atom (selenides, tellurides, sulfides) and one of electropositive element such as CdS, ZnS, CdSe, WS_2, WoS_2 and ZnSe have attracted great attention in recent years. Their shape, size and optical properties makes them suitable for multiple applications such as electroluminescence devices, gas sensor, laser, infrared detectors, photocatalysis and more (Boxi and Paria, 2014).

Zinc sulphide (ZnS) is one of the chalcogenides that has been investigated in photocatalysis application due to its remarkable properties compared to other metal sulfides. A zinc sulphide (ZnS) semiconductor has a band gap of 3.6 eV and large exciton-binding energy (∼40 meV) (Boxi and Paria, 2014). It exists in two different phases: cubic phase (Blende) or spherical and hexagonal phase (Wurtzite) with a band gap of 3.66 eV and 3.67 eV at room temperature, respectively. Their structures are shown in Figure 2.7. ZnS cubic phase has been determined as the most stable phase in the bulk and can be transformed in wurtzite phase at temperature 1020℃. The both polymorphs are used in industrial applications (Ramasamy et al., 2012).

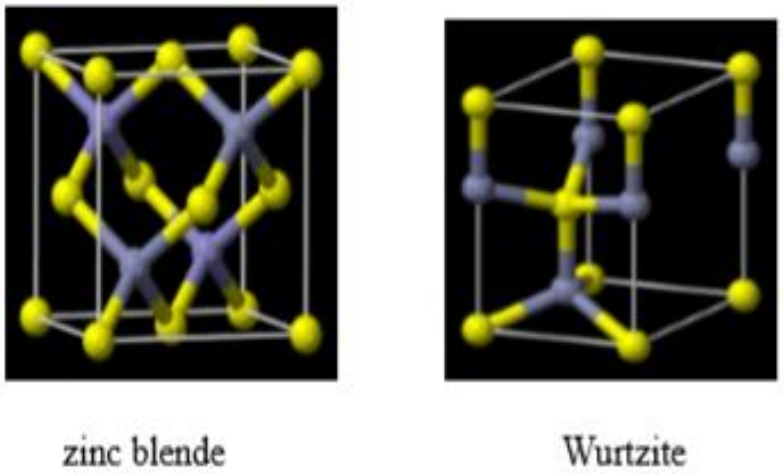

Figure 2.7: ZnS crystal structures (Kaur, 2010)

Zinc sulphide (ZnS) is the only chalcogenide which can behave as n-type and p-type semiconductor contrary to other II-VI semiconductors. ZnS nanoparticles attracted attention due to their unique properties compared to the bulk material, their quantum size effect and surface defect (Ramasamy et al., 2012). In addition, ZnS is interesting due to properties such as the polar surface, good thermal stability and high electronic mobility. As a result, it has used in many applications such as light-emitting devices, anti-reflecting coatings, and bio-electronics, photoluminescence and photoconductor (Sivakumar et al., 2014).

Most of the studies on nanoparticles have focused in its luminescence application such as photoluminescence (PL), electroluminescence (EL) and cathodoluminescence (CL).However its photoluminescence properties allow it to have fluorescence emission in the UV region, but the emission can be done in the visible region by adding a suitable doping ion. In this case the dopant acts as recombination centres for the excited electron-hole pairs and a strong luminescence in visible region can take place (Ramasamy et al., 2012).

ZnS nanostructures have been widely proposed by researchers in photocatalytic application to resolve wastewater problems caused by organic pollutants discarded by industry and municipality because of their unique properties, such as high chemical stability, non-toxicity, surface polarity, high electronic mobility, good thermal stability and being environmentally friendly (Viswanath et al., 2014). It is also a good photocatalyst due to its rapid generation of e^-/h^+ pair and highly negative reduction potential of excited electrons (Madkour and Al Sagheer, 2017).

In addition to this, ZnS has attracted attention due to its photocatalytic properties which does not occur only in the photoreductive phase by involving the formation of H_2 from water and photoreduction of CO_2 but also in phototransformation of organic pollutants (Kaur, 2010; Abbasi et al., 2017). However, its large band gap, rapid rate of oxidation and reduction in the photocatalytic activity limits its practical application in photocatalysis (Madkour and Al Sagheer, 2017).

In order to improve its photocatalytic efficiency, the problem of rapid photogenereated electron-hole pairs recombination must be resolved. In the past researchers tried to improve the absorption of ZnS in the visible region by introducing an impurity (dopant ion); hence the result is an enhancement of its photocatalytic efficiency. Several reports have been made on the enhancement of photocatalytic efficiency of ZnS by combining metal or non-metal by using different techniques. For instance, Fe (Li et al., 2011), Cr (Eyasu et al., 2013), Ni (Jothibas et al., 2018), transition metal (Mn, Co, Ni, Cu, Ag and Cd) doped ZnS (Ramasamy et al., 2012), as well as ZnS doped Pb (Borse et al., 2006) were synthesized using chemical precipitation.

2.4.3. Parameters Influencing the Photocatalytic Activity of Semiconductors Photocatalysts.

During the photocatalysis process, the oxidation rates and efficiency of the photocatalytic system are dependent on a number of parameters that govern the photodegradation of the organic pollutants (Gnanaprakasam et al., 2015). The following parameters play an important role in the semiconductor photocatalytic activity.

2.4.3.1. Crystal Composition and Catalyst Type

Structural and surface properties of semiconductors such as particle size distribution, crystal composition, surface area, band gap and surface hydroxyl density, play important roles in the activity of a photocatalyst semiconductor. The average crystal size is one of the most significant parameters in heterogeneous catalysis. It determines the efficiency in catalysis for studies dealing with degradation of organic compounds such as phenolic compounds and dyes in wastewater using some commercial catalyst. Presently, most of the research is focused on enhancing the photocatalytic activity of synthesized catalysts (Mai et al., 2008).

Luo et al. (2007) studied the degradation of methyl orange with synthesized rutile phase of titanium and the P25 rutile under visible light. After 2 hours of irradiation, the photocatalytic degradation of methyl orange was 94.85% for P25 rutile and 82.33% for the rutile titanium. However, it was observed that the particles sizes of the catalysts were smaller for the P25 (30nm) compared to the rutile titanium (70-90 nm).

The photocatalytic degradation rate efficiencies of acridine orange have also been shown to be higher for ZnO compared to TiO_2 and CdS (Pare et al. (2008). The lower degradation rate efficiency was attributed to its smaller band gaps. Similarly, ZnO exhibited higher efficiencies compared to TiO_2 anatase, ZnS, SnO_2, Fe_2O_3 and CdS for the degradation of Acid red 18 under UV irradiation (Sobana et al., 2006; Sobana et al., 2008). Insignificant activities were recorded for SnO_2, Fe_2O_3, CdS and ZnS for Acid Red 18 decolourization due to their smaller band gap which permits rapid recombination of hole and electron. Several other studies have also shown that ZnO is an important competitor of TiO_2 and it is sometimes preferred because of its higher photon adsorption (Mohabansi et al., 2011; Kalnaowakul et al., 2017).

2.4.3.2. Catalyst Loading Effect

The initial mass (m) of catalyst is proportional to the rate of reaction (Vaidya and Mahajani, 2002; Shankar et al., 2004). It has also been observed that as the mass increases, the reaction rate becomes independent of the mass at a point or after optimum mass. The increase of catalyst loading results in increase in surface area and consequently active sites, and hence the rate of photocatalytic degradation (Zanta and Martínez-Huitle, 2009; Liu et al., 2010).It is important to ascertain the optimum mass of a photocatalyst for effective degradation in order to avoid waste of resources leading to increase in the opacity and increased light scattering, reduction of the photons on the photocatalyst surface and the agglomeration of the nanoparticles which will reduce the number of active sites (Zhang and Lei, 2008).

2.4.3.3. Calcination Temperature

Calcination temperature has a strong effect on the crystal size, crystal structure and optical properties of a prepared photocatalyst (Liang et al., 2007). The synthesis of photocatalysts sometimes involves higher calcination temperatures to transform the amorphous phase to a crystal structure, possibly resulting in particle growth and increase in surface area and photocatalytic efficiency than the original particles.

Several studies have investigated the dependence of photocatalytic activity on reaction temperature (Ahmed et al., 2011). For instance, Pecchi et al. (2001) studied the effect of calcination temperature on the photocatalytic degradation of pentachlorophenol using the sol-gel method under different pH. They observed that increasing the calcination temperatures resulted in a decrease of particle size and surface area. When the calcination temperature was increased from 300 to 500°C at pH 3 and 5 the degradation rate increased from 300 to 500°C. Cun et al. (2002) reported the photocatalytic degradation of methyl orange using calcined at different temperatures; 600°C was found to be the optimum temperature for the degradation of methyl orange. Shi et al. (2009) studied the preparation, characterization and photocatalytic activities of holmium doped titanium dioxide nanoparticles. They observed that there was a shift of absorption to a longer wavelength (red-shift) with increase of calcination temperature.

V dopedTiO_2 nanoparticles with enhanced photocatalytic activity under visible light were studied by (Tian et al., 2009). They observed that increasing of calcination temperature changed the phase of TiO_2 from anatase to rutile phase. Like other researchers they noticed that the anatase phase has a higher thermal stability than the rutile phase (Zhou and Smith, 2002; Shi et al., 2009). The anatase phase has a low recombination of election-hole pair and easily absorbed organic molecule compared to the rutile phase.

2.4.3.4. Initial Substrate Concentration and Type

The investigation of the efficiency of a photocatalyst, the effect of the initial substrate concentration may give an idea of the efficacy of the photocatalyst at different concentrations. It has been reported that the high initial substrate concentration leads to a reduction of the photocatalyst degradation efficiency due to adsorption of many molecules on the photocatalyst surface resulting in unavailability of catalyst surface to produce $OH^{\bullet}$ radical (Ahmed et al., 2010). Moreover, increasing the pollutant concentration decreases the number of photons absorbed on photocatalyst surface which reduces the excitation of e^- from the valence band to the conduction band. Several studies have shown that increasing initial substrate concentration reduces the degradation efficiency of the photocatalyst (Bahnemann et al., 2007; Gaya et al., 2010; Jothibas et al., 2018; Kotlhao et al., 2018a).

This trend has been reported for several pollutants including azo dyes, phenol, m-nitrophenol, amido black dye, 4-chlorophenol, Chromotrope 2B, 2-chlorophenol,2,4- dichlorophenol, 2,4,6-trichlorophenol, chrysodine Y, amaranth, xylenol orange, and acridine orange (Sauer et al., 2002)

2.4.3.5. pH Effect

pH in the photocatalytic degradation process plays an important role in the preparation of the catalyst. The pH of the solution influences the adsorption and dissociation of the substrate photocatalyst surface charge, the oxidation potential of the valence band (Shankar et al., 2004; Venkatachalam et al., 2007) check all your references and put the older one first- arrange them from oldest to newestand physicochemical properties of the system. According to Nerst' law varying the pH of solution, tends to shift the energy of the valence band and conduction band edges by 0.059 per pH at ambient temperature (25°C) (Hoffmann et al., 1995).

Increasing the pH beyond the isoelectric point of a nano-photocatalyst leads to limiting the presence of negative charge at the photocatalyst surface. On the other hand, when the pH is reduced the positive charge (H^+) is dominant at the photocatalyst surface (Zhang et al., 2007). The amphoteric behaviour of the semiconductor and the charge surface of the photocatalyst are affected by the pH values around its point zero charge. For example, TiO_2 behaviour follows the following equation (Zhang et al., 2007)

$$pH < pzc \qquad TiOH + H^+ \longrightarrow TiOH_2^+ \qquad (1)$$

$$pH > pzc \qquad TiOH + OH^- \longrightarrow TiO^- + H_2O \qquad (2)$$

Zhu et al (2005) investigated the point of zero charge of TiO_2 which is equal to 6.25.

Ba-Abbad et al. (2017) investigated the photocatalytic degradation of 2-chlorophenol under solar light using ZnO under different pH conditions. They observed lower degradation efficiency at pH< 6 due to the high concentration of protons on the ZnO surface. However, an increase of pH up to 6 increases degradation efficiency, due to the lower concentration of photons which react with hydroxyl ions. Furthermore, a decrease of degradation efficiency was observed when the pH was above the optimum pH value (pH = 9) because of the charge repulsion with an excess of negative charge on the catalyst surface. Similar observations were made by other researchers (Akbal and Onar 2003; Chiou et al., 2008b and Prado and Costa, 2009).

On other hand Kotlhao et al. (2018a) studied the photocatalytic degradation of selected chlorophenol and in their study the effect of pH in the range of 4, 8 and 11 was investigated. The highest percentage degradation was obtained at pH = 11, because the hydroxide ions became predominant and the generated hole could interact with hydroxide ions for the production of hydroxyl radicals which would oxidize the organic molecules. Similar observation was made by (Devadi et al.; 2014).

2.5. Synthesis Method for Doped Nanoparticles.

Several processes have been employed for the production of doped and undoped TiO_2, ZnO and ZnS nanoparticles. These include deposition method, solvothermal, chemical precipitation and sol-gel methods. Here, the choices of the sol-gel and chemical precipitation methods will be discussed.

2.5.1. Sol-gel Method

The sol-gel process involves the transformation of a solution from a liquid "sol" into a solid "gel" phase. In this method, the precursors are usually inorganic metal salts or metal organic compounds such as metal alkoxide. The process involves two steps: (i) hydrolysis, and (ii) condensation. In hydrolysis, the precursor is hydrolyzed first to produce a hydrated metal hydroxide. Then the hydrated metal hydroxide can produce an oxo bridge (-M-O-M) by condensation and the sol can be formed. The wet gel is obtained after allowing the sol to age, followed by drying and heating (Nachit et al., 2016). Since 1971, the sol-gel method has been mainly used for synthesis and was applied in the production of multiple doped oxide component such as Ni (Caratto et al., 2012), Mg (Ansari et al., 2015), Cu (Yang et al., 2015), Co (Ba-Abbad et al., 2016), Ba (Yang et al., 2018) doped ZnO; Ag, Au and Pt (Karmaoui et al., 2017) doped TiO_2.

The sol-gel has been widely applied for the synthesis of TiO_2 nanoparticles. It allows photo-induced molecular reactions to take place on a titanium dioxide surface due to its simple process, low temperature chemical method, chemical homogeneity, low requirements for the substrates, stoichiometric control, high purity of the product and ease of dopant introduction (Liang et al., 2018).

A typical reaction scheme is written as follows:

a) Hydrolysis

$$\text{Ti-OR} + \text{H}_2\text{O} \rightarrow \text{Ti-OH} + \text{R-OH} \quad (1)$$

b) Condensation

$$\text{Ti-OH} + \text{RO-Ti} \rightarrow \text{Ti-O-Ti} + \text{R-OH} \quad (2)$$

$$\text{Ti-OH} + \text{HO-Ti} \rightarrow \text{Ti-O-Ti} + \text{H}_2\text{O} \quad (3)$$

R in the equation may represent ethyl, i-propyl or n-butyl groups (Yahaya et al., 2017). However, a titanium precursor is often diluted with an organic solvent before addition of water. This is to reduce the reaction rate of the hydrolysis process.

2.5.2. Chemical Precipitation method

The chemical precipitation method is a reaction that occurs between two aqueous solutions of anions and cations which combine resulting in the formation of an insoluble substance (Kaur, 2010). The method takes place in three steps which are nucleation, growth, and agglomeration. In this process both the soluble and insoluble salts react together to give a precipitate reaction in aqueous phase; the formed particles are called the embryos. After the liquid reaction, there is a formation of solid particles in the growth step. The growth step is when the embryos are diffused to the nuclei surface and finally the formation of large size nanoparticles take place due to the agglomeration.

Chemical precipitation has been used for the synthesis of a variety of doped nanomaterials such as Mn, Co, Ni, Cu, Ag and Cddoped ZnS Nanoparticles (Ramasamy et al., 2012); for example, Ni doped ZnO (Udaykumar et al., 2012), Mn doped ZnS (Chandrasekar et al., 2015), Co (Devi and Velu, 2016); Ag doped ZnO (Gayathri et al., 2015). This method has some advantages over other synthesis methods. The method is simple to operate, less time consuming, inexpensive, high yield process, size controllable, and inhibit the agglomeration of particles. However, it is suitable for the synthesis of ZnS and ZnO nanoparticles (Boxi and Paria, 2014).

Chapter 3: Methodology

3.1. Materials and Method of Preparation

3.1.1. Chemicals and Materials

3.1.1.1. Chemicals

Chemicals used for this study include zinc acetate, zinc nitrate, silver nitrate, titanium-(triethanolaminato) isopropoxide, 2-chlorophenol, sodium hydroxide, ethanol, sodium sulphate, methanol, 2-clorophenol, distilled water and hydrochloric acid

3.1.1.2. Materials

Beakers (250 mL), thermometer, stirring hotplate, 250 mL three-neck flasks, volumetric flask (100 mL and 50 mL), pH meter, furnace, oven, centrifuge, syringe, 0.45 µm filter, vacuum pump.

3.1.2. Preparation of Solutions

Stock solution preparation: 2-chlorophenol stock solution (500 ppm) was prepared by pouring 390 µl of 2-chlorophenol into a 500 mL volumetric flask and dilute with distillated water to 500 mL line. The solution was kept in the fridge and covered with a foil to avoid light penetration. Various concentrations (5, 10, 20, 30, 40, 50, 60, 70 and 80 ppm) were prepared from the stock solution

A buffer solution of 0.1M HCl and NaOH were prepared for the purpose of controlling the pH of the solution during the photocatalytic degradation experiments.

3.2. Methods used for the Preparation of Nanoparticles

3.2.1. Sol-gel Method for the Synthesis of Undoped TiO_2 Nanoparticles

The undoped titanium dioxide nanoparticles were synthesized by the sol-gel method. Titanium dioxide nanoparticles were obtained by taking 4.5 mL of titanium isopropyl oxide and 21 mL of ethanol were mixed with 3.5 mL of distilled water. The solution was stirred at 3500 rpm in a 250 mL beaker flask at room temperature for 4 hours. During the stirring a white gel was formed (titanium dioxide nanopowder), that was washed twice with deionized water and ethanol, then dried overnight at room temperature. The white powder was calcined at 500°C for 1 hour.

3.2.1.1. Preparation of Ag Doped TiO_2 Nanoparticles

The Ag doped TiO_2 nanoparticles were synthesized by the sol-gel method. A 4.5 mL of titanium isopropyl oxide and 21 mL of ethanol were dissolved in 3.5 mL of distilled water followed by $AgNO_3$with the molar ratios of Ag equal to 1%, 3% and 5%. The solution was stirred at 3500 rpm in a 250 mL beaker at room temperature for 4 hours. During the stirring a white gel that was formed was washed twice with distillated water and ethanol and dried overnight at room temperature. The obtained doped nanoparticles were calcined at 500°C for 1 hour.

3.2.2. Synthesis of Undoped ZnO Nanoparticles.

The undoped ZnO nanoparticles were synthesized by chemical precipitation. In a typical synthesis process, 0.1M solutions of $Zn(NO_3)_2.6H_2O$ and NaOH were prepared separately in 100 mL volumetric flask filled to the mark with deionized water. Sodium hydroxide was added dropwise into a vigorously stirred zinc nitrate solution in (1:2) ratio. The mixture was stirred at (4000 rpm) for 2 hours after addition of sodium hydroxide solution to obtain the white colored zinc hydroxide precipitate. After obtaining the precipitate, the reaction was allowed to settle overnight and the clear liquid on top (supernatant) was then discarded. The precipitate was washed 3 times with distilled water and ethanol and centrifuged at 5000 rpm to get the final product.

The white powder then was dried in an oven at 110℃ for 2 hours and calcined at 500℃ for 1 hour using a muffle furnace. During the calcinations process, there was a complete conversion of $Zn(OH)_2$ into ZnO.

3.2.1.1. Preparation of Ag Doped ZnO Nanoparticles

To synthesize Ag doped ZnO nanoparticles a chemical precipitation method was adopted. In a typical synthesis process, 0.1M solutions of $Zn(NO_3)_2.6H_2O$ and NaOH were prepared separately in 100 mL volumetric flask filled to the mark with deionized water. Sodium hydroxide was added dropwise into a vigorously stirred zinc nitrate solution in (1:2) ratio. The mixture was stirred at (4000 rpm) for 2 hours after addition of all the sodium hydroxide solution. A white colored zinc hydroxide precipitate was obtained. The $AgNO_3$ with various molar ratios of Ag equal to1%, 3% and 5% was added drop by drop into Zinc hydroxide precipitate.

A brown precipitate was obtained; the reaction was allowed to settle overnight and the clear liquid on top (supernatant) was then discarded. The precipitate was washed 3 times with distilled water and ethanol and centrifuged at 5000 rpm to get the final product. The brown powder was dried in an oven at 110℃ for 2 hours and calcined at 500℃ for 1 hour using a muffle furnace. Then 1%, 3% and 5% Ag-ZnO nanoparticles were obtained.

3.2.3. Synthesis of Undoped ZnS Nanoparticles

The synthesis of undoped ZnS nanoparticles was processed by chemical precipitation. Zn $(CH_3COO)_2.2H_2O$ (5.48g (0.5 M)) in aqueous (50 mL) was stirred magnetically at 80℃ in a three neck flask until a homogeneous solution was obtained. An amount of 2.75 g of Na_2S was dissolved in 50 mL of deionized water; the mixture was added dropwise to the zinc acetate solution under vigorous stirring. During the addition of Na_2S, a white precipitate appeared; the mixture was allowed to stir for 30 min at 80℃ at 60 rpm. The mixture was washed, centrifuged 3 times with a mixture of water/ethanol in (1:2) ratio at 5000 rpm for 5 min and dried in oven at 80℃ for 24 hours. The dried powder was calcined at 500℃ for 1 hour using the muffle furnace.

3.2.3.1. Preparation of Ag Doped ZnS Nanoparticles

The synthesis of Ag doped zinc sulfide nanoparticles was processed by chemical precipitation. $Zn(CH_3COO)_2.2H_2O$ (5.48 g (0.5 M)) in aqueous (50 mL) was stirred magnetically at 80℃ in a three neck flask until a homogeneous solution was obtained. The Na_2S solution was prepared by dissolving 2.75 g of Na_2S in 50 mL of deionized water, the mixture was added dropwise to the zinc acetate solution under vigorous stirring. During the addition of Na_2S, a white precipitate appeared. An addition of $AgNO_3$ solution with different molar ratios of Ag equal to 1%, 3% and 5% was added in the ZnS nanoparticles. The mixture was stirred for 30 min at 80℃ at 60 rpm and a black precipitated was obtained.

The precipitated was washed, centrifuged 3 times with a mixture of water/ethanol in (1:2) ratio at 5000 rpm for 5min and dried in oven at 80℃ for 24 hours. The dried powder was calcined at 500℃ for 1 hour using the muffle furnace. Then 1%, 3% and 5% Ag-ZnS nanoparticles were obtained.

3.2.4. Particle Characterization

The physical and chemical characteristics of the synthesized nanoparticles were obtained using many techniques. The size and the shape of the nanoparticles were observed under a transmission electron microscope (TEM). The crystallinity of the synthesised nanoparticles was recorded using *X*-ray diffraction (XRD) Philips (XPERT PROdiffractometer (Cu Kα radiation)) with a scanning rate of 0.01°/sec in the 2θ range of 10° to 90°. The light absorbance properties and the band gap of nanoparticles were determined by using UV-VIS spectroscopy (T80$^+$ UV), luminescence properties of the particles was determined by Photoluminescence (PL) (FP-8600 spectrofluorometer). Fourier-transform infrared (FT-IR) spectra were recorded with a Perkin Elmer FT-IR/ FT-NIR spectrometer (model 400).

3.3. Photocatalytic Degradation Process

3.4.1. Degradation of 2-chlorophenol without Catalyst

The photocatalytic degradation of 2-chlorophenol was performed with the photocatalytic reactor system. The photocatalytic system is composed of a cylindrical pyrex reactor with a capacity of 400 mL containing a 16 W Ultra-violet light. A 16 W Ultra-Violet lamp was used as a UV source. The photoreactor was filled with 300 mL of a specific concentration of 2-chlorophenol varying from 50, 20 to 8 ppm. The solution was stirred and aerated using a vacuum pump for oxygen supply and to allow the complete homogeneity of the solution. The suspension was adjusted at specific pH (4, 7, and 10.5). The solutions were kept and stirred in the dark for 30 min to allow the adsorption and desorption equilibrium to take place. Then the UV light was switched on for 150 min irradiation and 5 mL of aliquot was taken using a 0.45 µm filter membrane at interval time of 25 min for analysis. The absorption was measured before and after exposure to UV light at each time interval using T80$^+$ UV/VIS spectrometer.

3.4.2. Photocatalytic Degradation of 2-chlorophenol in the Presence of Catalyst

The photocatalytic activities of the synthesized undoped and silver doped TiO_2, ZnO and ZnS nanoparticles were studied by the photodegradation of 2-chlorophenol in an aqueous solute at room temperature. A mixture of 300 mL of a specific concentration of 2-CP with a specific catalyst dose was conducted in a photoreactor equipped with a 16 W Ultra-violet lamp. The mixture was kept under stirring. The mixture was stirred for 30 min in the dark to allow the adsorption and desorption equilibrium.

Then the light was turned on to investigate the photocatalytic degradation process. A 5 mL aliquot was taken out from the photoreactor using a 0.45 µm filter membrane to avoid the presence of the nanoparticles in the solution after each 25 min interval time. The absorption of solution after and before irradiation was analyzed using a $T80^{+}$ UV/VIS spectrometer. The percentage degradation was determined by the following formula.

$$D = \left(\frac{C_i - C_t}{C_i}\right) \times 100 \ or \left(\frac{A_i - A_t}{A_i}\right) \times 100$$

Where C_i and A_i are the initial concentration and initial intensity after the adsorption period and C_t and A_t are the concentration and intensity at any time.

Chapter 4: Results and Discussion

4.1. Characterization of Pure and Ag Doped TiO_2 Nanoparticles

4.1.1. *UV*-Visible Diffuse Reflectance spectroscopy (*UV*DRS)

The optical absorption properties of pure TiO_2 and Ag doped TiO_2 nanopowder calcined at 500℃ were studied using the *UV*DRS spectrometer as shown in Figure 4.1. It was observed that the band gap for the synthesized TiO_2 nanoparticles that was (3.42 eV) blue shifted from the band gap of the bulk band gap of TiO_2 nanomaterial (3.2 eV). This blue shifting is attributed to the reduction of the particle size. As shown in Figure 4.1. (a) Addition of Ag into the nanoparticles showed a shift of the absorption edge at 350 nm towards a higher wavelength for 1%, 3% but a red shift through the visible region was observed at 5% Ag. In addition, a weak broad peak with the absorption edge between 530 and 600 nm was observed in the spectrum as the concentration of silver increased. This is can be attributed to the plasmonic resonance peak of silver in Ag-TiO_2 spectra. This is supporting by the research of Ozimek et al. (2016).

The energy band gap (E_g) was determined by using the Tauc equation by plotting the Kubelka Munk function $(F(R)\ h\nu)^{2}$ versus the photon energy (hv) and extrapolating the Kubelka Munk function. Where F (R) is the Kubelka Munk reflectance, and *hv* is the photon energy.

The bang gap energies of the synthesized nanoparticles were 3.42 eV (TiO_2), 3.23 eV (1% Ag-TiO_2), 3.13 eV (3% Ag-TiO_2) and 3.10 eV (5% Ag-TiO_2). The result shows that addition of Ag doped ion into the TiO_2 nanoparticles reduced the band gap from 3.42 eV to 3.23 eV, and then with an increasing of the amount of silver decreases to 3.10 eV for the 5% Ag doped. This may result in improvement of their photocatalytic activity. This result was supported by the work of Naraginti et al. (2015) which showed that Ag/Sr doped TiO_2 nanoparticles exhibited a decrease in the energy gap and wavelength (red shift) and the doped nanoparticles enhanced the photocatalytic activity of the semiconductor.

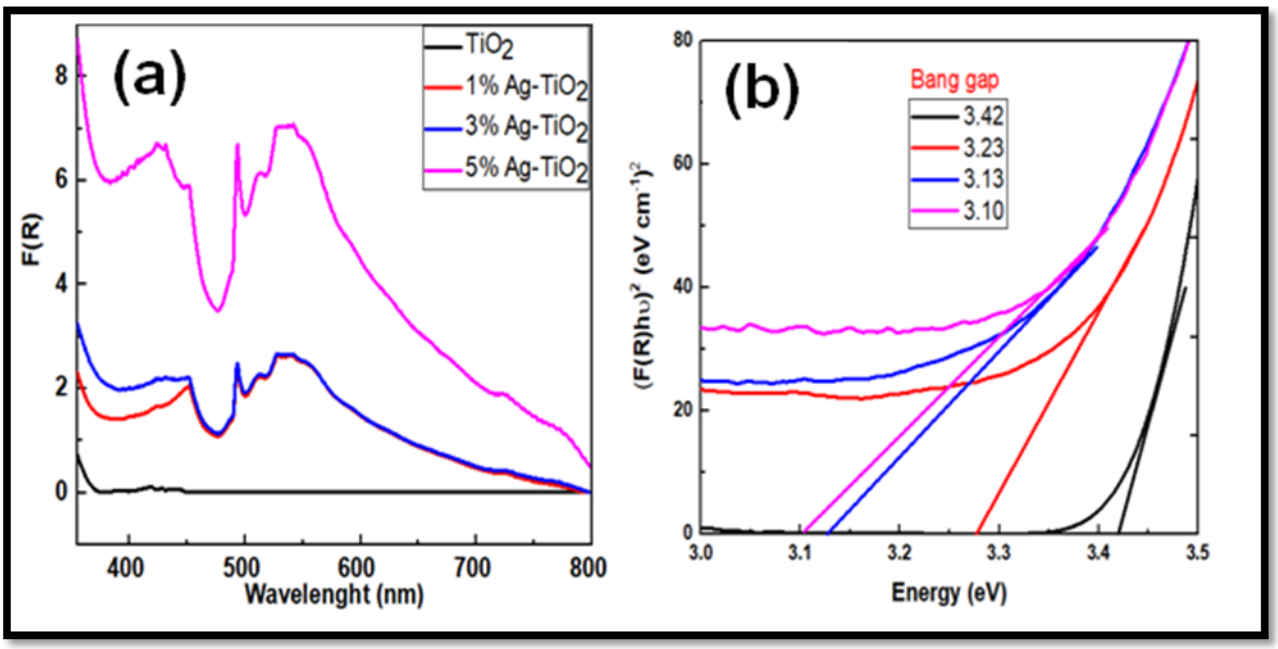

Figure 4.1: (a) Normalized *UV*DRS spectra, (b) Tauc plot of synthesized undoped and Ag doped TiO_2 nanoparticles

4.1.2 Photoluminescence (PL) spectroscopy

The emission spectra of pure TiO_2 and Ag doped TiO_2 are shown in Figure 4.2. Their photoluminescence was investigated in the range of 200 - 900 nm and the spectra patterns are shown in Figure 4.2. which shows the PL spectra of undoped and Ag doped TiO_2 nanoparticles with different amounts of Ag were excited at 325 nm. The PL emission spectra exhibited emission peaks at a range of 360 -600 nm. A decrease in intensity was observed as the amount of silver increased from 1 to 5%. This was attributed to the delay of electron-holes recombination, and this is believed to improve the photocatalytic activity (Tryba et al., 2010).The PL results are in agreement with *UV*DRS results because the red shift of the band gap observed in the UV after doping with Ag confirmed the delay of the recombination e^-/ h^+ species, which enhances the photocatalytic activity of the photocatalyst.

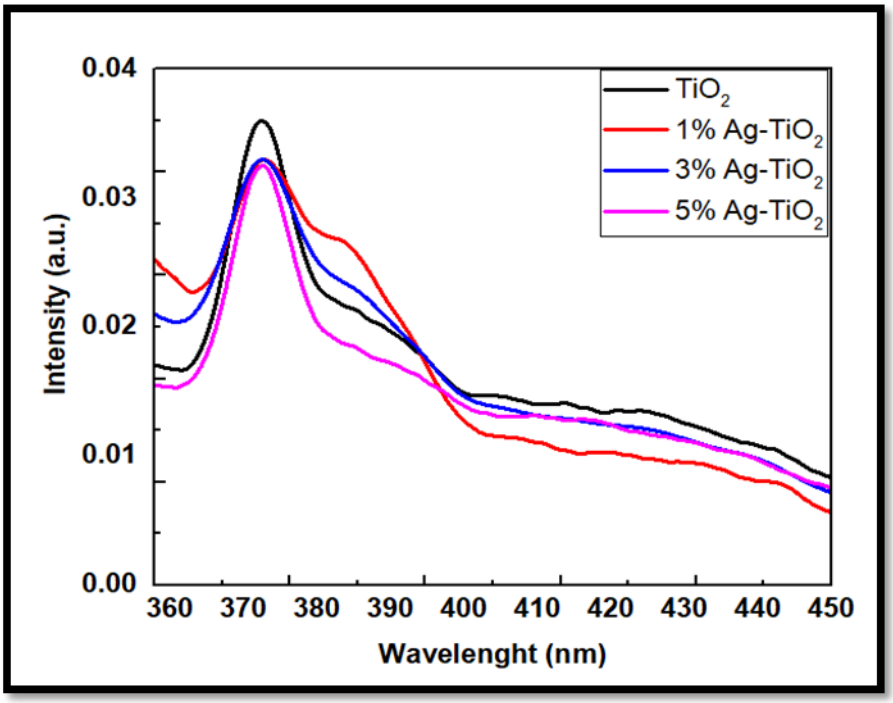

Figure 4.2: Normalized PL spectra of undoped and Ag doped TiO_2 nanoparticles

4.1.3 *X*- Ray Diffraction (XRD) spectroscopy

The crystallographic structure and the crystalline size of the synthesized nanopowders were determined by using XRD technique. The *X*-ray diffraction 2θ peak was carried out between 10 - 80° for undoped and Ag doped TiO_2 calcined at 500°C as shown in Figure 4.3. The peaks at 37.51, 47.82, 55.03, 53.89, 62.40, 69.9 , 74.69and 76.33° were attributed to (004), (200), (211), (105), (204), (220), (215) and (301) crystalline planes, respectively. This corresponded to (JCPDS 06-083) card of the anatase phase of TiO_2.For the photocatalytic activity of the TiO_2, the crystal and crystalline phase are important factors. It has been revealed that the crystalline anatase phase is more active than the rutile and brookite phase (Lei et al., 2014). It was also observed that the major [101] diffraction peak of the anatase phase increased in intensity and shifted from 25.2 to 25.7 two theta after doping Ag to the nanomaterial and the width of the [101] peak broadened. The broadness of the peak indicated that the particle crystalline or semi-crystalline sizes are decreasing (Perumal and Gnana-Sambandam, 2014).

There was no pure Ag peak in all the Ag doped TiO_2 samples which revealed that doping was achieved through substitution mechanism. This can be attributed to the low concentration level of the Ag used which was well dispersed on TiO_2 surface. This shows that Ag did not bring any change to the phase crystallinity and the observation suggests that doping agent is probably sited on the crystal surface (Perumal and Gnana-Sambandam, 2014). The average crystalline size was calculated by using the classical Scherrer equation $D = K\lambda/\beta\cos\theta$, where D is the crystallite size, λ is the wavelength of the X-ray radiation (Cu Kα-1 radiation=1.54060 Å), K is the Scherrer constant (usually taken as 0.9) for spherical shape, and β is the full width at half-maximum height, θ is the Bragg's diffraction angle. It was observed that TiO_2 has an average size of 15.62 nm and the crystalline size decreased up to 10.62 nm when Ag was added which could led to the assumption that Ag-TiO_2 inhibited the particles growth. The difference in particles size could be related to their radius ionic (Boxi and Paria, 2014).

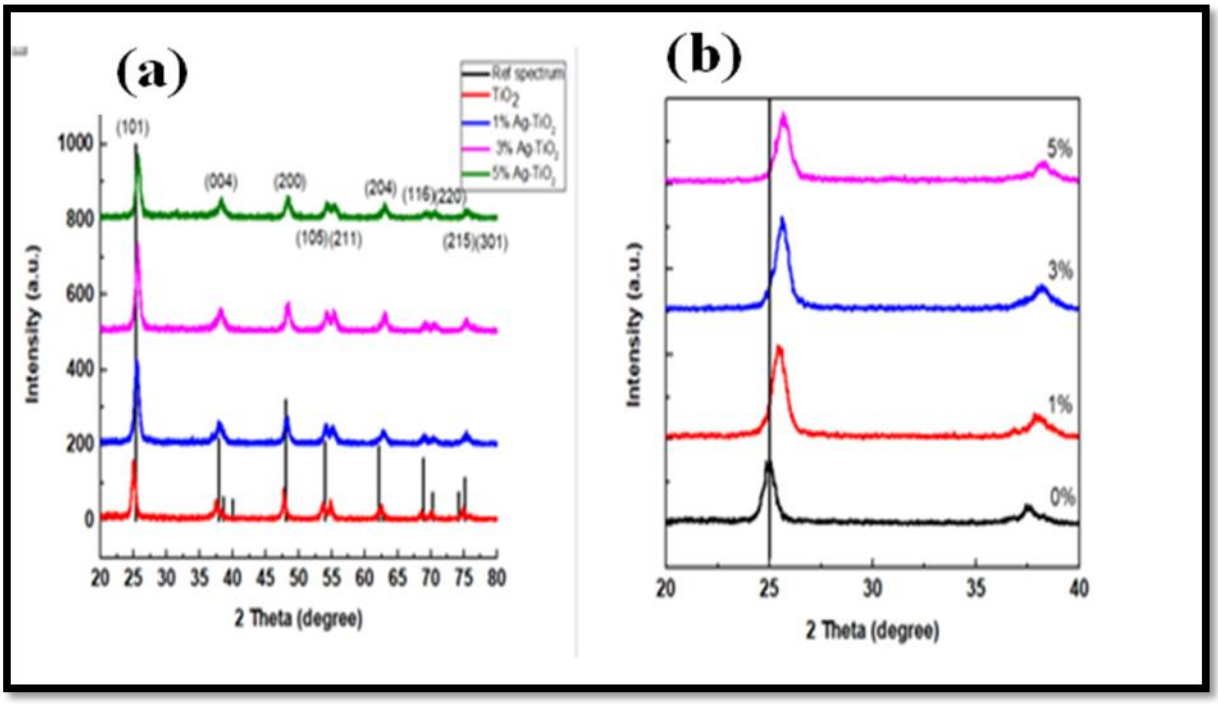

Figure 4.3: (a) XRD patterns of TiO_2; the reference spectrum is 06-083 anatase phase, TiO_2 and 1, 3 and 5% Ag doped TiO_2 nanoparticles. (b) Enlarged regions of XRD patterns

Table 4 : Crystallite size of TiO_2 and silver doped TiO_2 nanoparticles

Particles	Particles size (nm)
TiO_2	15.69
1%Ag-TiO_2	10.40
3% Ag-TiO_2	11.62
5% Ag-TiO_2	11.00

4.1.4. Fourier Transform Infrared (FTIR) spectroscopy

The Fourier transform infrared (FTIR) spectroscopy of the pure TiO_2 and Ag-TiO_2 nanoparticles were recorded in the range of 4000 - 400 cm^{-1}as shown in Figure 4.4. The peaks around 2982 cm^{-1} and 2993 cm^{-1} correspond to C-H vibration mode of CH_2 groups, the peak at 2982 $cm^{-1}$was attributed to anti-symmetric and 2993 cm^{-1} is attributed to symmetric mode of CH_2; these organic peaks are due to the remnants of organic solvent (ethanol) used for the sample preparation. The peaks around 3679 cm^{-1} are assigned to OH stretching vibration groups. This confirms the existence of free hydroxyl groups in all prepared samples; it has been reported that doping can improve the surface state of the material and may also generate more surface OH groups (Lei et al., 2014). It has been observed previously that the materials with more surface hydroxyl groups are more conducive for the production of $OH^{\cdot}$ radical and improves the photocatalytic activity.

The sharp peak at 1063 cm^{-1} for pure TiO_2 became more intense and shifted when silver was added. This peak corresponds to the vibration mode of the anatase skeletal Ti-O-Ti bond (Taylor, 1988; Pant et al., 2013; Suwarnkar et al., 2014).

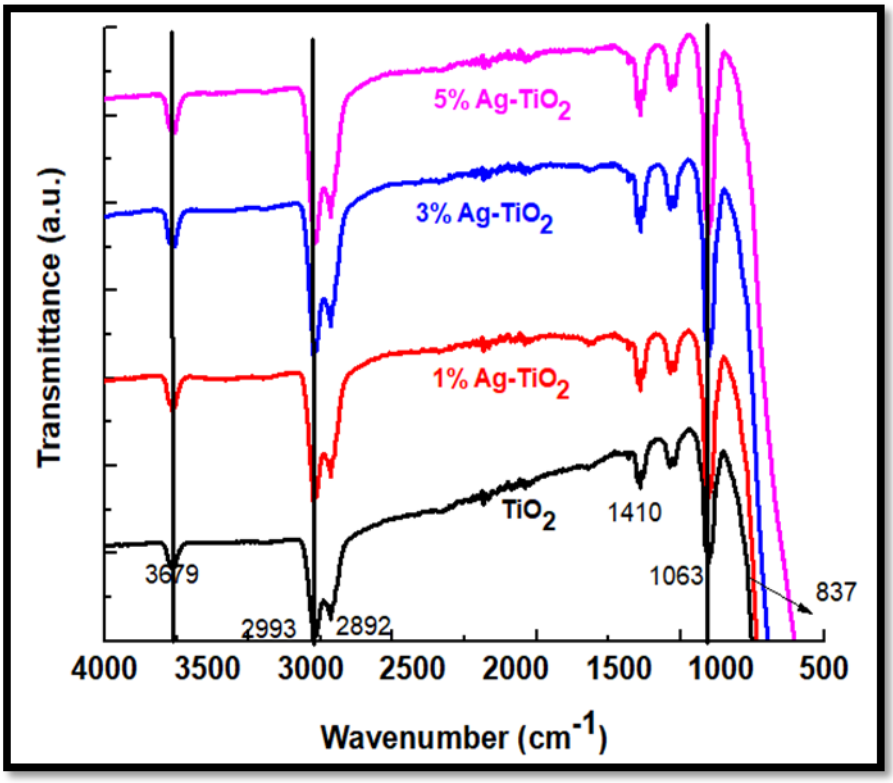

Figure 4.4: FTIR spectrum of undoped and Ag doped TiO_2 nanoparticles

4.1.4. Transmission Electron Microscope (TEM) analysis

Transmission electron microscope (TEM) was performed to investigate the crystal morphology of the TiO_2 and Ag-TiO_2nanoparticles. The TEM image of TiO_2 and Ag-TiO_2 are shown in Figure 4.5 (a) and (b), respectively. It has been observed that TiO_2 and Ag-TiO_2 particles are round with slight agglomeration due to the non-uniform morphology and have a uniform grain size as indicated by the XRD data.

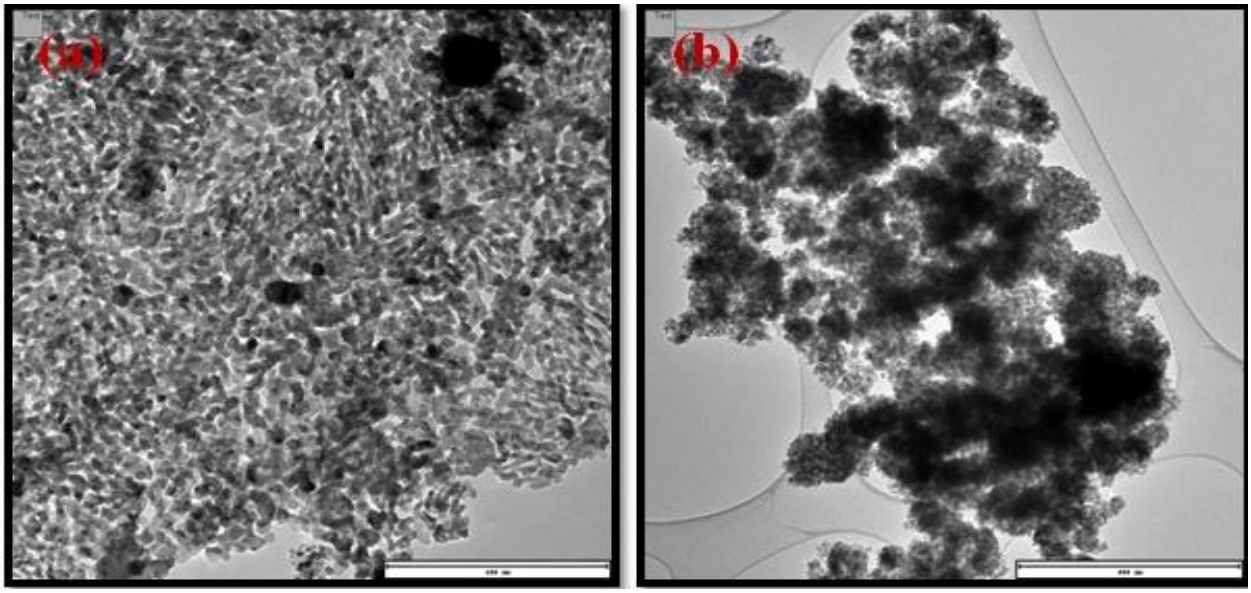

Figure 4.5: The TEM image of (a) TiO_2 and (b) 5% Ag doped TiO_2 nanoparticles

4.2. Characterization of Pure and Ag Doped ZnO Nanoparticles

4.2.1. *UV*-Vis Diffuse Reflectance spectroscopy (*UV*DRS)

The optical properties of the synthesized (undoped and Ag doped ZnO) nanoparticles were investigated to determine the effect of Ag amount on ZnO nanoparticles. Figure.4.6 shows *UV*DRS spectra of the ZnO and Ag doped ZnO. The absorption wavelength was observed in the range of 350 - 800 nm for ZnO and Ag doped nanoparticles. The band gap of the synthesized ZnO (3.23 eV) was red shifted compared toits bulk material band gap (3.3 eV). This red shift is attributed to increased particles size. A red shift of absorption edge was noticed as silver was doped into ZnO nanoparticles. As Ag concentration increased the absorption edge increased to a higher wavelength; this may be an indication of enhancement in the photocatalytic activity under UV irradiation for the synthesized samples. A similar observation was made by Bechambi et al. (2015). The addition of silver to ZnO reduced the band gap from 3.2 eV (ZnO) to 3.19 eV (1% Ag), 3.14 eV (3% Ag) and 3.13 eV for 5% Ag. A broad peak around 500 - 600 nm was attributed to the silver plasmonic resonance.

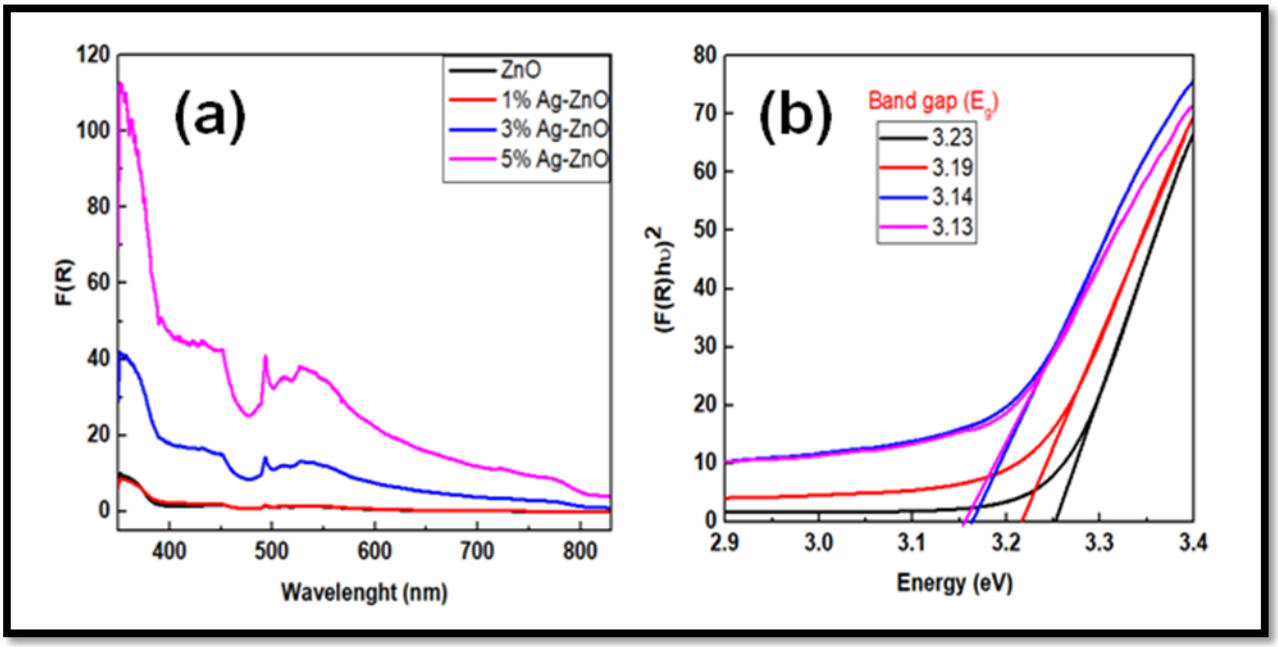

Figure 4.6: (a) Normalized *UV*DRS spectra; (b) The tauc plot of synthesized ZnO, 1, 3 and 5% Ag-ZnO nanoparticles

4.2.2. Photoluminescence (PL) spectroscopy

Photoluminescence of the synthesized undoped and Ag doped ZnO nanoparticles were investigated in the range of 200 - 900 nm and the spectra patterns are shown in Figure 4.7. In the photocatalytic process, the separation and the recombination of the photo generated electron-holes are competitive pathways. Figure 4.7 shows the PL spectra of undoped and Ag doped ZnO nanoparticles with different amounts of Ag were excited at 320 nm. It was observed that all samples (undoped and silver doped ZnO) exhibited two peaks at 413 nm and 533 nm. The peak at 413 nm may be due to the transitions from conductive band to the Zn vacancy. Then the peak at 533 nm referred to the emission from the interstitial Zn to the valence band. This observation is similar to that reported in the literature (Bechambi et al., 2015). It was observed that the PL intensity decreased first and then increased with an increase in Ag content.

At lower Ag (1 and 3%) molar ration, silver is able to accept electrons and reduce the recombination of photogenerated electron-hole onto ZnO surface. However, at higher Ag amount (5%), silver may act as a recombination centre for the photoinduced electron-hole and hence decrease the photocatalytic activity (Zhang, 2012). The lowest PL intensity of all synthesized photocatalysts was observed to be at 1 and 3% Ag doped ZnO. This is may be good for the photocatalytic activity, because at these percentages the dopant ion acts as a trapper of electron-hole pairs and this will reduce the electron-hole pairs recombination.

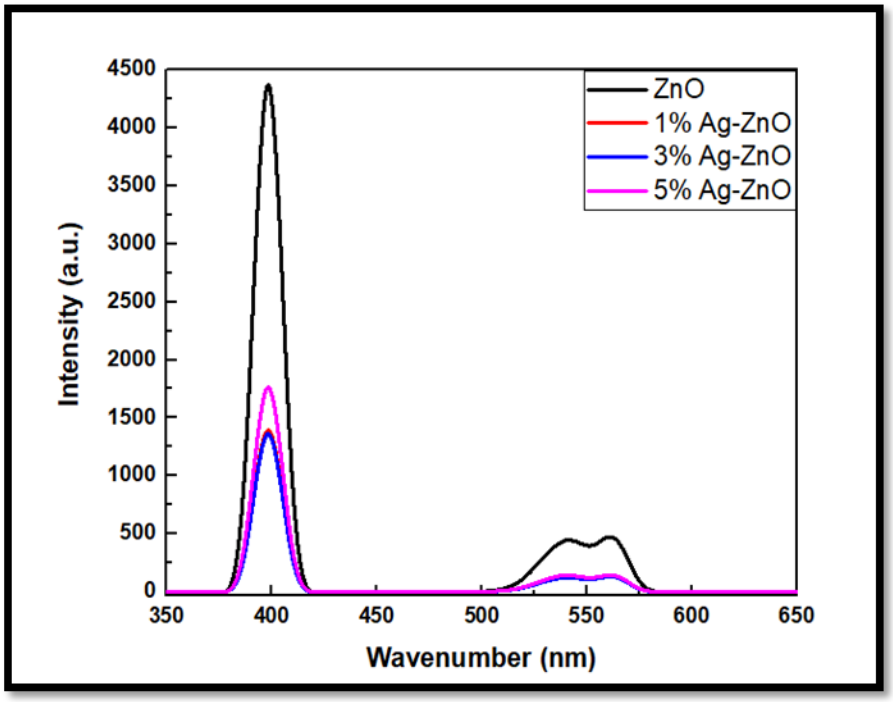

Figure 4.7: PL spectra of ZnO, 1, 3 and 5% Ag-ZnO nanoparticles

4.2.3. *X*-Ray Diffraction (XRD) spectroscopy

The XRD patterns of ZnO and Ag-ZnO nanoparticles synthesized by chemical precipitation with different amount of Ag incorporation (1, 3 and 5%) are shown in Figure 4.8. which shows that wurtzite is the only crystal phase of the ZnO according to the diffraction peaks at 2θ angles of 31.9˚, 34.5˚, 36.2˚, 47.7˚, 56.5˚, 62.9˚, 68.1˚ which corresponded to the refection at (100), (002), (101), (102), (110), (103) and (200), respectively.

There were an additional three new peaks at 38.28˚, 44.19˚and 64.76˚when silver was doped on ZnO nanoparticles, which corresponded to (111), (200) and (220) of the metallic silver, respectively.

These additional peaks suggested the formation of a second phase cluster. Figure.4.8 shows that the diffraction peaks (100), (002) and (101) of ZnO shifted to lower 2θ values with the addition of Ag^+ ion into the ZnO lattice. According to previous studies, the peak shifts to lower or higher 2θ values is due to the substitution or interstitial incorporation of Ag into the lattice of ZnO (Yıldırım et al., 2013). In addition, the peak shifts to lower 2θ values may be due to the difference in ionic radii between Ag^+ (1.26 Å) and ZnO (0.74 Å) (Yıldırım et al., 2013). In this case, since the peak positions shifted to the lower 2θ values, it suggests that substitution of Ag^+ ions into ZnO lattice occurred. The intensity and the broadness of the peaks decreased with doping of Ag on ZnO compared to the pristine ZnO nanoparticles. This ultimately increased the crystallinity and crystallite sizes which were determined using the following Scherrer equation.

$$D = 0.9\,\lambda / (\beta \times cos\theta) \qquad (2)$$

Where D is the average crystalline diameter, λ is the wavelength in angstrom, β is the line width at half maximum and θ is the Bragg angle.

The average crystallite size for undoped ZnO was 13.64 nm while it was 21.72 nm for 5% Ag doped ZnO. It was observed that the crystallite size increased as the amount of Ag metal increased as shown in the Table 6 below.

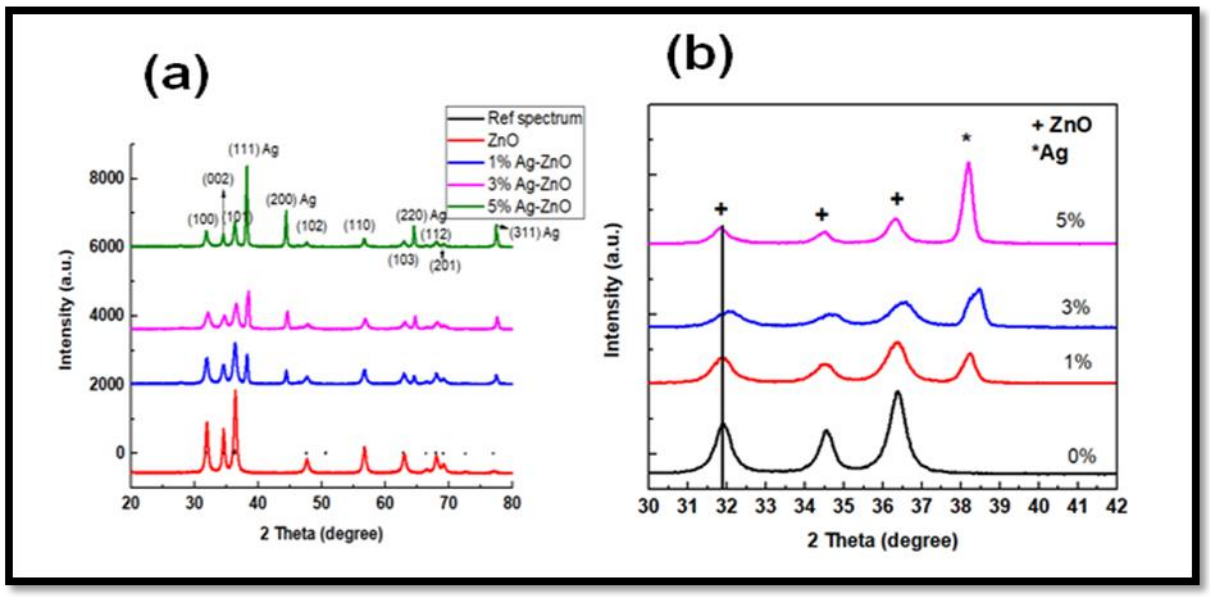

Figure 4.8: (a) XRD patterns of ZnO, 1, 3 and 5% Ag-ZnO nanoparticles. (b) Enlarged regions of the XRD patterns

Table 5: XRD crystalline size of ZnO and Ag doped ZnO nanoparticles

Nanoparticles	Crystalline size (nm)
ZnO	13.94
1% Ag-ZnO	14.97
3% Ag-ZnO	15.88
5% Ag-ZnO	21.72

4.2.4. Fourier Transform Infrared (FTIR) spectroscopy

The functional groups present in the undoped and Ag doped ZnO nanoparticles were also investigated with the FTIR spectroscopy in the range of 4000 - 400 cm^{-1}. The spectra of ZnO and various percentage doped Ag-ZnO nanoparticles are shown in Figure 4.9. The spectrum of ZnO sample shows bands located at 400 - 650 cm^{-1} which was attributed to ZnO stretching bands (Gnanaprakasam et al., 2016), and at 1383 and 1621 cm^{-1} which corresponded to C=O and OH bending vibration , respectively (Jose et al., 2017). The peaks at 2911 and 2995 cm^{-1} bands are

attributed to C-H stretching vibrations (Murtaza et al., 2014; Gayathri et al., 2015); these organic peaks are due to the remaining ethanol used for the sample preparation. The 3382 cm^{-1} peak has been ascribed to OH groups indicating the presence of absorbed water on the surface of the ZnO photocatalyst (Siva Vijayakumar et al., 2013; Gayathri et al., 2015). The peak at 1076 cm^{-1} could be attributed to bending vibrational modes (Zandi et al., 2011). All the functional groups peaks were shifted to the lower wavenumber and the intensity of their peaks increased with an addition of metallic silver into the undoped material. This could be attributed to the substitution of Ag^{+} ion on the ZnO lattice. The OH peaks were more intense in the 1 and 5% Ag-ZnO compared to the pristine ZnO. No absorption band for AgO or Ag_2O was observed; therefore there was no chemical attachment between AgO and Ag-ZnO, an indication that Ag may be in metallic form. This result supports the XRD spectral results which showed that Ag was incorporated onto the ZnO lattice by substitution without disturbing the crystal structure of the pristine ZnO. This result is in line with the findings of Yıldırım et al. (2013)

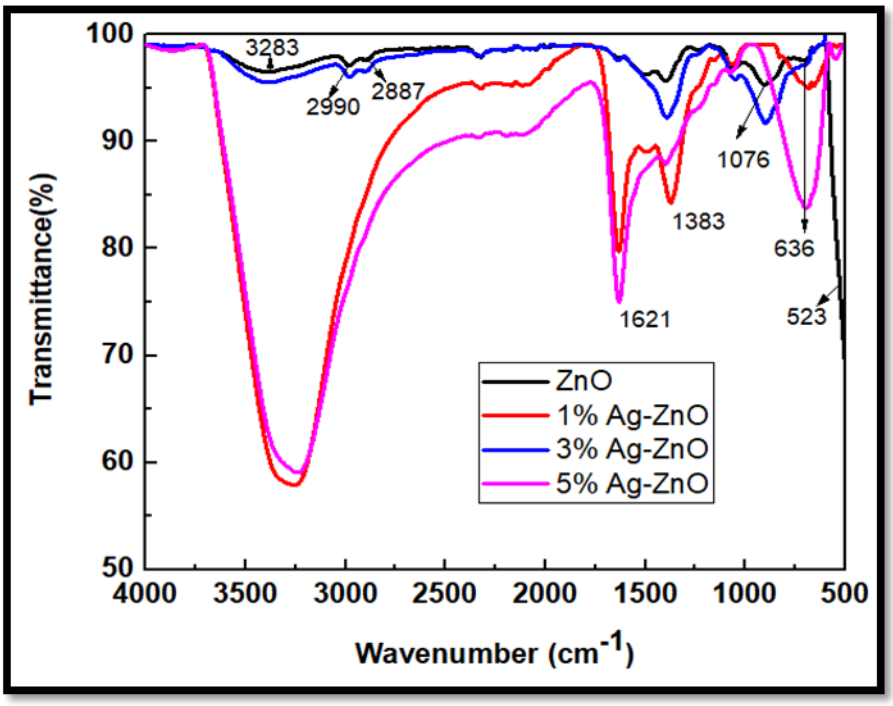

Figure 4.9: FTIR spectrum of ZnO, 1, 3 and 5% Ag-ZnO nanoparticles

4.2.5. Transmission Electron Microscope (TEM) analysis

The TEM images of the synthesized undoped ZnO and Ag doped ZnO (1% Ag) nanoparticles are shown in Figure 4.10 (a) and (b). It was observed that the particles were agglomerated and spherical in shape for the undoped and Ag doped ZnO nanoparticles. A slight increase in particles size was observed for the Ag doped ZnO suggesting that doping with Ag has an influence on the particles size of ZnO.

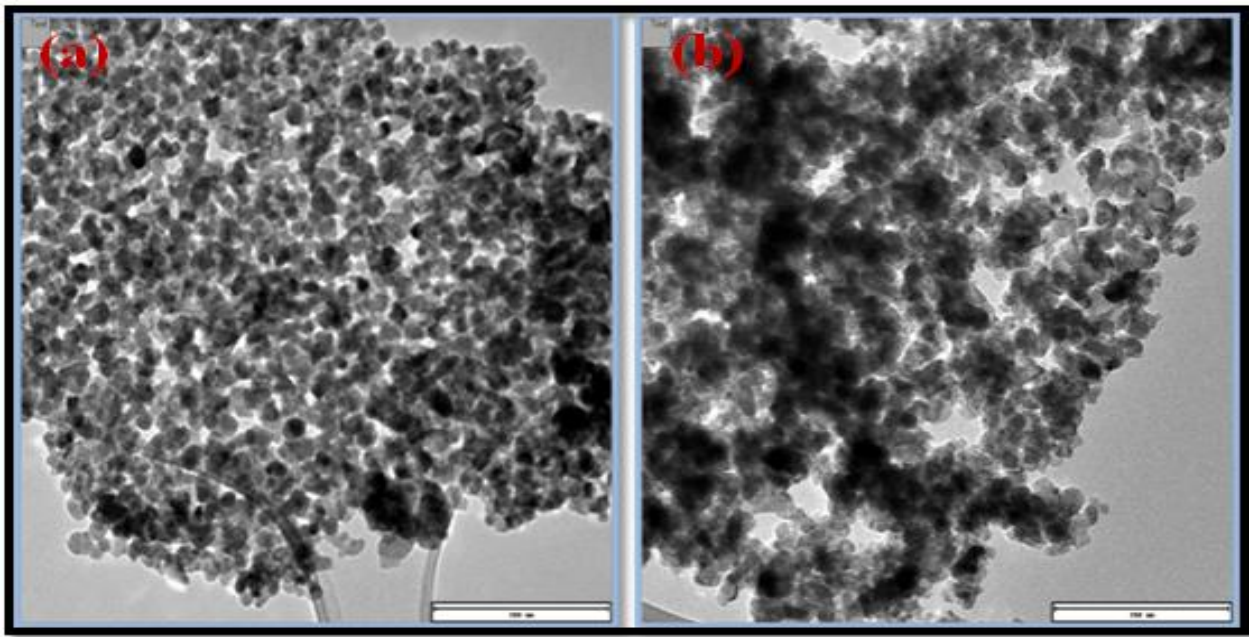

Figure 4.10: TEM images (a) ZnO and (b) 1% Ag-ZnO nanoparticles

4.3. Characterization of Pure and Ag Doped ZnS Nanoparticles

4.3.1 *UV*-Vis Diffuse Reflectance (*UV*DRS) spectroscopy

The *UV*DRS of the pristine ZnS and the various percentage Ag doped ZnS were investigated to study the optical properties of the photocatalyst, and the results are presented in Figure 4.11. The band gap of the synthesized ZnS (3.12eV) was smaller than the bulk (3.6 eV). This red shift of the band gap suggested that the particles sizes were bigger. The absorption edge of all nanoparticles was observed in slightly in UV region and an increase toward a higher wavelength observed in the presence of Ag doping to ZnS nanoparticles.

The band gap energy (E_g) of the synthesized photocatalyst was found using the plot of Kubelka Munk equation against the photon energy, and the band gap energy values obtained are 3.12, 3.10, 2.95 and 2.92 eV for ZnS, 1% Ag-ZnS, 3% Ag-ZnS and 5% Ag-ZnS nanoparticles, respectively. A red shift of the band gap was observed upon doping with Ag; this may be is due to quantum energy effect of Ag which has an influence on band gap of ZnS (Madkour and Al Sagheer, 2017). Addition of Ag delays the fast photogenerated electron-hole recombination and enhances the photocatalytic degradation.

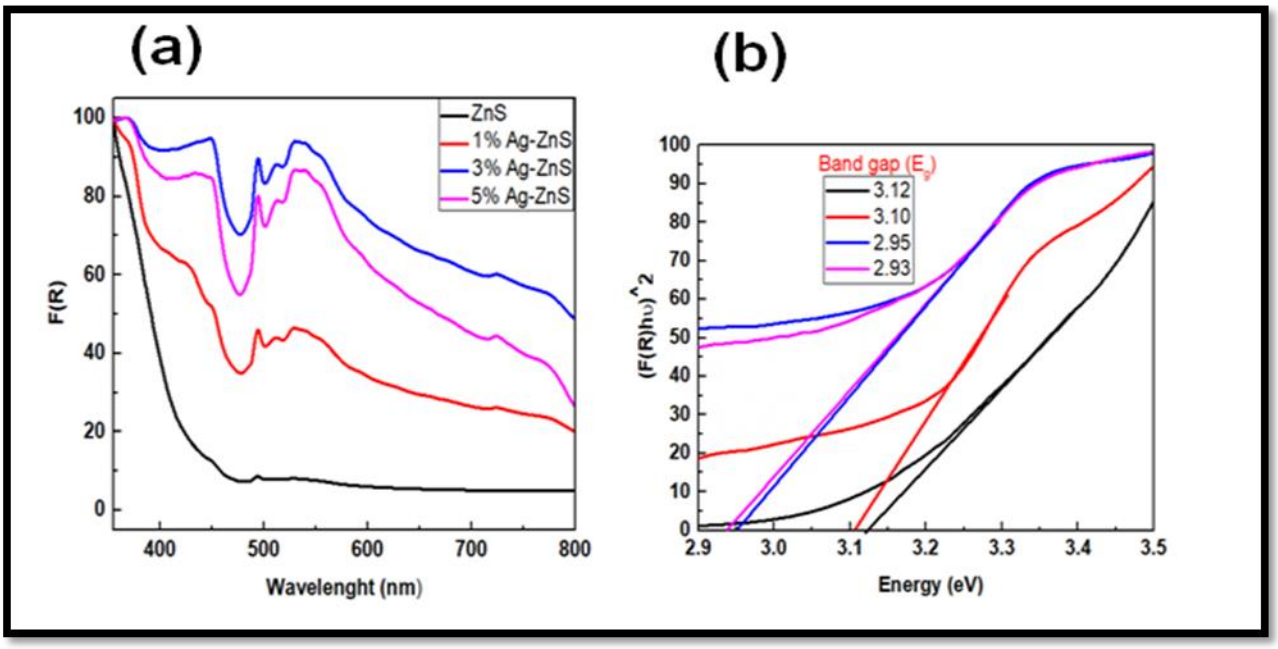

Figure 4.11: (a) Normalized *UV*DRS spectra and (b) Tauc plot of synthesized ZnS and 1, 3 and 5% Ag-ZnS nanoparticles

4.3.2. Photoluminescence (PL) spectroscopy

The photoluminescence (PL) spectra of undoped and doped ZnS nanoparticles with different percentages of Ag (1, 3 and 5%) under an excitation wavelength of 343 nm are shown in Figure 4.12. It was observed that both the undoped and Ag doped ZnS nanoparticles exhibited two emission peaks at 418 and 550 nm, while the addition of Ag into the particles resulted in a decrease in intensity.

This supports the results obtained from the *UV*DRS spectroscopy and indicates that increasing the amount of Ag decreases the band gap energy of nanoparticles which results in the red-shift of the PL emission peak. Similar trend has been reported in literature (Qin et al., 2012).

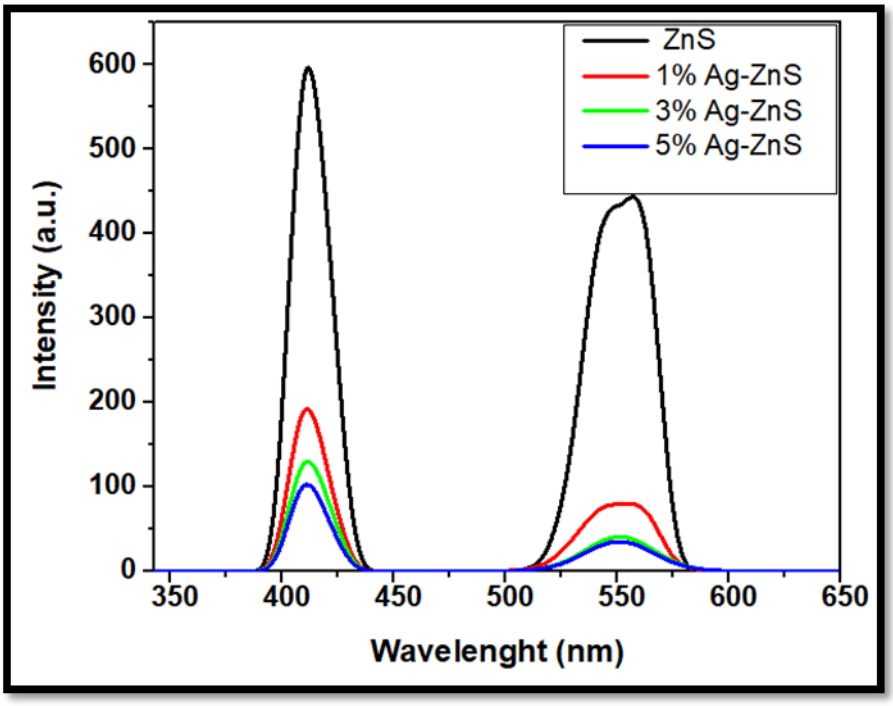

Figure 4.12: PL spectra of ZnS, 1, 3 and 5% Ag-ZnS nanoparticles

4.3.3. *X*- ray diffraction (XRD) spectroscopy

The *X*-ray diffraction patterns (XRD) of Ag doped and undoped ZnS are presented in Figure 4.13. The pattern for undoped ZnS shows diffraction peaks at 2θ values of 28.38, 47.84 and 56.55 corresponding to the respective diffraction planes of (111), (220) and (311) (Synnott et al., 2013).The XRD patterns for Ag doped ZnS nanoparticles contains new diffraction peaks at 2θ values of 38.11, 43.57, 62.83 and 76.81 corresponding to metallic silver (Li et al., 2012). The appearance of Ag peaks in the doped ZnS nanoparticles was in contrast to results obtained for the ZnO and TiO_2 nanoparticles above and suggested that Ag was deposited on the ZnS crystal lattice (Murugadoss and Chattopadhyay, 2008; Ramasamy et al., 2012; Sivakumar et al., 2014). Their crystallite size was determined from using the Debye-Scherrer formula (Lv et al., 2011).

$$D = 0.94.\lambda // (\beta.\cos\theta) \quad (4)$$

Where, *D* is average size of particle; λ is the X-ray wavelength (= 0.15406 nm), β is full width at half-maxima of diffraction peak (at $2\theta = 27^{\circ}$); and θ is the angle of diffraction with geometric factor equal to 0.94. The crystallite size increases as the doping agent was added from 13.48 to 18.12 nm.

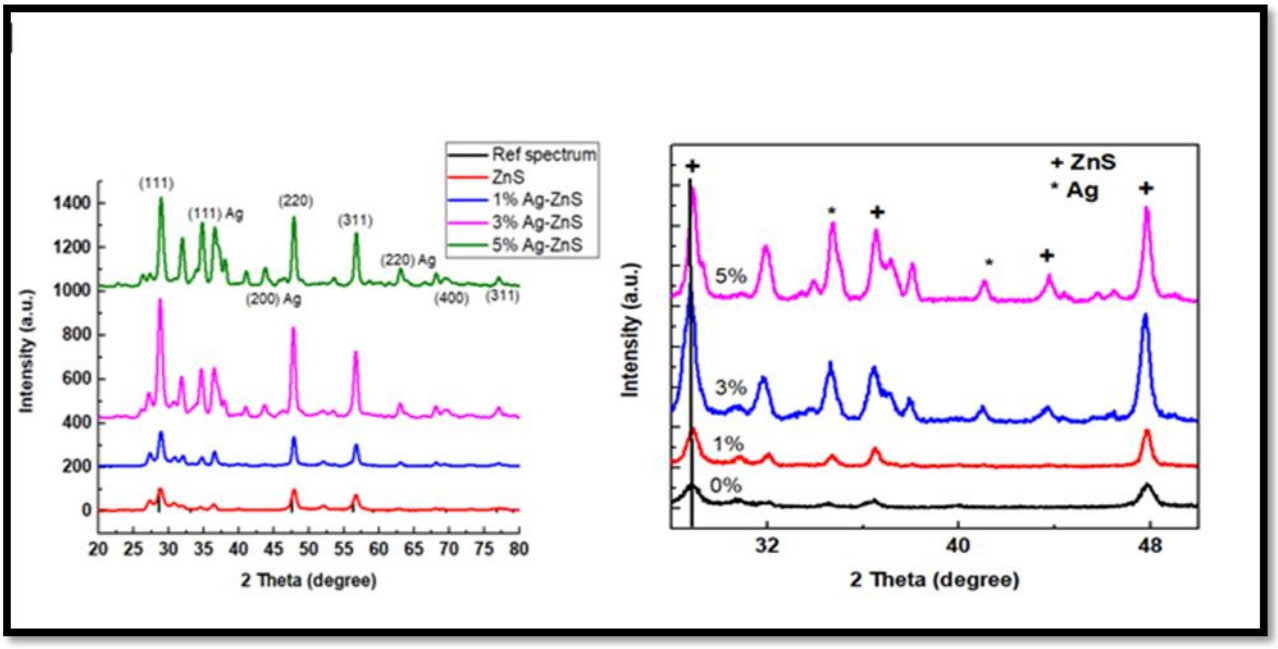

Figure 4.13: XRD spectrum of ZnS, 1, 3 and 5% Ag-ZnS nanoparticles and (b) enlarged regions of the XRD patterns

Table 6: Crystallite size of ZnS and silver doped nanoparticles

Particles	Crystallite size (nm)
Pure ZnS	13.48
1% Ag-ZnS	14.70
3% Ag-ZnS	16.42
5% Ag-ZnS	18.12

4.3.4. Fourier Transform Infrared (FTIR) spectroscopy

The FTIR spectra of ZnS and Ag-ZnS nanoparticles was also performed to identify the functional groups present and Figure 4.14 shows the spectra. The peaks at 1065, 627 and 497 cm^{-1} is due to Zn-S vibrations and those observed at 1063, 1121, 1212, 1975, 2157, 2984, 2907, 2144 cm^{-1} represented the microstructural formations (Devi et al., 2007; Kuppayee et al., 2011).The broad absorption peak centered at 3671 cm^{-1} corresponds to the OH group which indicates the existence of absorbed water on the surface of the nanocrystals. A shift of the peaks of the functional groups toward a higher wavenumbers was observed and became more intense as the amount of Ag increased. The peak around 3000 and 3500 cm^{-1} of 5% Ag-ZnS is broader compared to other samples. This confirms the existence of more OH group on the surface which is believed to favour the good photocatalytic activity. In comparison to other percentage doped ZnS, the more intense peak around 876 cm^{-1} for 5% Ag suggests that the higher doping quantity affected the structure of the ZnS crystal**.**

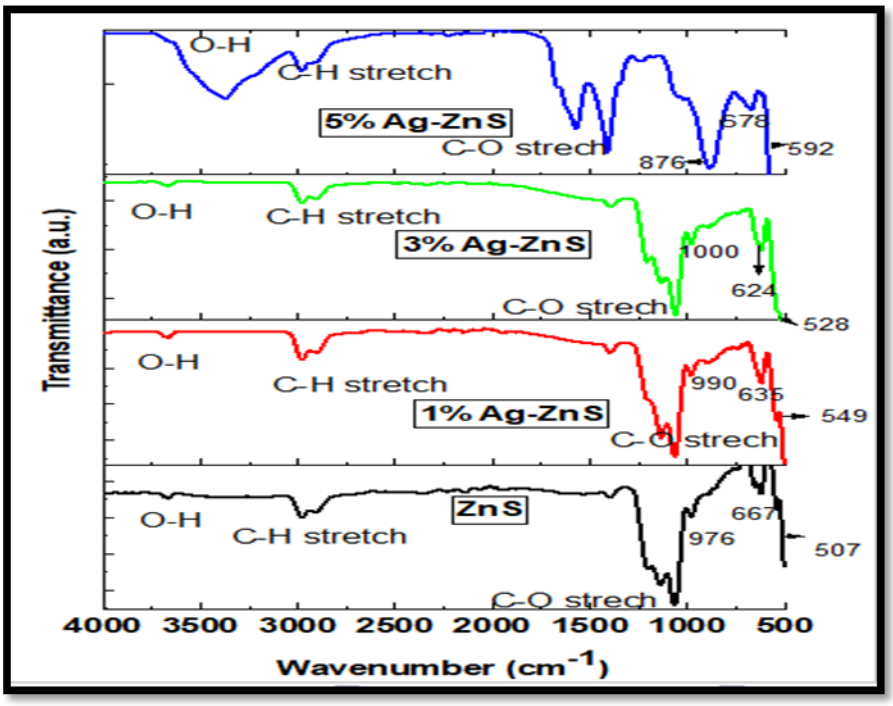

Figure 4.14: FTIR of ZnS, 1, 3 and 5% Ag-ZnS nanoparticles

4.3.5. Transmission Electron Microscope (TEM) analysis

The morphology of the obtained ZnS and 5% Ag doped ZnS synthesized by the chemical precipitation method has been determined by TEM. Figure 4.15 (a) and (b) show that the particles were spherical and agglomerated.

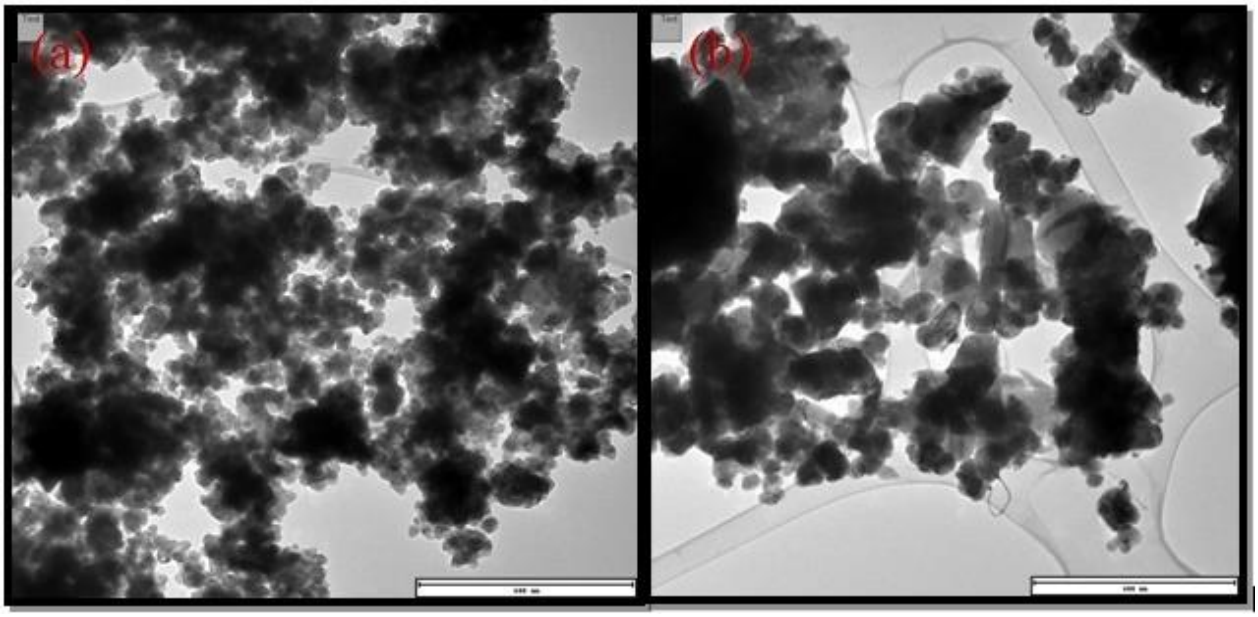

Figure 4.15: TEM images of (a) ZnS and (b) 5% Ag-ZnS nanoparticles

4.4. Degradation of 2-chlorophenol

The absorption peaks of 2-chlorophenol (2-CP) were determined before degradation using *UV*-Vis spectra. Figure 4.16 shows the absorption spectra of 50 ppm of 2-CP and it was observed that 2-CP exhibited two emissions peaks at 220 and 274 nm. The absorption spectra of the different 2-CP concentration (8, 20 and 50 ppm) were measured at a maximum wavelength of 220 nm.

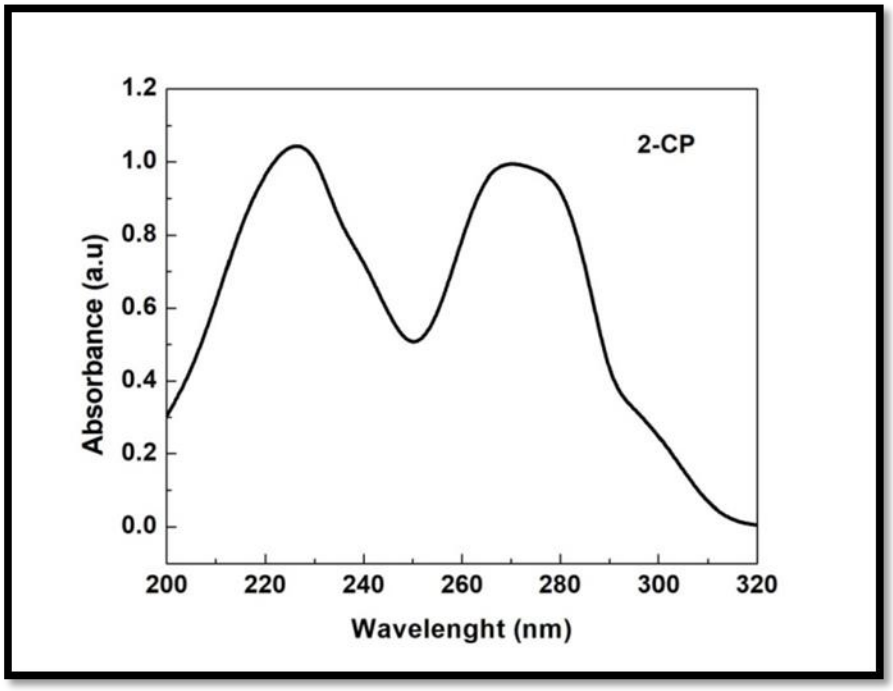

Figure 4.16: UV-Vis spectra of 2-chlorophenol

4.4.1. Degradation of 2-chlorophenol using Undoped and Ag Doped TiO_2 Nanoparticles

4.4.1.1. Degradation of 2-CP without Catalyst/Undoped TiO_2 Nanoparticles

A preliminary 2-CP degradation experiment was carried out in the absence and presence of the TiO_2 nanoparticles using 50 ppm 2-CP and 5mg of TiO_2 nanoparticles at pH of 10.5 for a period of 150 min. The percentage degradations are shown in Figure 4.17 which shows that irradiation of 2-CP with UV light for a period of 150 min resulted in an approximate mineralization of 4.6 percent.

However, irradiation of 2-CP at the same condition in the presence of TiO_2 nanoparticles enhanced the 2-CP degradation resulting about 16 percent 2-CP degradation. The degradation percentage was calculated using the expression below.

$$\%D = (C_0 - C_t \,/\, C_0) \times 100$$

Where C_0 (mg/L) is the concentration of 2-CP at t = 0 min, C_t (mg/L) is the concentration at each intervals of the radiation time.

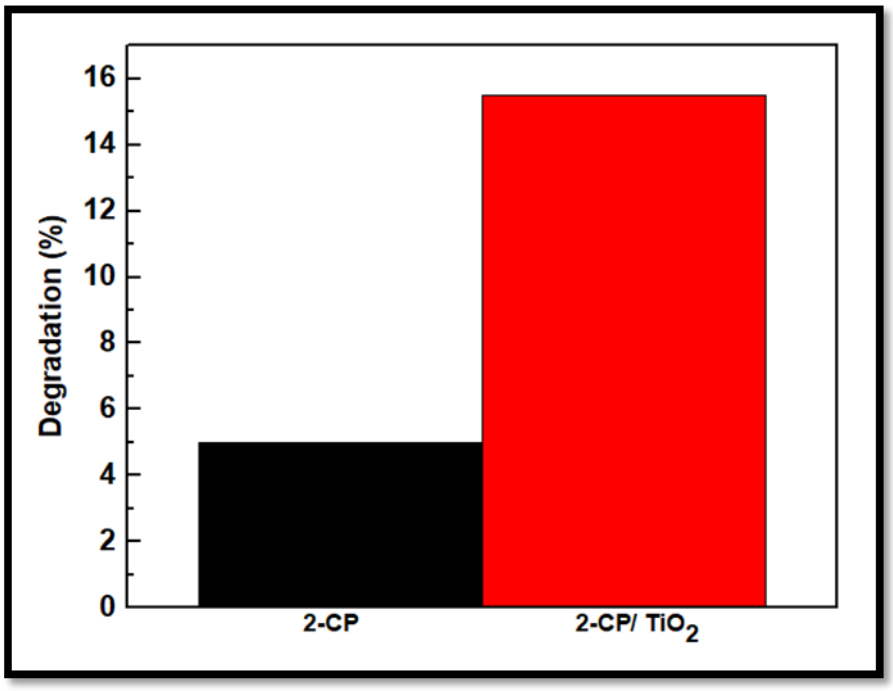

Figure 4.17: Degradation of 2-CP without and withTiO_2 nanoparticles using 50 ppm (2-CP) and 5 mg of TiO_2 nanoparticles at pH = 10.5, irradiation time = 150 min

4.4.1.2. Degradation of 2-chlorophenol with Ag Doped TiO_2 Nanoparticles

Further 2-CP degradations comparisons were carried out using both the different percentages of Ag doped and undopedTiO_2 nanoparticles. All experiments were performed using 300 mL of 50 ppm of 2-CP and 5 mg catalyst. The mixture was initially stirred for 30 min in the dark to allow for the adsorption of the 2-CP onto the TiO_2 nanoparticles surfaces and then the mixture was irradiated for 150 min. The results of these experiments are shown in Figure 4.18. It was observed that the solutions with Ag doped TiO_2 nanoparticles showed a better degradation percentage for 2-CP than the undoped TiO_2nanoparticles. The total degradation percentages after 150 min of irradiation for each photocatalyst was 4.98%, 15.5%, 20.5%, 26.76% and 30.36% for UV light only, undoped TiO_2, 1% Ag-TiO_2, 3% Ag-TiO_2, and 5% Ag-TiO_2, respectively. The results clearly confirm that the addition of doping of TiO_2 surfaces improves the degradation performance.

A similar observation showing that doping of Ag onto TiO_2 surface enhances it photocatalytic activity and expands the response range of the photocatalyst to the visible light region has been reported (Ilyas et al., 2011; Park and Lee, 2014). The Figure 4.18 showed that the best degradation result was achieved with the 5% Ag-TiO_2; this confirms that the amount of Ag doped onto the TiO_2 surface plays important role in the degradation efficiency of the pollutant. At higher dopant ion concentration (5% Ag), silver can easily accept the electrons and reduce the rapid recombination rate of photogenerated electron-hole pairs. Following the results of this experiment, further studies were carried out using the 5% Ag-TiO_2 nanoparticles due to its high degradation percentage.

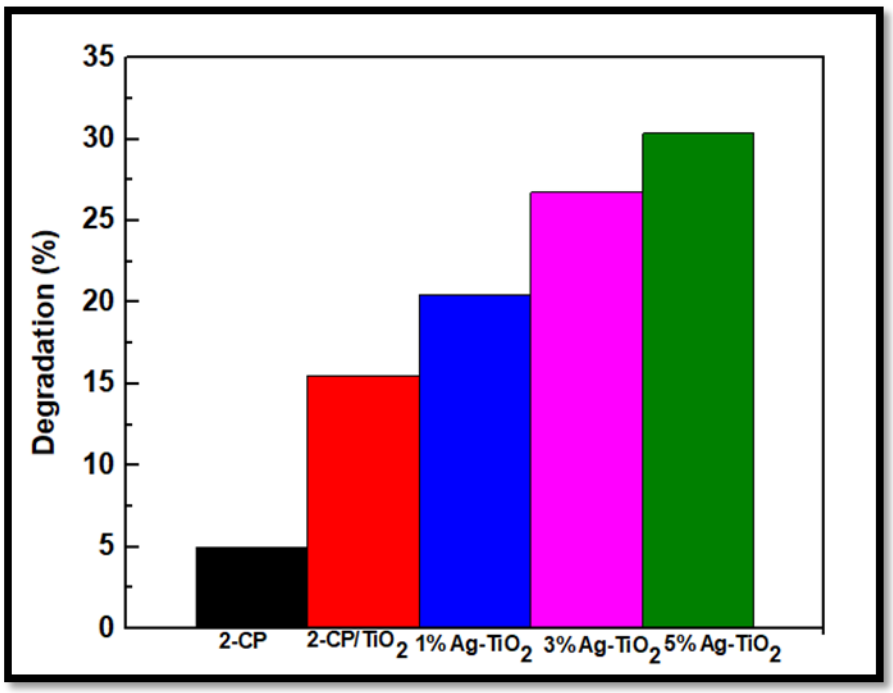

Figure 4.18: Comparative 2-CP degradation of undoped and Ag doped TiO_2 nanoparticles using 2-CP concentration of 50 ppm at pH = 10.5 and catalyst dosage of 5 mg, irradiation time = 150 min

4.4.1.3. Factors Influencing the Photocatalytic Degradation of 2-chlorophenol

4.4.1.3.1. Effect of 2-CP Initial Concentration

The starting concentration of 2-CP is an important factor in the performance of the catalyst. The effect of 2-CP starting concentrations was investigated from 8 to 50 ppm using Ag doped TiO_2

nanoparticles dosage of 11.25 mg at an irradiation time of 150 min and the results are shown in Figure.4.19. It was observed that with an increase of initial concentration of 2-CP, the percentage degradation of 2-CP by the 5% Ag-TiO_2 decreased. The percentage removals were 74.4, 45.5 and 30.4 % for 8, 20 and 50 ppm of the initial 2-CP concentrations solutions, respectively. Similar results were reported by Rideh et al. (1997). This could be attributed to the fact that at higher concentration, the UV light is blocked from reaching the surfaces of the Ag doped TiO_2 nanoparticles. Thus the number of photons or path length of photons which strikes the surface of the photocatalystis reduced leading to decrease the number of electrons excited (Sobana et al., 2008; Pouretedal et al., 2009b).

Consequently the amount of hydroxyl radicals formed on the surface to attack the organic pollutant is reduced, resulting in the decreased photocatalytic efficiency (Rashid et al., 2015b). The best percentage degradation of 2-CP was obtained at 8 ppm. This implies that at lower concentration, smaller amounts of 2-CP molecules are absorbed and there is availability of photogenerated holes for the production of hydroxyl radicals (Behnajady et al., 2006; Karunakaran and Dhanalakshmi, 2008; Ba-Abbad et al., 2016).

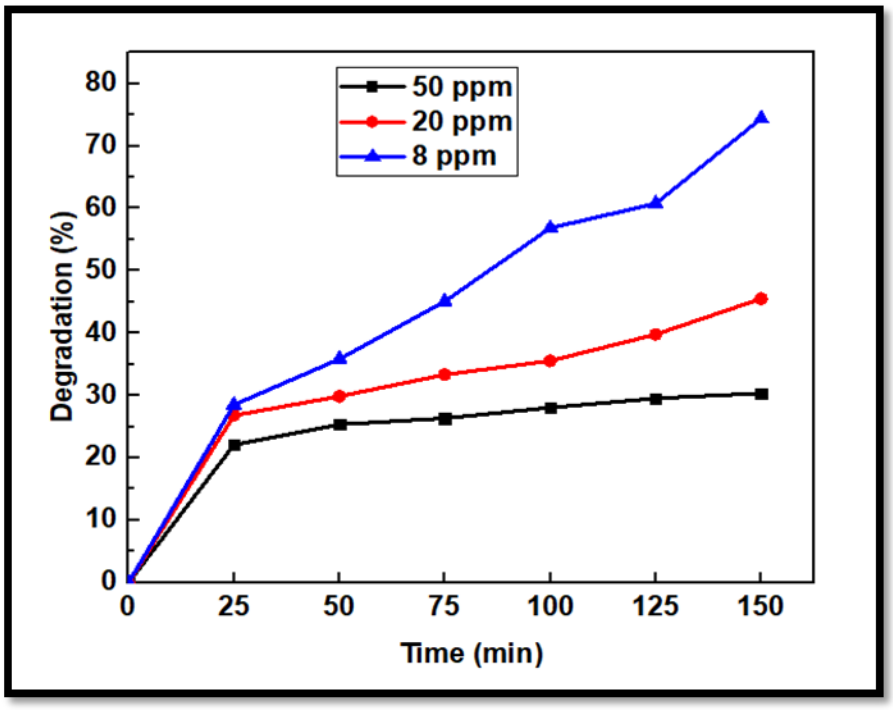

Figure 4.19: Effect of pollutant concentration. Catalyst loading (5% Ag-TiO_2) = 11.25 mg, pH = 10.5, irradiation time = 150 min

4.4.1.3.2. Effect of Catalyst Loading

The effect of Ag doped TiO_2 nanoparticles loading experiments was investigated to determine the optimum amount of the Ag doped TiO_2 nanoparticles on the degradation efficiency of 2-CP. Various masses (5, 7.5 and 11.25 mg) of the Ag doped TiO_2 nanoparticles were employed in the degradation of 8 ppm of 2-CP at pH 10.5, and the experimental results are depicted in Figure 4.20. The maximum degradation of 2-CP was observed with the Ag doped TiO_2 nanoparticles dose of 11.25 mg as shown in Figure 4.19. This trend was attributed to the fact that increases in the Ag doped TiO_2 nanoparticles dosage led to increase in the amount of $OH^{\bullet}$ radical produced from irradiated photocatalyst and enhanced the degradation efficiency.

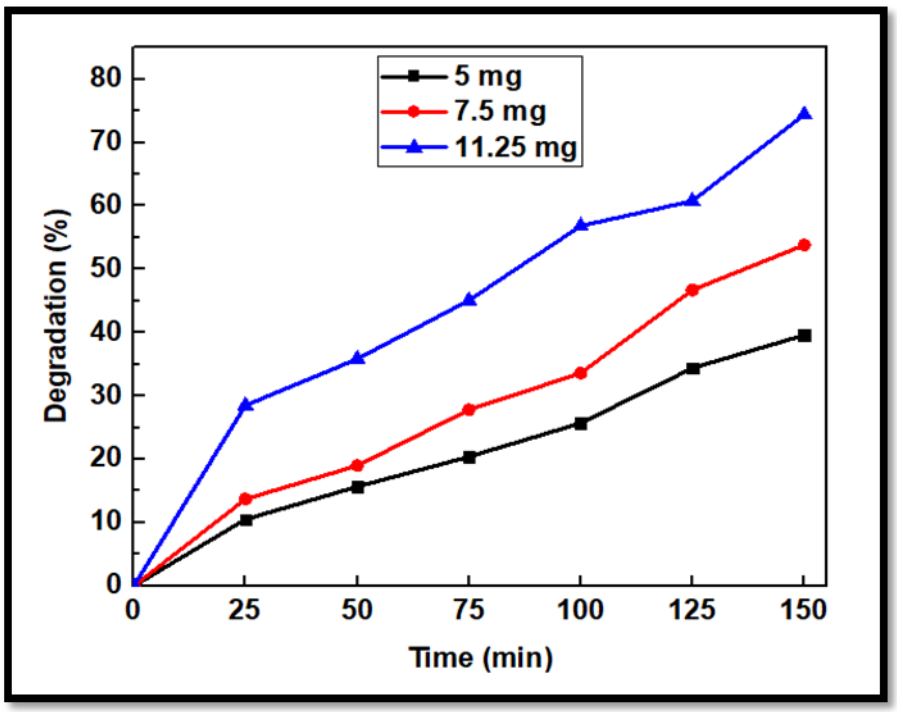

Figure 4.20: Effect of catalyst loading (5% Ag-TiO_2), 2-CP = 8 ppm, pH = 10.5, irradiation time = 150 min

4.4.1.3.3 Effect of pH

The pollutant solution pH is a crucial parameter for the photocatalytic reaction. The effect of pH on the degradation of 2-CP by the Ag doped TiO_2 nanoparticles was investigated in the pH range of 4 to 10.5. The pH was adjusted by using 0.1 M of HCl or 0.1 M NaOH. Figure 4.21 shows the

effect of pH on 8 ppm of 2-CP degradation using Ag doped TiO_2 nanoparticles dose of 11.25 mg. Figure 4.21 showed that the photo-degradation efficiency of 2-CP was affected by the change of pH; the degradation percentages are 45.7, 60.1 and 74.4 % for pH 4.11, 7.05 and 10.5, respectively. In acidic medium (pH lower than its pH_{PZC} = 5.6 – 6.4 for 2-CP), the surface of TiO_2 is protonated and positively charged, while in basic medium (pH higher than its pH_{PZC} = 5.6 – 6.4), TiO_2 surface is deprotonated and it is negatively charged (Rashid et al., 2015a); the deprotonation results in the release of more hydroxyl ions which reacts with electron holes to produce $OH^{\cdot}$ radicals that enhances the degradation efficiency. Thus, the degradation of 2 CP increased as the pH increased from 4.5 to 10.5.

A similar observation has been noted by (Barakat et al., 2005) who investigated the photocatalytic degradation of 2-CP using Co-TiO_2 with up to 93.41% efficiency at pH of 9.

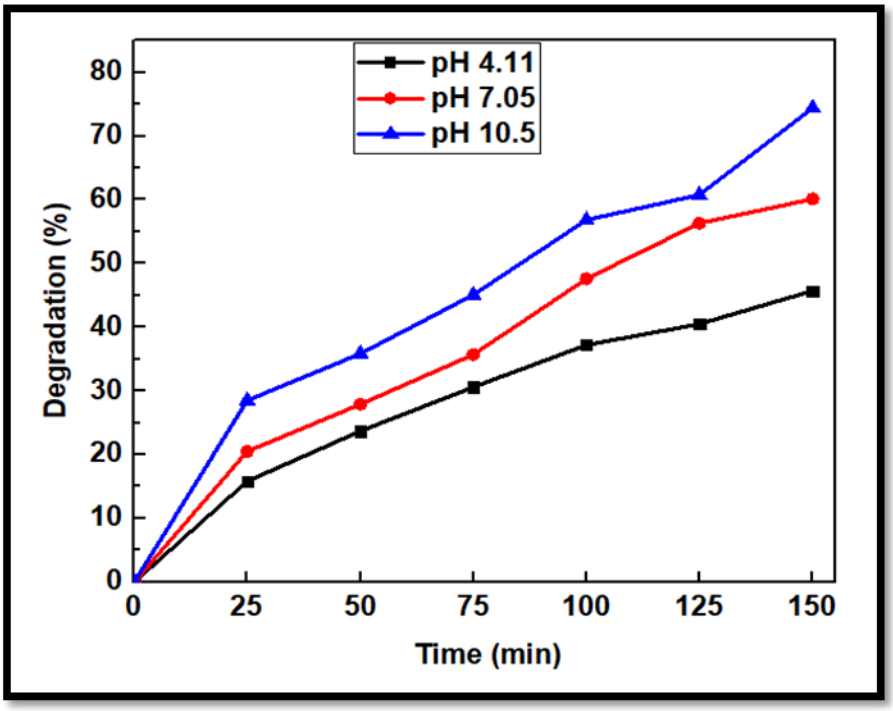

Figure 4.21: Effect of pH, 2-CP = 8 ppm, catalyst dosage (5% Ag-TiO_2) = 11.25 mg, irradiation time = 150 min

4.4.1.4. Conclusions

The study assessed the degradation of 2-chlorophenol in the absence and presence of Ag doped TiO_2 nanoparticles, as well as the effect of various ambient conditions on the degradation efficiency. Degradation efficiency of 2-CP was not significant in the absence of the Ag doped TiO_2 nanoparticles but with the TiO_2 nanoparticles, the efficiency was improved. Doping of Ag in the Ag doped TiO_2 nanoparticles greatly enhanced the degradation efficiency. The 5% Ag doped TiO_2 nanoparticles had the best 2-CP degradation capacity when compared to other doping percentages. The Ag doped TiO_2 nanoparticles works best at lower 2-CP concentration, and high Ag doped TiO_2 nanoparticles loading seemed to show corresponding degradation while the optimum pH for degradation is 10.5.

4.4.2. Degradation of 2-chlorophenol using ZnO and Ag Doped ZnO Nanoparticles

4.4.2.1. Degradation of 2-CP without Catalyst/ Undoped ZnO Nanoparticles

The photocatalytic degradation of 2-CP without a catalyst and in the presence of undoped ZnO nanoparticles were investigated with 50 ppm of 2-CP and 5 mg of catalyst loading under UV irradiation. The pH was adjusted at 4.11, 7.05 and 10.5 using HCl and NaOH. Figure 4.22 shows the results of 2-CP degradation at pH 10.5. Figure 4.22 shows that a better percentage of 2-CP was obtained in the presence of ZnO catalyst, with a percentage degradation of 12.56% compared to 2-CP without catalyst after 150 min of irradiation.

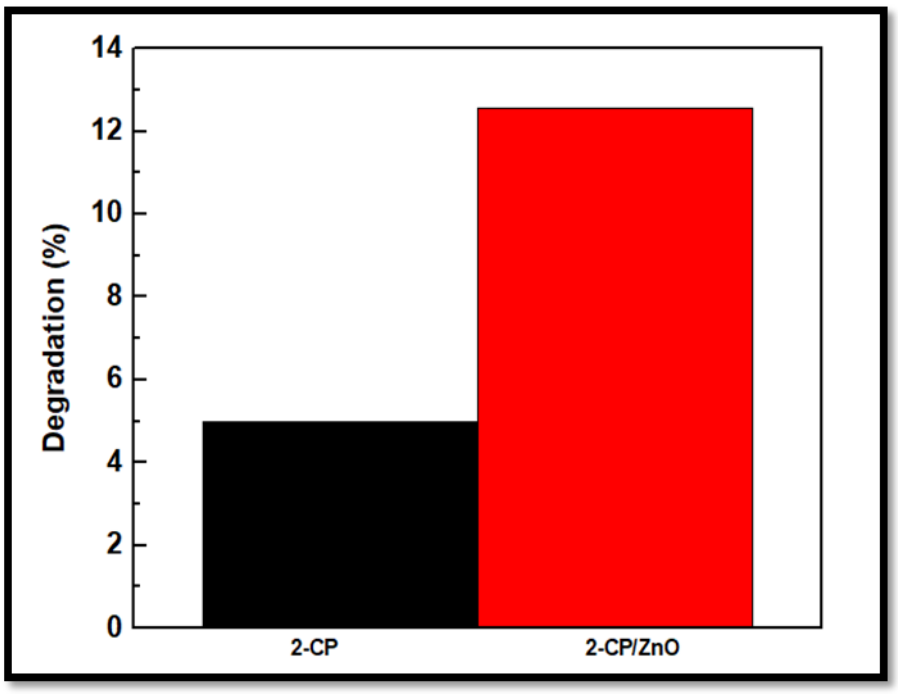

Figure 4.22: Degradation of 2-CP without catalyst and with undoped ZnO catalyst. Catalyst loading = 5 mg, pH = 10.5, irradiation time = 150 min

4.4.2.2. Degradation of 2-CP with Undoped/ Ag Doped ZnO Nanoparticles

Figure 4.23 shows that the addition of Ag into ZnO surface resulted in the improvement of the degradation percentage removal of 2-CP. The maximum degradation of 2-CP were 28.9%, 28.2% and 23.5% for 1% Ag-ZnO, 3% Ag-ZnO and 5% Ag-ZnO nano-photocatalyst, respectively, after 150 min irradiation as shown in Figure 4.23.

The efficiency of degradation with the addition of Ag into ZnO surface indicated that Ag plays a significant role in the photocatalyst activity for the degradation of 2-chlorophenol. The 1% Ag was the most efficient concentration of silver compared to 3 and 5% Ag. This showed that 1% is the optimum concentration dopant ion, and at this amount the penetration of the light in the solution occurred easily. In contrary at 3 and 5% Ag-ZnO the degradation percentage may decrease due to the excess amount of Ag which covers the surface preventing the light and pollutant adsorption.

In addition, at higher dopant ion concentration, the dopant ion can react as a recombination centre due to an excess of electrons accumulated. This increases the reaction between the dopant ion sites and the photogenerated holes and promoted the electron-hole recombination (Gnanaprakasam et al., 2016; Cardoza-Contreras et al., 2019). The photocatlytic degradation of 2-chlorophenol was further studied with 1% Ag-ZnO nanoparticles by investigating parameters such as catalyst mass, pollutant concentration and pH of the solution.

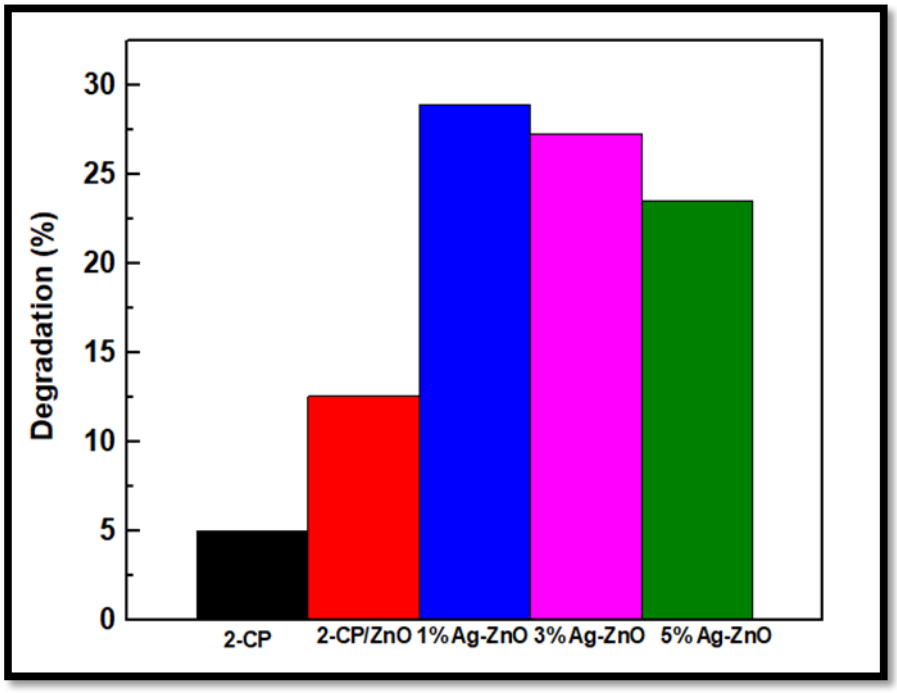

Figure 4.23: Comparative study between undoped and Ag doped ZnO nanoparticles for the photocatalytic degradation of 2-CP (50 ppm), pH = 10.5 and catalyst loading = 5 mg, irradiation time = 150 min

4.4.2.3. Factors Influencing the Photocatalytic Degradation of 2-chlorophenol

4.4.2.3.1. Effect of 2-CP Initial Concentration

The initial pollutant concentration of 2-CP was investigated by varying the concentration from 8, 20 and 50 ppm. Figure 4.24 shows the results of the photocatalytic degradation of 2-CP at pH 10.5 with 1% Ag-ZnO nano-photocatalyst. The maximum percentage degradation of 57.8%, 50.4% and 28.9% was obtained with 8 ppm, 20 ppm and 50 ppm, respectively.

At a higher concentration, the percentage degradation is lower because of the insufficient number of the active sites on the photocatalyst surface for 2-chlorophenol to degrade.

In addition, the insufficient number of active sites reduces the available actives sites for the generation of hydroxyl radicals (OH·) (Ba-Abbad et al., 2013a). In addition, an increase of the initial pollutant concentration decreases the number of photons reaching the catalyst surface and reduces their adsorption by the photocatalyst and decreases the 2-CP degradation efficiency (Krishnakumar et al., 2010). A similar observation was made for the degradation of phenol and benzoic acid (Benhebal et al., 2013).

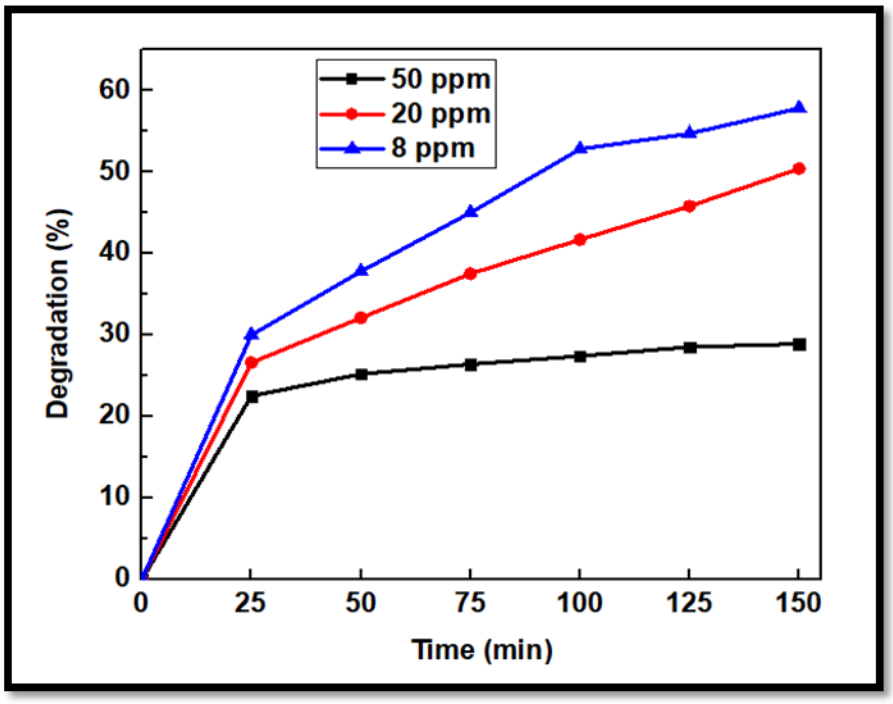

Figure 4.24: Effect of initial concentration of 2-CP. Catalyst loading (1% Ag-ZnO) = 5 mg, pH = 10.5, irradiation time = 150 min

4.4.2.3.2. Effect of Catalyst Loading

The catalyst loading effect was investigated from 5, 7.5 and 11.25 mg at optimum values. Figure 4.25 shows the photocatalytic degradation of 8 ppm of 2-CP at pH 10.5 with different amounts of 1% Ag-ZnO nano-photocatalyst. The results show that an increase in the amount of catalyst

loading lead to a decrease the photocatalytic degradation efficiency and the degradation percentage of 57.8%, 42.3% and 35.25% were obtained with 5, 7.5 and 11.25 mg, respectively. At higher catalyst loading, the number of exposed catalyst active sites on the catalyst surface is reduced which in turn reduces the number of hydroxyl radicals ($OH^{\bullet}$) formed. The hydroxyl radicals ($OH^{\bullet}$) are the main reactive species for the oxidation of 2-CP molecules. Also, at higher catalyst loading, the turbidity of the solution increases and this blocks the penetration of the light into the solution which reduces the availability of the photon for the degradation of the adsorbed 2-CP molecules on the catalyst surface (Gnanaprakasam et al., 2016). Similar results have been reported for the photodegradation of others organic pollutants (Barakat et al., 2005).

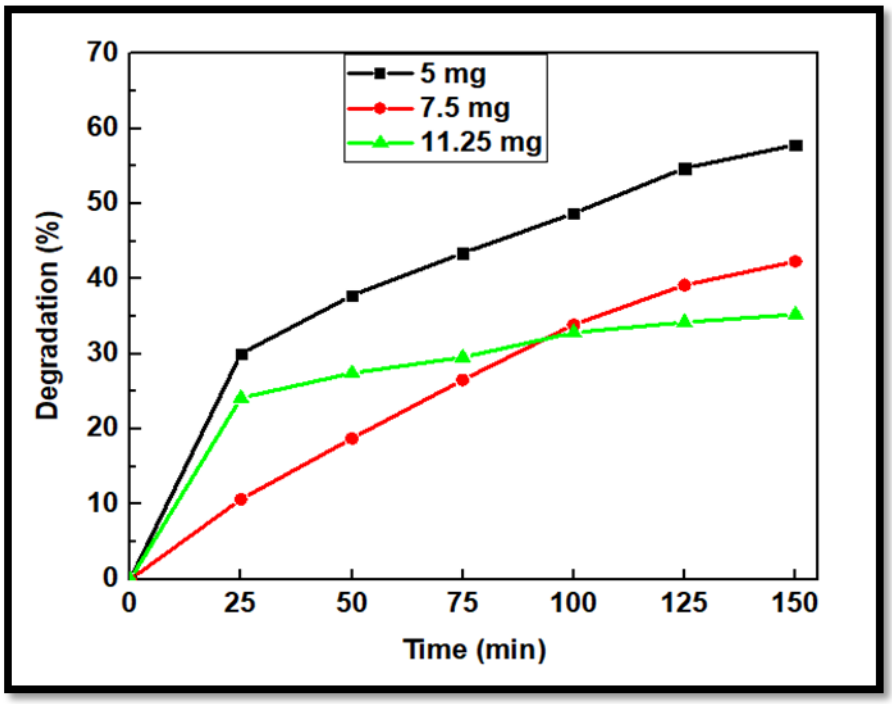

Figure 4.25: Effect of catalyst loading (1% Ag-ZnO), [2-CP] = 8 ppm, pH = 10.5, irradiation time = 150 min

4.4.2.3.3. Effect of pH

The effect of pH on the photocatalytic degradation of 2-chlorophenol was carried out at different pH values (4.11, 7.05 and 10.5) with the optimized experimental condition (A mixture of 300 mL of 8 ppm of 2-CPsolutionand 5 mg of 1 % Ag-ZnO loading as shown in Figure 4.26).

The pH is crucial for the degradation because it affects the surface charge of the catalyst surface (Sivakumar et al., 2014; Gnanaprakasam et al., 2016; Kotlhao et al., 2018b). It has been reported that undoped and silver doped ZnO catalysts have the same pH zero point charge of 9.0 (Tan et al., 2003; Ba-Abbad et al., 2013b).

At pH below its pHzcp value (pHzcp< 9), the surface of ZnO is protonated (positively charged) and deprotonated (negatively charged) at pH above 9.0.Thus, the ionization state of the photocatalyst can be an advantage or disadvantage for the photocatalytic degradation of the organic pollutant. It was observed in Figure 4.26 that the highest photocatalytic degradation of 2-CP was obtained at alkaline pH (10.5). The results have shown a total degradation of 57.8%, 52.5% and 40.45% for pH 10.5, 7.05 and 4.11, respectively.

Similar results have been reported in the literature for the photodegradation of other organic pollutants using doped ZnO (Degen and Kosec, 2000; Habibi and Rahmati, 2015). In acidic pH, low degradation percentage of 2-CP was obtained due to the lower number of OH^- ions which resulted in less production of $OH^\cdot$ radicals; hence the photocatalytic degradation of 2-CP decreases (Ravishankar et al., 2014; Bechambi et al., 2016). On the other hand at alkaline medium (pH =10.5) the surface of the catalyst is negatively charged, hydroxide ions became the predominant species and the surface concentration of 2-CP is higher (Bechambi et al., 2015; Kotlhao et al., 2018b). In addition, at pH 10.5 a constant number of OH^- ions and 2-CP concentration is produced which will react with holes on the valence band to produce hydroxide radical species; these hydroxyl radicals will oxidize 2-CP molecules. In order at acidic pH ZnO molecules dissolved due to its amphoteric nature in the solution and the main existing Zinc species are Zn^{2+} and $Zn(OH)^{2+}$ (Behnajady et al., 2006). At basic pH, ZnO molecules are in the form of zincates such as $Zn(OH)_4^{2-}$ (Ba-Abbad et al., 2013a) and enhance the degradation efficiency of 2-chlorophenol.

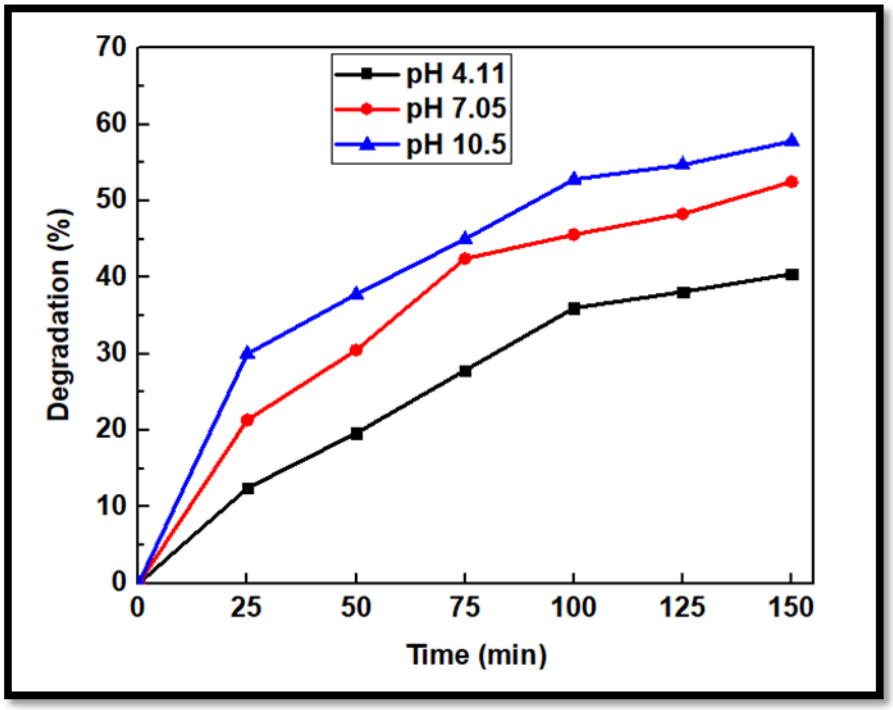

Figure 4.26: Effect of pH; [2-CP] = 8 ppm, catalyst loading (1% Ag-ZnO) = 5 mg, irradiation time = 150 min

4.4.2.4. Conclusions

The photocatalytic degradation of 2-CP is enhanced with the addition of a catalyst compared to the presence of 2-CP without catalyst. However, it has been observed that addition of Ag into ZnO nanoparticles showed an improvement in the photocatalyst activity. The 1% Ag doped ZnO was shown to be the best photocatalyst for the degradation of 2-CP under UV irradiation compared to undoped and 3 and 5% Ag doped ZnO nanoparticles. It was observed that 57.8% of removal of 2-CP was obtained at optimum value of 8 ppm as initial concentration of 2-CP, 5 mg of catalyst loading and 10.5 of pH.

4.4.3. Degradation of 2-chlorophenol using ZnS and Ag Doped ZnS Nanoparticles

4.4.3.1. Degradation of 2-CP without Catalyst/Undoped ZnS Nanoparticles

The photocatalytic activity of the synthesized undoped and ZnS nanoparticles was assessed for the degradation of 2-CP using 50 ppm as a starting 2-CP concentration at pH 10.5 in absence of the catalyst and in the presence of undoped ZnS nanoparticles.

It was observed that 4.98% of 2-CP was degraded after 150 min of irradiation time in the absence of ZnS nanoparticles. The addition of the pristine ZnS in the mixture resulted in an increase in 2-CP photocatalytic degradation of 7 % after 150 min of irradiation time as shown in Figure 4.27.

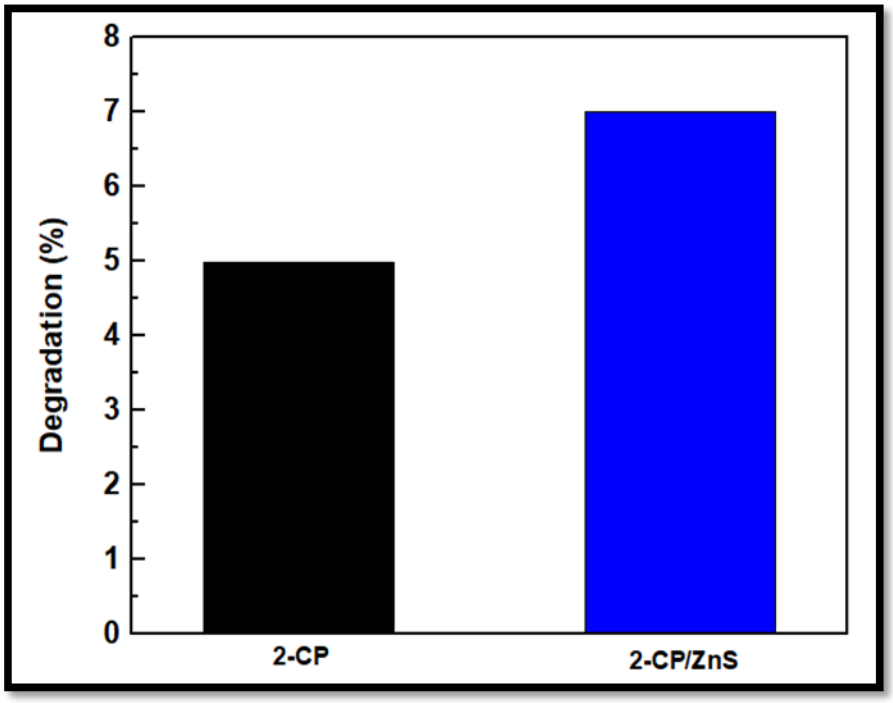

Figure 4.27: Degradation of 2-CP without catalyst and with undoped ZnS catalyst. Catalyst loading = 5 mg, pH = 10.5, irradiation time = 150 min

4.4.3.2. Degradation of 2-CP with Ag Doped ZnS Nanoparticles

The effect of Ag doping on the ZnS nanoparticles was investigated. Figure 4.28 shows the degradation of 50 ppm of 2-CP at pH 10.5 with ZnS nanoparticles dosage of 5 mg. It was revealed in Figure 4.28 that the degradation efficiency of 2-CP increased upon Ag doping; the highest degradation of 16.4% was obtained with 5% Ag-ZnS catalyst. A similar observation was made by Gupta et al. (2018).

This enhancement was attributed to the role Ag plays in electrontrapping which delays e^-/h^+ rapid recombination and thus enhancing the percentage degradation of the organic pollutants (Wang et al., 2004; Abdennouri et al., 2015). Figure 4.28 showed a percentage degradation of 11.2, 12.3 and 16% for the 1, 3 and 5 % Ag doped ZnS nanoparticles, respectively.

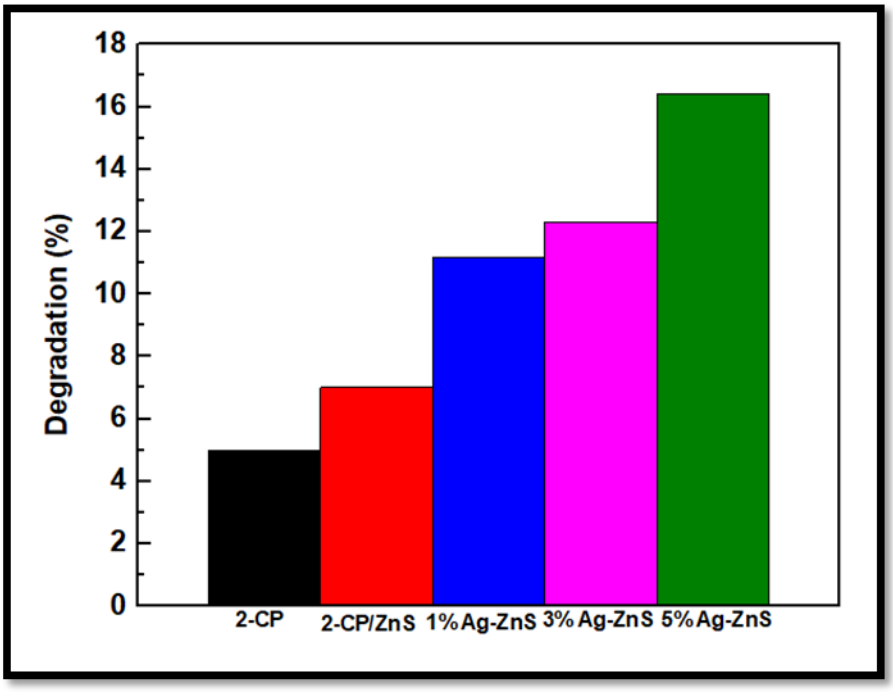

Figure 4.28: Comparative study between the undoped and Ag doped ZnS nanoparticles. [2-CP] = 50 ppm, pH = 10.5, catalyst loading = 5 mg, irradiation time = 150 min

The investigation of effect of catalyst loading, initial pollutant concentration and pH were done with the 5% Ag doped ZnS nanoparticles which exhibited the best degradation potential.

4.4.3.3. Factors Influencing the Photocatalytic Degradation of 2-chlorophenol by Ag doped ZnS Nanoparticles

4.4.3.3.1. Effect of 2-CP Initial Concentration

The photocatalytic activity of 5% Ag-ZnS nanoparticles was investigated under 150 min of UV-Vis irradiation. The effect of initial pollutant concentration was carried out using 8, 20 and 50 ppm concentrations of 2-CP, and the results are depicted in Figure 4.29. which shows that with an increase in the initial concentration of 2-CP, the degradation percentage of 2-CP by the nanophotcatalyst decreased. This was attributed to the fact that at higher concentrations of the Ag-ZnS nano-photocatalyst, the 2-CP percentage degradation was lower because of the because of the insufficient number of the active sites on the photocatalyst surface for 2-chlorophenol to degrade because these sites have been blocked by the numerous 2-CP in solution.

In addition the insufficient number of active sites causes the unavailability of actives sites for the generation of hydroxyl radicals ($OH^{\cdot}$). A similar observation has been reported by Han et al. (2009) and Anjum et al. (2017).

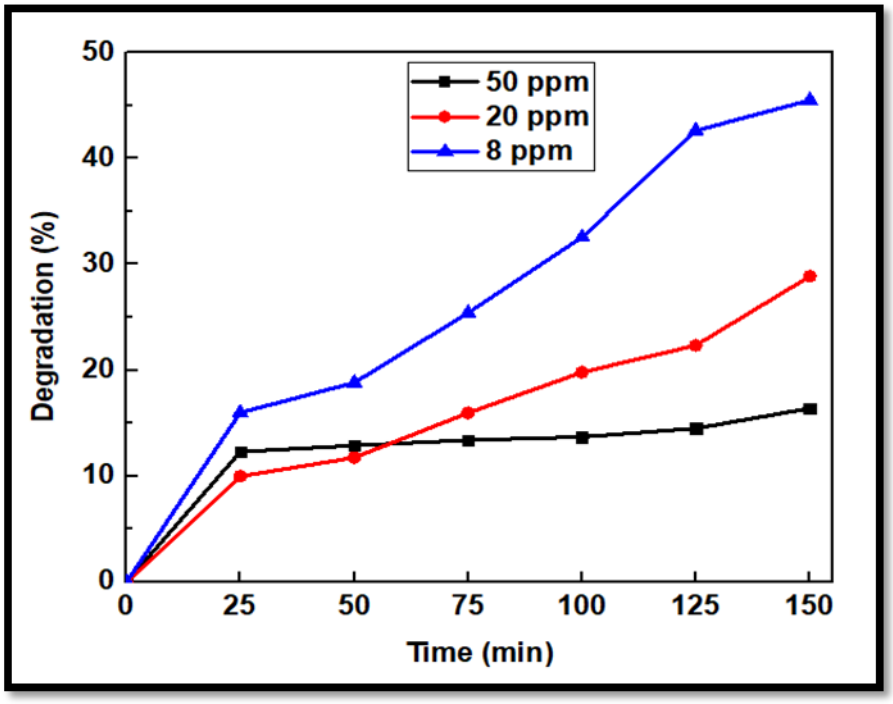

Figure 4.29: Effect of 2-CP initial concentration, catalyst loading (5% Ag-ZnS) = 5 mg, pH = 10.5, irradiation time = 150 min

4.4.3.3.2. Effect of Catalyst Loading

The effect of catalyst dose was studied using different amounts (5, 7.5 and 11.25 mg) of the Ag-ZnS photocatalyst, with the concentration of 2-CP kept constant (8 ppm) throughout the experiment. The results of the experiment are shown in Figure 4.30; it was observed that increasing of the Ag doped ZnS photocatalyst dosage above 5 mg resulted in reduced percentage degradation of 2-CP. A maximum percentage degradation of 52% was obtained at Ag doped ZnS photocatalyst dose of 5 mg, while 48.1% and 38.2% were obtained at 7.5 mg and 11.25 mg doses, respectively. At Ag doped ZnS photocatalyst dose of 5 mg, the actives sites are well dispersed which which facilitates the optimal penetration of UV light across to the pollutant (Daneshvar et al., 2004).

On the other hand, an increase in the catalyst dose increases the turbidity of the pollutant medium leading to a reduced amount of photons which can penetrate the surface and hence the photocatalytic activity of the pollutant decreases (Sivakumar et al., 2014).

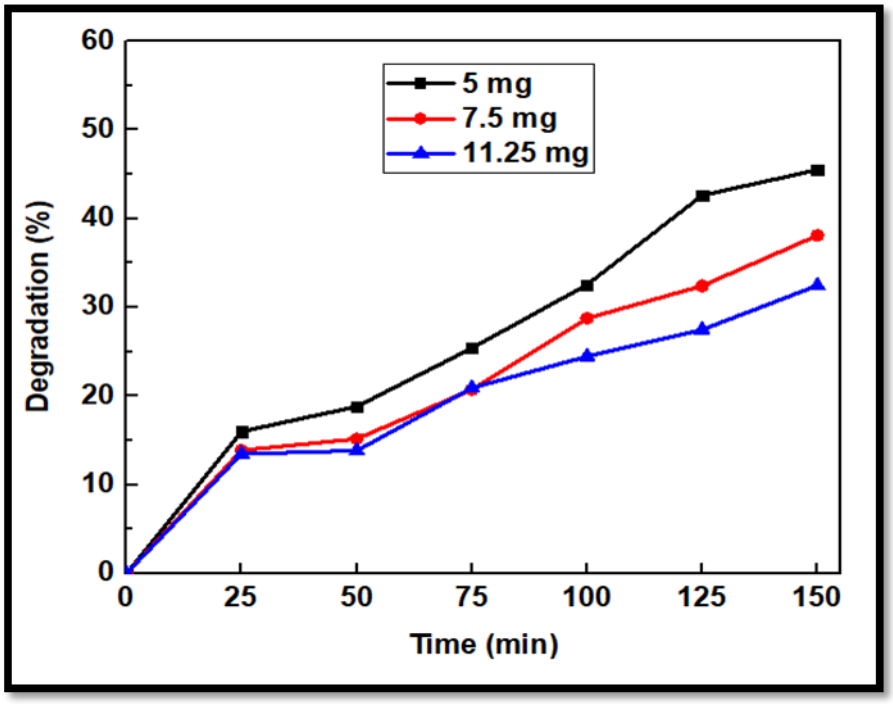

Figure 4.30: Effect of catalyst loading. [2-CP] = 8 ppm, catalyst used (5% Ag-ZnS), pH = 10.5, irradiation time = 150 min

4.4.3.3.3. Effect of pH

The pH is the most crucial parameter for the photocatalytic degradation analysis of organic compounds and in the generation of actives sites. The effect of pH on the photocatalytic degradation of 2-CP was investigated at different pH values (4.1, 7.0 and 10.5) with 8ppm of 2-CP, 5 mg of 5% Ag-ZnS and results are shown in Figure 4.31. It was observed that that the percentage degradation of 2-CP increased as the pH increased resulting in a maximum degradation of 45.5% at pH = 10.5. The results also showed that degradations of 31.8 and 25.2 % were obtained at pH 4.11 and 7.05, respectively. Thiscan be attributed to the fact that in acidic pH and neutral pH (pH below the point of zero charge for ZnS , pH ≤ 7-7.5(Gupta et al., 2018)), the surface of the photocatalyst is predominated by positive charges which reduces the production of hydroxyl radicals.

In addition, a low degradation value at pH ≤ pHzpc of ZnS may be due to the presence of excess Cl^- ions (from HCl solution used to adjust the pH of the solution), which will react with $OH^•$ radicals by forming the inorganic $ClO^{-•}$ (hyperchlorite) ion radicals which are known as less reactive species compare to $OH^•$ radicals. The percentage degradation was favoured at pH above the pHpzc value. At higher pH, the surface of the photocatalyst is mostly dominated by negative charges, and there is formation of OH^- species. In addition, alkaline medium facilitates van der Waals interactions between 2-CP and the nano-photocatalyst; this enhances the adsorption of 2-CP to the catalyst surface and results in increased photocatalytic activity. Similarly $OH^•$ radicals can be formed due to a reaction between the hole in the valence band or molecules of water with hydroxide ions which favors the production of $OH^•$ radicals, the primary species responsible for photodegradation (Barjasteh-Moghaddam and Habibi-Yangjeh, 2011).

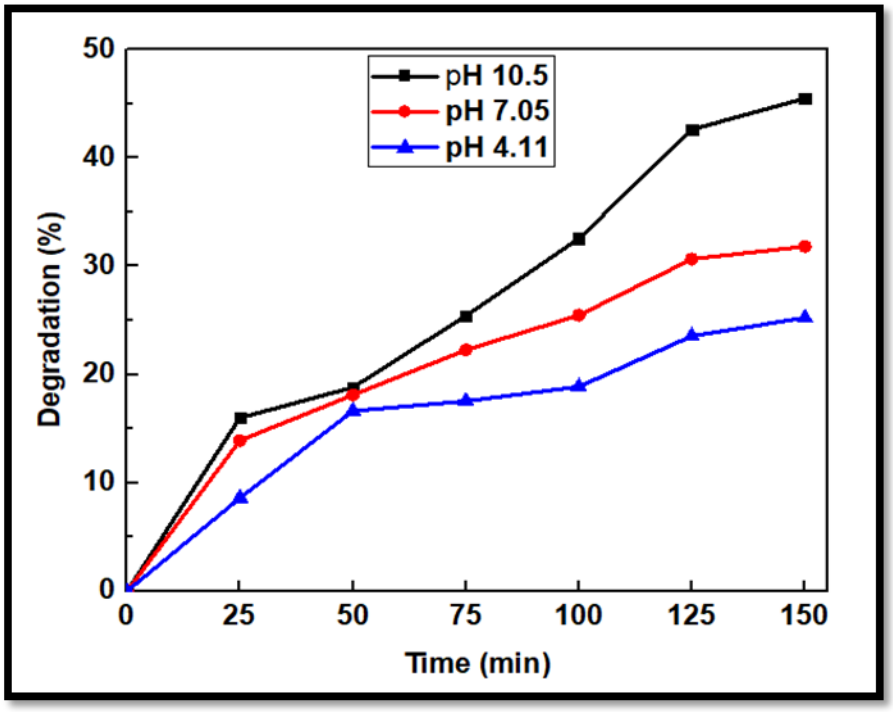

Figure 4.31: Effect of pH. [2-CP] = 8 ppm, catalyst loading (5% Ag-ZnS) = 5 mg, pH = 10.5, irradiation time = 150 min

4.4.4.4. Conclusions

The degradation results of 2-CP showed that the addition of Ag into ZnS nanoparticles enhanced the degradation of 2-CP better than the undoped ZnS nanoparticles. The best degradation result was obtained at Ag doping of 5% with 45.5 % 2-CP degradation capacity, at optimuim pH of 10.5 and 2-CP concentration of 8 ppm.

Chapter 5: General Conclusions and Recommendations

5.1. General Conclusions

Undoped and silver doped TiO_2, ZnO and ZnS nanoparticles were synthesized and used for the UV photocatalytic degradation of degradation of 2-chlorophenol. The TiO_2 and Ag doped TiO_2 nanoparticles were synthesized using the sol-gel method, while the chemical precipitation method was used for the synthesis of undoped and Ag doped ZnO and ZnS nanoparticles. The *UV*DRS results of the characterization forTiO_2, ZnO and ZnS showed band gap changes (reduction) after doping. The PL results exhibited reduced intensities upon doping suggesting that Ag delays the recombination of the photogenerated electron-hole pairs thus enhancing their photoactivity. The XRD analysis showed that the anastase, wurtzite and blende were the phases obtained for the TiO_2, ZnO and ZnS nanoparticles, respectively. It was noticed that addition of silver ion did not affected their respective structures. There was particle size reduction for the Ag doped TiO_2 upon doping; however, the particle sizes increased for ZnO and ZnS; all the particle sizes were within the nanoparticles range. The FTIR spectra results exhibited peaks unique to the synthesized TiO_2, ZnO and ZnS nanoparticles, while the TEM results showed shapes which were spherical and uniform in size. The degradation efficiency of all undoped nanoparticles was lower than Ag doped nanoparticles. However, different doping percentages gave optimum degradation efficiencies of the 2-chlorophenol. Parameters such as catalyst mass, initial pollutant concentration and pH played important roles that affect the degradation efficiencies. The optimum percentage degradation of 2-CP were 74.4, 57.8, and 45.5 % for 5% Ag-TiO_2, 1% Ag-ZnO and 5% Ag-ZnS, respectively, The amount of photocatalysts that produced optimum percentage degradation were 11.25 mg for TiO_2 and 5mg for the other two catalysts at pH 10.5 and 8 ppm of 2-CP.The Ag-TiO_2 proved to be the most efficient photocatalyst. Due to its cost and low toxicity, TiO_2 was adjudged the best photocatalyst for the degradation of 2-chlorophenol compared to the others two semiconductor photocatalysts.

5.2. Recommendations

Based on the study presented in this dissertation, it is strongly advised to perform further studies for the degradation of 2-chlorophenol under UV irradiation specifically with the following points in mind:

- Using the same preparation method for the preparation of the different nanoparticles for a better comparison.
- Study the effect of the different parameters for a longer time.
- Determine the secondary products formed during the degradation of 2-chlorophenol.
- Perform a reusability test.

References

ABBASI, M., RAFIQUE, U., MURTAZA, G. & ASHRAF, M. A. 2017. Synthesis, characterisation and photocatalytic performance of ZnS coupled Ag2S nanoparticles: A remediation model for environmental pollutants. *Arabian Journal of Chemistry*, 11, 827-837.

ABDENNOURI, M., ELHALIL, A., FARNANE, M., TOUNSADI, H., MAHJOUBI, F., ELMOUBARKI, R., SADIQ, M., KHAMAR, L., GALADI, A. & BAÂLALA, M. 2015. Photocatalytic degradation of 2, 4-D and 2, 4-DP herbicides on Pt/TiO2 nanoparticles. *Journal of Saudi Chemical Society,* 19**,** 485-493.

AHMAD, K. S. & JAFFRI, S. B. 2018. Phytosynthetic Ag doped ZnO nanoparticles: Semiconducting green remediators. *Open Chemistry,* 16**,** 556-570.

AHMED, S., RASUL, M., MARTENS, W. N., BROWN, R. & HASHIB, M. 2010. Heterogeneous photocatalytic degradation of phenols in wastewater: a review on current status and developments. *Desalination,* 261**,** 3-18.

AHMED, S., RASUL, M., MARTENS, W. N., BROWN, R. & HASHIB, M. 2011. Advances in heterogeneous photocatalytic degradation of phenols and dyes in wastewater: a review. *Water, Air, & Soil Pollution,* 215**,** 3-29.

AKBAL, F. & ONAR, A. N. 2003. Photocatalytic degradation of phenol. *Environmental Monitoring and Assessment,* 83**,** 295-302.

ALL-ABOUT-WATER-FILTERS. 2019. *7 Biggest Culprits Behind Water Pollution Around the World* [Online]. Available: http://all-about-water-filters.com/producers-water-pollution-around-the-world/#Water-Pollution-in-the-World-Today [Accessed].

ANJUM, M., OVES, M., KUMAR, R. & BARAKAT, M. 2017. Fabrication of ZnO-ZnS@ polyaniline nanohybrid for enhanced photocatalytic degradation of 2-chlorophenol and microbial contaminants in wastewater. *International Biodeterioration & Biodegradation,* 119**,** 66-77.

ANSARI, M. M., ARSHAD, M. & TRIPATHI, P. (2014). 'Study of ZnO and Mg doped ZnO nanoparticles by sol-gel process'. In S. Bhattacharyya, R. Chitra & N.K Sahoo (eds.), *Solid State Physics: Proceeding of The 59th DAE Solid State Physics Symposium, 2014, 16*-20 December, Taminau, India. America Institute of Physic, 123.

AUGUGLIARO, V., LITTER, M., PALMISANO, L. & SORIA, J. 2006. The combination of heterogeneous photocatalysis with chemical and physical operations: A tool for improving the photoprocess performance. *Journal of Photochemistry and Photobiology C: Photochemistry Reviews,* 7**,** 127-144.

AWAZU, K., FUJIMAKI, M., ROCKSTUHL, C., TOMINAGA, J., MURAKAMI, H., OHKI, Y., YOSHIDA, N. & WATANABE, T. 2008. A plasmonic photocatalyst consisting of silver nanoparticles embedded in titanium dioxide. *Journal of the American Chemical Society,* 130**,** 1676-1680.

BA-ABBAD, M. M., KADHUM, A. A. H., MOHAMAD, A. B., TAKRIFF, M. S. & SOPIAN, K. 2013a. Photocatalytic degradation of chlorophenols under direct solar radiation in the presence of ZnO catalyst. *Research on Chemical Intermediates,* 39**,** 1981-1996.

BA-ABBAD, M. M., KADHUM, A. A. H., MOHAMAD, A. B., TAKRIFF, M. S. & SOPIAN, K. 2013b. Visible light photocatalytic activity of Fe3+-doped ZnO nanoparticle prepared via sol–gel technique. *Chemosphere,* 91**,** 1604-1611.

BA-ABBAD, M. M., TAKRIFF, M. S., KADHUM, A. A., MOHAMAD, A. B., BENAMOR, A. & MOHAMMAD, A. W. 2017. Solar photocatalytic degradation of 2-chlorophenol with ZnO nanoparticles: optimisation with D-optimal design and study of intermediate mechanisms. *Environmental Science and Pollution Research,* 24**,** 2804-2819.

BA-ABBAD, M. M., TAKRIFF, M. S. & MOHAMMAD, A. W. 2016. Enhancement of 2-chlorophenol photocatalytic degradation in the presence Co2+-doped ZnO nanoparticles under direct solar radiation. *Research on Chemical Intermediates,* 42**,** 5219-5236.

BABU, N. S. & KHADAR, M. A.(2011) 'Photoluminescent effect of Ag 2 S coated ZnS nanoparticles'. *3rd International Congress on Ultra Modern Telecommunications and Control Systems (ICUMT)*, 2011, Buapet, Hungary, 5-7 October. Institute of Electrical and Electronics Engineers, 1-4.

BAHNEMANN, D. 2004. Photocatalytic water treatment: solar energy applications. *Solar energy,* 77**,** 445-459.

BAHNEMANN, W., MUNEER, M. & HAQUE, M. M. 2007. Titanium dioxide-mediated photocatalysed degradation of few selected organic pollutants in aqueous suspensions. *Catalysis Today,* 124**,** 133-148.

BAKARDJIEVA, S., STENGL, V., SZATMARY, L., SUBRT, J., LUKAC, J., MURAFA, N., NIZNANSKY, D., CIZEK, K., JIRKOVSKY, J. & PETROVA, N. 2006. Transformation of brookite-type TiO2 nanocrystals to rutile: correlation between microstructure and photoactivity. *Journal of Materials Chemistry,* 16**,** 1709-1716.

BAMUZA-PEMU, E. E. 2014. '*Photocatalytic degradation of phenolic compounds and algal metabolites in water*'*.* Doctoral dissertation, University of Pretoria.

BARAKAT, M., AL-HUTAILAH, R., QAYYUM, E., RASHID, J. & KUHN, J. 2014. Pt nanoparticles/TiO2 for photocatalytic degradation of phenols in wastewater. *Environmental technology,* 35**,** 137-144.

BARAKAT, M., SCHAEFFER, H., HAYES, G. & ISMAT-SHAH, S. 2005. Photocatalytic degradation of 2-chlorophenol by Co-doped TiO2 nanoparticles. *Applied Catalysis B: Environmental,* 57**,** 23-30.

BARJASTEH-MOGHADDAM, M. & HABIBI-YANGJEH, A. 2011. Effect of operational parameters on photodegradation of methylene blue on ZnS nanoparticles prepared in presence of an ionic liquid as a highly efficient photocatalyst. *Journal of the Iranian Chemical Society,* 8**,** S169-S175.

BECHAMBI, O., CHALBI, M., NAJJAR, W. & SAYADI, S. 2015. Photocatalytic activity of ZnO doped with Ag on the degradation of endocrine disrupting under UV irradiation and the investigation of its antibacterial activity. *Applied Surface Science,* 347**,** 414-420.

BECHAMBI, O., NAJJAR, W. & SAYADI, S. 2016. The nonylphenol degradation under UV irradiation in the presence of Ag–ZnO nanorods: effect of parameters and degradation pathway. *Journal of the Taiwan Institute of Chemical Engineers,* 60**,** 496-501.

BEHNAJADY, M., MODIRSHAHLA, N. & HAMZAVI, R. 2006. Kinetic study on photocatalytic degradation of CI Acid Yellow 23 by ZnO photocatalyst. *Journal of Hazardous Materials,* 133**,** 226-232.

BENHEBAL, H., CHAIB, M., SALMON, T., GEENS, J., LEONARD, A., LAMBERT, S. D., CRINE, M. & HEINRICHS, B. 2013. Photocatalytic degradation of phenol and benzoic acid using zinc oxide powders prepared by the sol–gel process. *Alexandria Engineering Journal,* 52**,** 517-523.

BORSE, P. H., VOGEL, W. & KULKARNI, S. 2006. Effect of pH on photoluminescence enhancement in Pb-doped ZnS nanoparticles. *Journal of colloid and interface science,* 293**,** 437-442.

BOXI, S. S. & PARIA, S. 2014. Effect of silver doping on TiO2, CdS, and ZnS nanoparticles for the photocatalytic degradation of metronidazole under visible light. *RSC Advances,* 4**,** 37752-37760.

CALLAHAN, M., SLIMAK, M., GABEL, N., MAY, I., FOWLER, C., FREED, J., JENNINGS, P., DURFREE, R., WHITMORE, F. & MESTRI, B. 1979. *Water-related environmental fate of 129 priority pollutants: Introduction and technical background, metals and inorganics, pesticides and PCBs*.Volume 1. Washington D.C: U.S Environmental Protection Agency.

CAO, Y., TAN, H., SHI, T., TANG, T. & LI, J. 2008. Preparation of Ag-doped TiO2 nanoparticles for photocatalytic degradation of acetamiprid in water. *Journal of Chemical Technology & Biotechnology: International Research in Process, Environmental & Clean Technology,* 83**,** 546-552.

CAO, Y., YU, Y., ZHANG, P., ZHANG, L., HE, T. & CAO, Y. 2013. An enhanced visible-light photocatalytic activity of TiO2 by nitrogen and nickel–chlorine modification. *Separation and Purification Technology,* 104**,** 256-262.

CARATTO, V., SETTI, L., CAMPODONICO, S., CARNASCIALI, M., BOTTER, R. & FERRETTI, M. 2012. Synthesis and characterization of nitrogen-doped TiO 2 nanoparticles prepared by sol–gel method. *Journal of sol-gel science and technology,* 63**,** 16-22.

CARDOZA-CONTRERAS, M. N., VÁSQUEZ-GALLEGOS, A., VIDAL-LIMON, A., ROMO-HERRERA, J. M., ÁGUILA, S. & CONTRERAS, O. E. 2019. Photocatalytic and Antimicrobial Properties of Ga Doped and Ag Doped ZnO Nanorods for Water Treatment. *Catalysts,* 9**,** 165.

CHANDRASEKAR, L. B., CHANDRAMOHAN, R., VIJAYALAKSHMI, R. & CHANDRASEKARAN, S. 2015. Preparation and characterization of Mn-doped ZnS nanoparticles. *International Nano Letters,* 5**,** 71-75.

CHAUHAN, R., KUMAR, A., CHAUDHARY, R. P. & EDUCATION, T. 2010. Synthesis and characterization of silver doped ZnO nanoparticles. *Archives of Applied Science Research,* 2(5)**,** 378-385.

CHEN, C., LEI, P., JI, H., MA, W., ZHAO, J., HIDAKA, H. & SERPONE, N. 2004. Photocatalysis by titanium dioxide and polyoxometalate/TiO2 cocatalysts. Intermediates and mechanistic study. *Environmental science & technology,* 38**,** 329-337.

CHEN, T., ZHENG, Y., LIN, J.-M. & CHEN, G. 2008. Study on the photocatalytic degradation of methyl orange in water using Ag/ZnO as catalyst by liquid chromatography electrospray ionization ion-trap mass spectrometry. *Journal of the American Society for Mass Spectrometry,* 19**,** 997-1003.

CHIOU, C.-H., WU, C.-Y. & JUANG, R.-S. 2008a. Influence of operating parameters on photocatalytic degradation of phenol in UV/TiO2 process. *Chemical Engineering Journal,* 139**,** 322-329.

CHIOU, C.-H., WU, C.-Y. & JUANG, R.-S. 2008b. Photocatalytic degradation of phenol and m-nitrophenol using irradiated TiO2 in aqueous solutions. *Separation and Purification Technology,* 62**,** 559-564.

CHOQUETTE-LABBÉ, M., SHEWA, W. A., LALMAN, J. A. & SHANMUGAM, S. R. 2014. Photocatalytic degradation of phenol and phenol derivatives using a nano-TiO2 catalyst: Integrating quantitative and qualitative factors using response surface methodology. *Water,* 6**,** 1785-1806.

CUN, W., JINCAI, Z., XINMING, W., BIXIAN, M., GUOYING, S., PING'AN, P. & JIAMO, F. 2002. Preparation, characterization and photocatalytic activity of nano-sized ZnO/SnO2 coupled photocatalysts. *Applied Catalysis B: Environmental,* 39**,** 269-279.

CZAPLICKA, M. 2004. Sources and transformations of chlorophenols in the natural environment. *Science of the Total environment,* 322**,** 21-39.

DANESHVAR, N., SALARI, D. & KHATAEE, A. 2004. Photocatalytic degradation of azo dye acid red 14 in water on ZnO as an alternative catalyst to TiO2. *Journal of Photochemistry and Photobiology A: Chemistry,* 162**,** 317-322.

DEGEN, A. & KOSEC, M. 2000. Effect of pH and impurities on the surface charge of zinc oxide in aqueous solution. *Journal of the European Ceramic Society,* 20**,** 667-673.

DENG, Y. & ZHAO, R. 2015. Advanced oxidation processes (AOPs) in wastewater treatment. *Current Pollution Reports,* 1**,** 167-176.

DEVADI, M. A. H., KRISHNA, M., MURTHY, H. N. & SATHYANARAYANA, B. 2014. Statistical optimization for photocatalytic degradation of methylene blue by Ag-TiO2 nanoparticles. *Procedia Materials Science,* 5**,** 612-621.

DEVI, B. R., RAVEENDRAN, R. & VAIDYAN, A. 2007. Synthesis and characterization of Mn 2+-doped ZnS nanoparticles. *Pramana,* 68**,** 679-687.

DEVI, P. G. & VELU, A. S. 2016. Synthesis, structural and optical properties of pure ZnO and Co doped ZnO nanoparticles prepared by the co-precipitation method. *Journal of Theoretical and Applied Physics,* 10**,** 233-240.

ELSALAMONY, R. A. & MAHMOUD, S. A. 2017. Preparation of nanostructured ruthenium doped titania for the photocatalytic degradation of 2-chlorophenol under visible light. *Arabian Journal of Chemistry,* 10**,** 194-205.

EYASU, A., YADAV, O. & BACHHETI, R. 2013. Photocatalytic degradation of methyl orange dye using Cr-doped ZnS nanoparticles under visible radiation. *International Journal of ChemTech Research,* 5**,** 1452-1461.

FERNÁNDEZ, J., KIWI, J., BAEZA, J., FREER, J., LIZAMA, C. & MANSILLA, H. 2004. Orange II photocatalysis on immobilised TiO2: effect of the pH and H2O2. *Applied Catalysis B: Environmental,* 48**,** 205-211.

FOX, M. A. & DULAY, M. T. 1993. Heterogeneous photocatalysis. *Chemical reviews,* 93**,** 341-357.

FUJISHIMA, A., ZHANG, X. & TRYK, D. A. 2007. Heterogeneous photocatalysis: from water photolysis to applications in environmental cleanup. *International journal of hydrogen energy,* 32**,** 2664-2672.

GAYA, U. I. & ABDULLAH, A. H. 2008. Heterogeneous photocatalytic degradation of organic contaminants over titanium dioxide: a review of fundamentals, progress and problems. *Journal of Photochemistry and Photobiology C: Photochemistry Reviews,* 9**,** 1-12.

GAYA, U. I., ABDULLAH, A. H., ZAINAL, Z. & HUSSEIN, M. Z. 2010. Photocatalytic degradation of 2, 4-dichlorophenol in irradiated aqueous ZnO suspension. *International Journal of Chemistry,* 2**,** 180.

GAYATHRI, S., GHOSH, O. N., SATHISHKUMAR, S., SUDHAKARA, S., JAYARAMUDU, J., RAY, S. & VISWANATH, A. K. 2015. Investigation of physicochemical properties of Ag doped ZnO nanoparticles prepared by chemical route. *Applied Science Letters*, 1, 8-13.

GNANAPRAKASAM, A., SIVAKUMAR, V. & THIRUMARIMURUGAN, M. 2015. Influencing parameters in the photocatalytic degradation of organic effluent via nanometal oxide catalyst: a review. *Indian Journal of Materials Science,* 2015, 1-16.

GNANAPRAKASAM, A., SIVAKUMAR, V. & THIRUMARIMURUGAN, M. 2016. A study on Cu and Ag doped ZnO nanoparticles for the photocatalytic degradation of brilliant green dye: synthesis and characterization. *Water Science and Technology,* 74**,** 1426-1435.

GOGATE, P. R. & PANDIT, A. B. 2004. Sonophotocatalytic reactors for wastewater treatment: a critical review. *AIChE Journal,* 50**,** 1051-1079.

GUPTA, V. K., ALI, I., SALEH, T. A., NAYAK, A. & AGARWAL, S. 2012. Chemical treatment technologies for waste-water recycling—an overview. *Royal Society of Chemistry ,* 2**,** 6380-6388.

GUPTA, V. K., FAKHRI, A., AZAD, M. & AGARWAL, S. 2018. Synthesis and characterization of Ag doped ZnS quantum dots for enhanced photocatalysis of Strychnine as a poison: Charge transfer behavior study by electrochemical impedance and time-resolved photoluminescence spectroscopy. *Journal of colloid and interface science,* 510**,** 95-102.

HABIBI, M. H. & RAHMATI, M. H. 2015. The effect of operational parameters on the photocatalytic degradation of Congo red organic dye using ZnO–CdS core–shell nano-structure coated on glass by Doctor Blade method. *Spectrochimica Acta Part A: Molecular and Biomolecular Spectroscopy,* 137**,** 160-164.

HAN, R., ZHANG, J., HAN, P., WANG, Y., ZHAO, Z. & TANG, M. 2009. Study of equilibrium, kinetic and thermodynamic parameters about methylene blue adsorption onto natural zeolite. *Chemical Engineering Journal,* 145**,** 496-504.

HEATH, R., VAN ZYL, H., SCHUTTE, C. & SCHOEMAN, J. 2009. First order assessment of the quantity and quality of non-point sources of pollution associated with industrial, mining and power generation. A report presented to *The Water Research Commission*, WRC Report no. 1627/1/09.

HELMER, R., HESPANHOL, I. 1997. *Water pollution control: a guide to the use of water quality management principles.* London*: E & F. Spon*

HERRMANN, J.-M., DUCHAMP, C., KARKMAZ, M., HOAI, B. T., LACHHEB, H., PUZENAT, E. & GUILLARD, C. 2007. Environmental green chemistry as defined by photocatalysis. *Journal of hazardous materials,* 146**,** 624-629.

HOFFMANN, M. R., MARTIN, S. T., CHOI, W. & BAHNEMANN, D. W. 1995. Environmental applications of semiconductor photocatalysis. *Chemical reviews,* 95**,** 69-96.

HOSSEINI, S., SARSARI, I. A., KAMELI, P. & SALAMATI, H. 2015. Effect of Ag doping on structural, optical, and photocatalytic properties of ZnO nanoparticles. *Journal of Alloys and Compounds,* 640**,** 408-415.

HIGH LEVEL PANEL ON WATER 2017, March 21. *Why Waste water: World Water Day 2017*. [Online]. Available: https:// sustainabledevelopment.un.org/HPLWater 2017-03-21 [Accessed].

IBHADON, A. O. & FITZPATRICK, P. 2013. Heterogeneous photocatalysis: recent advances and applications. *Catalysts,* 3**,** 189-218.

ILYAS, H., QAZI, I. A., ASGAR, W. & AWAN, M. A. 2011. Photocatalytic degradation of nitro and chlorophenols using doped and undoped titanium dioxide nanoparticles. *Journal of Nanomaterials,* 2011**,** 21.

JANG, Y. H., KOCHUVEEDU, S. T., CHA, M.-A., JANG, Y. J., LEE, J. Y., LEE, J., LEE, J., KIM, J., RYU, D. Y. & KIM, D. H. 2010. Synthesis and photocatalytic properties of hierarchical metal nanoparticles/ZnO thin films hetero nanostructures assisted by diblock copolymer inverse micellar nanotemplates. *Journal of Colloid and Interface Science,* 345(1)**,** 125-130.

JOSE, Y. J., MANJUNATHAN, M. & SELVARAJ, S. J. 2017. Highly photocatalyst efficient in LEDs/solar active and reusable: Sm–ZnO–Ag nanoparticles for methylene blue degradation. *Journal of Nanostructure in Chemistry,* 7**,** 259-271.

JOTHIBAS, M., MANOHARAN, C., JEYAKUMAR, S. J., PRAVEEN, P., PUNITHAVATHY, I. K. & RICHARD, J. P. 2018. Synthesis and enhanced photocatalytic property of Ni doped ZnS nanoparticles. *Solar Energy,* 159**,** 434-443.

KALNAOWAKUL, P., PHAIRATANA, T. & RODCHANAROWAN, A. 2017 Photocatalytic Comparative Study of TiO2, ZnO, Ag-G-ZnO and Ag-G-TiO2 Nanocomposite Films. *Key Engineering Materials*, 751, . 825-830.

KARMAOUI, M., LAJAUNIE, L., TOBALDI, D., LEONARDI, G., BENBAYER, C., ARENAL, R., LABRINCHA, J. A. & NERI, G. 2017. *Modification of anatase using noble-metals (Au, Pt, Ag): Toward a nanoheterojunction exhibiting simultaneously photocatalytic activity and plasmonic gas sensing*.

KARUNAKARAN, C. & DHANALAKSHMI, R. 2008. Semiconductor-catalyzed degradation of phenols with sunlight. *Solar Energy Materials and Solar Cells,* 92**,** 1315-1321.

KAUR, J., 2010. '*Synthesis and Photo-Catalytic Studies of ZnS Nanoparticles',* Master thesis, Thapar University, Patiala.

KAWAHARA, T., KONISHI, Y., TADA, H., TOHGE, N., NISHII, J. & ITO, S. 2002. A patterned TiO2 (anatase)/TiO2 (rutile) bilayer-type photocatalyst: effect of the anatase/rutile junction on the photocatalytic activity. *Angewandte Chemie,* 114**,** 2935-2937.

KOOL, H., VAN KREIJL, C., ZOETEMAN, B. & TARDIFF, R. G. 1982. Toxicology assessment of organic compounds in drinking water. *Critical Reviews in Environmental Science and Technology,* 12**,** 307-357.

KOTLHAO, K., MTUNZI, F., PAKADE, V., EJIDIKE, I. & KLINK, M. 2018a. Synthesis, characterization and evaluation of Ag-TiO2 nanocomposites for photo-catalytic degradation of selected chlorophenols. *Digest Journal of Nanomaterial and Biostructures,* 13**,** 835-846.

KOTLHAO, K., MTUNZI, F. M., PAKADE, V., LALOO, N., EJIDIKE, I. P., MODISE, S. J., MOUTLOALI, R. M. & KLINK, M. J. 2018b. Enhancing the photocatalytic degradation of selected chlorophenols using Ag/ZnO nanocomposites. *Materials Research Society***,** 3, 2129-2136.

KRISHNAKUMAR, B., SELVAM, K., VELMURUGAN, R. & SWAMINATHAN, M. 2010. Influence of operational parameters on photodegradation of Acid Black 1 with ZnO. *Desalination and Water Treatment,* 24**,** 132-139.

KRISHNAN, S., RAWINDRAN, H., SINNATHAMBI, C. & LIM, J. 2017. Comparison of various advanced oxidation processes used in remediation of industrial wastewater laden with recalcitrant pollutants. *Materials Science and Engineering*, 206(1) 12-86.

KU, Y., LEU, R.-M. & LEE, K.-C. 1996. Decomposition of 2-chlorophenol in aqueous solution by UV irradiation with the presence of titanium dioxide. *Water Research,* 30**,** 2569-2578.

KU, Y., LI, Y. C., WANG, W. Y., MA, C. M. & CHOU, Y. C. 2010. Effect of platinum on the photocatalytic decomposition of 2-chlorophenol in aqueous solution by UV/TiO2. *Journal of the Chinese Institute of Engineers,* 33**,** 591-596.

KUMAR, P. S. S., RAJ, M. R. & ANANDAN, S. 2010. Nanoporous Au–TiMCM-41—An inorganic hybrid photocatalyst toward visible photooxidation of methyl orange. *Solar Energy Materials and Solar Cells,* 94**,** 1783-1789.

KUMAR, R., RASHID, J. & BARAKAT, M. 2015. Zero valent Ag deposited TiO2 for the efficient photocatalysis of methylene blue under UV-C light irradiation. *Colloids and Interface Science Communications,* 5**,** 1-4.

KUPPAYEE, M., NACHIYAR, G. V. & RAMASAMY, V. 2011. Synthesis and characterization of Cu2+ doped ZnS nanoparticles using TOPO and SHMP as capping agents. *Applied Surface Science,* 257**,** 6779-6786.

LEI, X., XUE, X. & YANG, H. 2014. Preparation and characterization of Ag-doped TiO2 nanomaterials and their photocatalytic reduction of Cr (VI) under visible light. *Applied Surface Science,* 321**,** 396-403.

LI, X., WANG, F., QIAN, Q., LIU, X., XIAO, L. & CHEN, Q. 2012. Ag/TiO2 nanofibers heterostructure with enhanced photocatalytic activity for parathion. *Materials Letters,* 66**,** 370-373.

LI, Y., CAO, C. & CHEN, Z. 2011. Magnetic and optical properties of Fe doped ZnS nanoparticles synthesized by microemulsion method. *Chemical Physics Letters,* 517**,** 55-58.

LIANG, J., KOMAROV, S., HAYASHI, N. & KASAI, E. 2007. Improvement in sonochemical degradation of 4-chlorophenol by combined use of Fenton-like reagents. *Ultrason Sonochem,* 14**,** 201-7.

LIANG, Y., SUN, S., DENG, T., DING, H., CHEN, W. & CHEN, Y. 2018. The preparation of TiO2 film by the sol-gel method and evaluation of its self-cleaning property. *Materials,* 11**,** 450.

LINSEBIGLER, A. L., LU, G. & YATES JR, J. T. 1995. Photocatalysis on TiO2 surfaces: principles, mechanisms, and selected results. *Chemical reviews,* 95**,** 735-758.

LIU, C., LI, F., MA, L. P. & CHENG, H. M. 2010. Advanced materials for energy storage. *Advanced materials,* 22(8). 28-62

LUO, X.-X., CAO, W.-H. & ZHOU, L.-X. 2007. Synthesis and luminescence properties of (Zn, Cd) S: Ag nanocrystals by hydrothermal method. *Journal of luminescence,* 122**,** 812-815.

LV, J., GONG, W., HUANG, K., ZHU, J., MENG, F., SONG, X. & SUN, Z. 2011. Effect of annealing temperature on photocatalytic activity of ZnO thin films prepared by sol–gel method. *Superlattices and Microstructures,* 50**,** 98-106.

MADKOUR, M. & AL SAGHEER, F. 2017. Au/ZnS and Ag/ZnS nanoheterostructures as regenerated nanophotocatalysts for photocatalytic degradation of organic dyes. *Optical Materials Express,* 7**,** 158-169.

MAHMOODI, N. M., ARAMI, M., LIMAEE, N. Y. & TABRIZI, N. S. 2006. Kinetics of heterogeneous photocatalytic degradation of reactive dyes in an immobilized TiO2 photocatalytic reactor. *Journal of colloid and interface Science,* 295**,** 159-164.

MAI, F., LU, C., WU, C., HUANG, C., CHEN, J. & CHEN, C. 2008. Mechanisms of photocatalytic degradation of Victoria Blue R using nano-TiO2. *Separation and Purification Technology,* 62**,** 423-436.

MALATO, S., BLANCO, J., ALARCÓN, D. C., MALDONADO, M. I., FERNÁNDEZ-IBÁÑEZ, P. & GERNJAK, W. 2007. Photocatalytic decontamination and disinfection of water with solar collectors. *Catalysis Today,* 122**,** 137-149.

METCALF, EDDY, BURTON, F. L., STENSEL, H. D. & TCHOBANOGLOUS, G. 2003. *Wastewater engineering: treatment and reuse*. New York: McGraw Hill.

MILLS, A., DAVIES, R. H. & WORSLEY, D. 1993. Water purification by semiconductor photocatalysis. *Chemical Society Reviews,* 22**,** 417-425.

MILLS, A. & MCFARLANE, M. 2007. Current and possible future methods of assessing the activities of photocatalyst films. *Catalysis Today,* 129**,** 22-28.

MOHABANSI, N., PATIL, V. & YENKIE, N. 2011. A comparative study on photo degradation of methylene blue dye effluent by advanced oxidation process by using TiO2/ZnO photo catalyst. *Rasayan Journal of Chemistry,* 4**,** 814-819.

MOHAMED, E. F. 2011. '*Removal of organic compounds from water by adsorption and photocatalytic oxidation',* Doctoral dissertation, University of Toulouse..

MOHAMMADI, N., KHANI, H., GUPTA, V. K., AMEREH, E. & AGARWAL, S. 2011. Adsorption process of methyl orange dye onto mesoporous carbon material–kinetic and thermodynamic studies. *Journal of colloid and interface science,* 362**,** 457-462.

MOYO, N. A. & PHIRI, C. 2002. The degradation of an urban stream in Harare, Zimbabwe. *African Journal of Ecology,* 40**,** 401-406.

MUNIR, T., KASHIF, M., MAHMOOD, K., IMRAN, M., ALI, A., SABIR, N., AMIN, N., MAHMOOD, A., ALI, H. & AHMED, N. 2019. Impact of silver dopant on structural, optical and electrical properties of zno nanoparticles. *Journal of Ovonic Research,* 15**,** 173-179.

MURTAZA, G., AHMAD, R., RASHID, M., HASSAN, M., HUSSNAIN, A., KHAN, M. A., UL HAQ, M. E., SHAFIQUE, M. & RIAZ, S. 2014. Structural and magnetic studies on Zr doped ZnO diluted magnetic semiconductor. *Current Applied Physics,* 14**,** 176-181.

MURUGADOSS, A. & CHATTOPADHYAY, A. 2008. Tuning photoluminescence of ZnS nanoparticles by silver. *Bulletin of Materials Science,* 31**,** 533-539.

MUSINGAFI, M. C. C. 2014. Fresh water sources pollution: a human related threat to fresh water security in South Africa. *Journal of Public policy and Governance*, 1, 72-81.

NACHIT, W., TOUHTOUH, S., RAMZI, Z., ZBAIR, M., EDDIAI, A., RGUITI, M., BOUCHIKHI, A., HAJJAJI, A. & BENKHOUJA, K. 2016. Synthesis of nanosized TiO2 powder by sol gel method at low temperature. *Molecular Crystals and Liquid Crystals,* 627**,** 170-175.

NAINANI, R., THAKUR, P. & CHASKAR, M. 2012. Synthesis of silver doped TiO2 nanoparticles for the improved photocatalytic degradation of methyl orange. *J. Mater. Sci. Eng. B,* 2**,** 52-58.

NARAGINTI, S., THEJASWINI, T., PRABHAKARAN, D., SIVAKUMAR, A., SATYANARAYANA, V. & PRASAD, A. A. 2015. Enhanced photo-catalytic activity of Sr and Ag co-doped TiO2 nanoparticles for the degradation of Direct Green-6 and Reactive Blue-160 under UV & visible light. *Spectrochimica Acta Part A: Molecular and Biomolecular Spectroscopy,* 149**,** 571-579.

NOMURA, K., OHTA, H., UEDA, K., KAMIYA, T., HIRANO, M. & HOSONO, H. 2003. Thin-film transistor fabricated in single-crystalline transparent oxide semiconductor. *Science,* 300**,** 1269-1272.

OTURAN, M. A. & AARON, J.-J. 2014. Advanced oxidation processes in water/wastewater treatment: principles and applications. A review. *Critical Reviews in Environmental Science and Technology,* 44**,** 2577-2641.

OZIMEK, M., PALEWICZ, M. & HRENIAK, A. 2016. Optical Properties of TiO2 Nanopowder Doped by Silver (Copper) during Synthesis or PVD Method. *Acta Physica Polonica, A.,* 129, 1214-1219.

PANT, H. R., PANT, B., SHARMA, R. K., AMARJARGAL, A., KIM, H. J., PARK, C. H., TIJING, L. D. & KIM, C. S. 2013. Antibacterial and photocatalytic properties of Ag/TiO2/ZnO nano-flowers prepared by facile one-pot hydrothermal process. *Ceramics International,* 39**,** 1503-1510.

PARASTAR, S., NASSERI, S., BORJI, S. H., FAZLZADEH, M., MAHVI, A. H., JAVADI, A. H. & GHOLAMI, M. 2013. Application of Ag-doped TiO2 nanoparticle prepared by photodeposition method for nitrate photocatalytic removal from aqueous solutions. *Desalination and Water Treatment,* 51**,** 7137-7144.

PARE, B., JONNALAGADDA, S., TOMAR, H., SINGH, P. & BHAGWAT, V. 2008. ZnO assisted photocatalytic degradation of acridine orange in aqueous solution using visible irradiation. *Desalination,* 232**,** 80-90.

PARK, J.-Y. & LEE, I.-H. 2014. Photocatalytic degradation of 2-chlorophenol using Ag-doped TiO 2 nanofibers and a near-UV light-emitting diode system. *Journal of Nanomaterials,* 2014**,** 1.

PEARTON, S., HEO, W., IVILL, M., NORTON, D. & STEINER, T. 2004. Dilute magnetic semiconducting oxides. *Semiconductor Science and Technology,* 19**,** R59.

PECCHI, G., REYES, P., SANHUEZA, P. & VILLASENOR, J. 2001. Photocatalytic degradation of pentachlorophenol on TiO2 sol–gel catalysts. *Chemosphere,* 43**,** 141-146.

PERA-TITUS, M., GARCíA-MOLINA, V., BAÑOS, M. A., GIMÉNEZ, J. & ESPLUGAS, S. 2004. Degradation of chlorophenols by means of advanced oxidation processes: a general review. *Applied Catalysis B: Environmental,* 47**,** 219-256.

PERUMAL, S. & GNANA SAMBANDAM, C. 2014. Synthesis and characterization studies of solvothermally synthesized undoped and Ag-doped TiO2 nanoparticles using toluene as a solvent. *Journal of Engineering Research and Applications,* 4**,** 184-187.

POURETEDAL, H. R., ESKANDARI, H., KESHAVARZ, M. H. & SEMNANI, A. 2009a. Photodegradation of Organic Dyes using Nanoparticles of Cadmium Sulfide Doped with Manganese, Nickel and Copper as Nanophotocatalyst. *Acta Chimica Slovenica,* 56.

POURETEDAL, H. R., NOROZI, A., KESHAVARZ, M. H. & SEMNANI, A. 2009b. Nanoparticles of zinc sulfide doped with manganese, nickel and copper as nanophotocatalyst in the degradation of organic dyes. *Journal of Hazardous Materials,* 162**,** 674-681.

PRADO, A. G. & COSTA, L. L. 2009. Photocatalytic decouloration of malachite green dye by application of TiO2 nanotubes. *Journal of hazardous materials,* 169**,** 297-301.

PRIYA, M. H. & MADRAS, G. 2006. Photocatalytic degradation of nitrobenzenes with combustion synthesized nano-TiO2. *Journal of Photochemistry and Photobiology A: Chemistry,* 178**,** 1-7.

QIN, D.-Z., YANG, G., HE, G.-X., ZHANG, L., ZHANG, Q.-X. & LI, L.-Y. 2012. The investigation on synthesis and optical properties of Ag-doped ZnS nanocrystals by hydrothermal method. *Journal Scope Chalcogenide Letters,* 9**,** 441-446.

RAMASAMY, V., PRABA, K. & MURUGADOSS, G. 2012. Synthesis and study of optical properties of transition metals doped ZnS nanoparticles. *Spectrochimica Acta Part A: Molecular and Biomolecular Spectroscopy,* 96**,** 963-971.

RAO, N., DUBEY, A., MOHANTY, S., KHARE, P., JAIN, R. & KAUL, S. 2003a. Photocatalytic degradation of 2-chlorophenol: a study of kinetics, intermediates and biodegradability. *Journal of hazardous materials,* 101**,** 301-314.

RASHID, J., BARAKAT, M., RUZMANOVA, Y. & CHIANESE, A. 2015a. Fe 3 O 4/SiO 2/TiO 2 nanoparticles for photocatalytic degradation of 2-chlorophenol in simulated wastewater. *Environmental Science and Pollution Research International,* 22**,** 3149-3157.

RAVISHANKAR, T., MANJUNATHA, K., RAMAKRISHNAPPA, T., NAGARAJU, G., KUMAR, D., SARAKAR, S., ANANDAKUMAR, B., CHANDRAPPA, G., REDDY, V. & DUPONT, J. 2014. Comparison of the photocatalytic degradation of trypan blue by undoped and silver-doped zinc oxide nanoparticles. *Materials Science in Semiconductor Processing,* 26**,** 7-17.

RIDEH, L., WEHRER, A., RONZE, D. & ZOULALIAN, A. 1997. Photocatalytic degradation of 2-chlorophenol in TiO2 aqueous suspension: modeling of reaction rate. *Industrial & Engineering Chemistry Research,* 36**,** 4712-4718.

RODRÍGUEZ, J. A. & FERNÁNDEZ-GARCÍA, M. 2007. *Synthesis, properties, and applications of oxide nanomaterials*. New Jersey: John Wiley & Sons.

SAFARZADEH-AMIRI, A. 2001. O3/H2O2 treatment of methyl-tert-butyl ether (MTBE) in contaminated waters. *Water Research,* 35**,** 3706-3714.

SALEM, A. A., KALIDINDI, S. R. & DOHERTY, R. D. 2003. Strain hardening of titanium: role of deformation twinning. *Acta Materialia,* 51**,** 4225-4237.

SARAVANAN, R., GRACIA, F. & STEPHEN, A. 2017. Basic principles, mechanism, and challenges of photocatalysis. *Nanocomposites for Visible Light-induced Photocatalysis*. New york: Springer.

SARAVANAN, R., MANOJ, D., QIN, J., NAUSHAD, M., GRACIA, F., LEE, A. F., KHAN, M. M. & GRACIA-PINILLA, M. 2018. Mechanothermal synthesis of Ag/TiO2 for photocatalytic methyl orange degradation and hydrogen production. *Process Safety and Environmental Protection,* 120**,** 339-347.

SATHISHKUMAR, P., MANGALARAJA, R. V., ANANDAN, S. & ASHOKKUMAR, M. 2013. CoFe2O4/TiO2 nanocatalysts for the photocatalytic degradation of Reactive Red 120 in aqueous solutions in the presence and absence of electron acceptors. *Chemical engineering journal,* 220**,** 302-310.

SAUER, T., NETO, G. C., JOSE, H. & MOREIRA, R. 2002. Kinetics of photocatalytic degradation of reactive dyes in a TiO2 slurry reactor. *Journal of Photochemistry and Photobiology A: Chemistry,* 149**,** 147-154.

SHAH, A., MANIKANDAN, E., AHAMED, M. B., MIR, D. A. & MIR, S. A. 2014. Antibacterial and Blue shift investigations in sol–gel synthesized CrxZn1− xO Nanostructures. *Journal of Luminescence,* 145**,** 944-950.

SHANKAR, S. S., RAI, A., AHMAD, A. & SASTRY, M. 2004. Rapid synthesis of Au, Ag, and bimetallic Au core–Ag shell nanoparticles using Neem (Azadirachta indica) leaf broth. *Journal of colloid and interface science,* 275**,** 496-502.

SHI, J.-W., ZHENG, J.-T. & WU, P. 2009. Preparation, characterization and photocatalytic activities of holmium-doped titanium dioxide nanoparticles. *Journal of Hazardous Materials,* 161**,** 416-422.

SIM, L. C., RAMANAN, S., ISMAIL, H., SEETHARAMU, K. & GOH, T. 2005. Thermal characterization of Al2O3 and ZnO reinforced silicone rubber as thermal pads for heat dissipation purposes. *Thermochimica acta,* 430**,** 155-165.

SINGH, R., BARMAN, P. & SHARMA, D. 2017. Synthesis, structural and optical properties of Ag doped ZnO nanoparticles with enhanced photocatalytic properties by photo degradation of organic dyes. *Journal of Materials Science: Materials in Electronics,* 28**,** 5705-5717.

SIVA VIJAYAKUMAR, T., KARTHIKEYENI, S., VASANTH, S., GANESH, A., BUPESH, G., RAMESH, R., MANIMEGALAI, M. & SUBRAMANIAN, P. 2013. Synthesis of silver-doped zinc oxide nanocomposite by pulse mode ultrasonication and its characterization studies. *Journal of Nanoscience,* 2013, 1-7.

SIVAKUMAR, P., KUMAR, G. G. & RENGANATHAN, S. 2014. Synthesis and characterization of ZnS-Ag nanoballs and its application in photocatalytic dye degradation under visible light. *Journal of Nanostructure in Chemistry,* 4**,** 107.

SOBANA, N., MURUGANADHAM, M. & SWAMINATHAN, M. 2006. Nano-Ag particles doped TiO2 for efficient photodegradation of direct azo dyes. *Journal of Molecular Catalysis A: Chemical,* 258**,** 124-132.

SOBANA, N., SELVAM, K. & SWAMINATHAN, M. 2008. Optimization of photocatalytic degradation conditions of Direct Red 23 using nano-Ag doped TiO2. *Separation and Purification Technology,* 62**,** 648-653.

STEPAN, S., SMITH, J. & RIHA, M. 1988. ‘ Movement and chemical change of organic pollutants in an aquifer’. Australian Water Resources Council. *Groundwater Pollution Conference*, Canberra , Australia.

STUMM, W. 1992. *Chemistry of the solid-water interface: processes at the mineral-water and particle-water interface in natural systems*. New York: John Wiley & Son Inc.

SUNDER, M. & HEMPEL, D.-C. 1997. Oxidation of tri-and perchloroethene in aqueous solution with ozone and hydrogen peroxide in a tube reactor. *Water Research,* 31**,** 33-40.

SUWARNKAR, M., DHABBE, R., KADAM, A. & GARADKAR, K. 2014. Enhanced photocatalytic activity of Ag doped TiO2 nanoparticles synthesized by a microwave assisted method. *Ceramics International,* 40**,** 5489-5496.

SYNNOTT, D. W., SEERY, M. K., HINDER, S. J., MICHLITS, G. & PILLAI, S. C. 2013. Anti-bacterial activity of indoor-light activated photocatalysts. *Applied Catalysis B: Environmental,* 130**,** 106-111.

TALEB, M. F. A. 2014. Adsorption and photocatalytic degradation of 2-CP in wastewater onto CS/CoFe2O4 nanocomposite synthesized using gamma radiation. *Carbohydrate polymers,* 114**,** 65-72.

TAN, T. T. Y., YIP, C. K., BEYDOUN, D. & AMAL, R. 2003. Effects of nano-Ag particles loading on TiO2 photocatalytic reduction of selenate ions. *Chemical Engineering Journal,* 95**,** 179-186.

TAYLOR, D. 1988. Optical properties of mixed crystals. In Elliott R.J, Ipatova I.P. (eds) *Modern Problems in Condensed Matter Sciences,* , 35-131, Elsevier, North Holland.

TIAN, B., LI, C., GU, F., JIANG, H., HU, Y. & ZHANG, J. 2009. Flame sprayed V-doped TiO2 nanoparticles with enhanced photocatalytic activity under visible light irradiation. *Chemical Engineering Journal,* 151**,** 220-227.

TIAN, B., ZHANG, J., TONG, T. & CHEN, F. 2008. Preparation of Au/TiO2 catalysts from Au (I)–thiosulfate complex and study of their photocatalytic activity for the degradation of methyl orange. *Applied Catalysis B: Environmental,* 79**,** 394-401.

TRYBA, B., PISZCZ, M. & MORAWSKI, A. 2010. Photocatalytic and self-cleaning properties of Ag-doped TiO2. *Open Materials Science Journal,* 4**,** 5-8.

UDAYKUMAR, S., RENUGA, V. & KAVITHA, K. 2012. synthesis and characterization of Ni–doped Zno by chemical precipitation method. *International Journal of Recent Scientific Research,* 3**,** 118-122.

ULLATTIL, S. G. & PERIYAT, P. 2017. Sol-gel synthesis of titanium dioxide. In Pillai S., Hehir S. (eds) *Sol-Gel Materials for Energy, Environment and Electronic Applications*, 271-283, Springer, Cham.

VAIDYA, P. D. & MAHAJANI, V. V. 2002. Insight into heterogeneous catalytic wet oxidation of phenol over a Ru/TiO2 catalyst. *Chemical Engineering Journal,* 87**,** 403-416.

VENKATACHALAM, N., PALANICHAMY, M. & MURUGESAN, V. 2007. Sol–gel preparation and characterization of alkaline earth metal doped nano TiO2: Efficient photocatalytic degradation of 4-chlorophenol. *Journal of Molecular Catalysis A: Chemical,* 273**,** 177-185.

VISWANATH, R., NAIK, H. S. B., SOMALANAIK, Y. K. G., NEELANJENEALLU, P. K. P., HARISH, K. N. & PRABHAKARA, M. C. 2014. Studies on characterization, optical absorption, and photoluminescence of yttrium doped ZnS nanoparticles. *Journal of Nanotechnology,* 2014.

VORA, J., CHAUHAN, S., PARMAR, K., VASAVA, S., SHARMA, S. & BHUTADIYA, L. 2009. Kinetic study of application of ZnO as a photocatalyst in heterogeneous medium. *Journal of Chemistry,* 6**,** 531-536.

WANG, R., XIN, J. H., YANG, Y., LIU, H., XU, L. & HU, J. 2004. The characteristics and photocatalytic activities of silver doped ZnO nanocrystallites. *Applied Surface Science,* 227**,** 312-317.

WANG, Y., HUANG, Y., HO, W., ZHANG, L., ZOU, Z. & LEE, S. 2009. Biomolecule-controlled hydrothermal synthesis of C–N–S-tridoped TiO2 nanocrystalline photocatalysts for NO removal under simulated solar light irradiation. *Journal of Hazardous materials,* 169**,** 77-87.

WATER, U. 2017, March 22. *World Water Development Report 2017* [Online]. Available: http://www.unwater.org/publications/world-water-development-report-2017/ [Accessed].

WU, H. B., HNG, H. H. & LOU, X. W. 2012. Direct synthesis of anatase TiO2 nanowires with enhanced photocatalytic activity. *Advanced Materials,* 24**,** 2567-2571.

WU, M., YANG, B., LV, Y., FU, Z., XU, J., GUO, T. & ZHAO, Y. 2010. Efficient one-pot synthesis of Ag nanoparticles loaded on N-doped multiphase TiO2 hollow nanorod arrays with enhanced photocatalytic activity. *Applied Surface Science,* 256**,** 7125-7130.

XU, A.-W., GAO, Y. & LIU, H.-Q. 2002. The preparation, characterization, and their photocatalytic activities of rare-earth-doped TiO2 nanoparticles. *Journal of Catalysis,* 207**,** 151-157.

YAHAYA, M. Z., AZAM, M. A., TERIDI, M. A. M., SINGH, P. K. & MOHAMAD, A. A. 2017. 'Recent Characterisation of Sol-Gel Synthesised TiO2 Nanoparticles', in U. Chandra (eds), *Recent Applications in Sol-Gel Synthesis*, 109-129, Intech, London.

YANG, R., QU, X. & WANG, M.-H. 2018. Sol–gel synthesis of Ba-doped ZnO nanoparticles and its use in varistor ceramics. *Micro & Nano Letters,* 13**,** 1506-1509.

YANG, X.-J., SHU, W., SUN, H.-M., WANG, X.-B. & LIAN, J.-S. 2015. Preparation and photocatalytic performance of Cu-doped TiO2 nanoparticles. *Transactions of Nonferrous Metals Society of China,* 25**,** 504-509.

YILDIRIM, Ö. A., UNALAN, H. E. & DURUCAN, C. 2013. Highly Efficient Room Temperature Synthesis of Silver-Doped Zinc Oxide (ZnO: Ag) Nanoparticles: Structural, Optical, and Photocatalytic Properties. *Journal of the American Ceramic Society,* 96**,** 766-773.

YU, T., TAN, X., ZHAO, L., YIN, Y., CHEN, P. & WEI, J. 2010. Characterization, activity and kinetics of a visible light driven photocatalyst: cerium and nitrogen co-doped TiO2 nanoparticles. *Chemical Engineering Journal,* 157**,** 86-92.

ZANDI, S., KAMELI, P., SALAMATI, H., AHMADVAND, H. & HAKIMI, M. 2011. Microstructure and optical properties of ZnO nanoparticles prepared by a simple method. *Physica B: Condensed Matter,* 406**,** 3215-3218.

ZANTA, C. & MARTÍNEZ-HUITLE, C. 2009. Degradation of 2-hydroxybenzoic acid by advanced oxidation processes. *Brazilian Journal of Chemical Engineering,* 26**,** 503-513.

ZHANG, D. 2012. Effects of deposited metallic Silver on nano-ZnO for the environmental purification of dye pollutants. *South African Journal of Chemistry,* 65**,** 98-103.

ZHANG, X. & LEI, L. 2008. Effect of preparation methods on the structure and catalytic performance of TiO2/AC photocatalysts. *Journal of hazardous materials,* 153**,** 827-833.

ZHANG, Y., ZHOU, M., HAO, X. & LEI, L. 2007. Degradation mechanisms of 4-chlorophenol in a novel gas-liquid hybrid discharge reactor by pulsed high voltage system with oxygen or nitrogen bubbling. *Chemosphere,* 67**,** 702-11.

ZHAO, J. & YANG, X. 2003. Photocatalytic oxidation for indoor air purification: a literature review. *Building and Environment,* 38**,** 645-654.

ZHOU, H. & SMITH, D. W. 2002. Advanced technologies in water and wastewater treatment. *Journal of Environmental Engineering and Science,* 1**,** 247-264.

ZHU, B.-Z. & SHAN, G.-Q. 2009. Potential mechanism for pentachlorophenol-induced carcinogenicity: a novel mechanism for metal-independent production of hydroxyl radicals. *Chemical research in toxicology,* 22**,** 969-977.

ZHU, B.-Z., ZHU, J.-G., FAN, R.-M. & MAO, L. 2011. Metal-independent pathways of chlorinated phenol/quinone toxicity. *Advances in Molecular Toxicology*, 5, 1-43.

ZHU, X., YUAN, C., BAO, Y., YANG, J. & WU, Y. 2005. Photocatalytic degradation of pesticide pyridaben on TiO2 particles. *Journal of Molecular Catalysis A: Chemical,* 229**,** 95-105.

ZORBA, T. B. Q. 2015. '*Photocatalytic Degradation of 2-Chlorophenol in Water with Direct Solar Light using Pristine and Kaolinite Supported ZnO'. Master thesis, An-Najah National University, Nablus.*